

**SUPRAMOLECULAR DISCOTIC LIQUID
CRYSTALS: TOWARDS FUNCTIONAL
NANOPOROUS SCAFFOLDS**

Andrew Stretton



MPhil

University of Edinburgh

2007



I declare that this thesis is entirely of my own composition unless otherwise stated, and that the work described herein has not been submitted for examination for any other research degree.

Andrew Stretton

Signature:

THE UNIVERSITY OF EDINBURGH: ABSTRACT OF THESIS

Name of Candidate: Andrew David Stretton

Address : 68, St. Laurence Rd.

Birmingham

Post Code: B31 2AY

Degree: MPhil

Title of Supramolecular discotic liquid crystals: towards functional nanoporous

Thesis: scaffolds

No. of words in the main text 15000

Considerable research efforts have been devoted to the creation of ordered arrays of nanopores on a variety of surfaces. Potential applications for such materials include highly efficient solar cells, real-time electrochemical sensors, miniaturised hard-disks, continuous flow reactors, catalytic supports, and drug delivery devices. Self-assembling organic 'building blocks' provide direct access to these complex multi-scale nanostructured materials i.e. a bottom-up approach. Derivatives of a known liquid crystalline complex were synthesised, incorporating a benzotri(imidazole) core binding three long-chain gallic acid derivatives. Thin films were prepared by spin-coating solutions of the complex on to microscope slides and gold coated silicon wafers. Slow cooling of these films from the isotropic phase provided a homeotropically aligned (or face on) hexagonal columnar mesophase. As the final etching stage has yet to be investigated, a new technique has been suggested to complete the fabrication of a nanoporous scaffold. Novel supramolecular building blocks were also investigated; these studies led to the synthesis of a highly distorted triphenylene derivative. In the solid-state, X-ray crystallographic studies reveal that 1,4,5,8,9,12-Hexamethyltriphenylene presents a highly distorted C_2 geometry with a 53° end-to-end twist. In solution, variable temperature ^1H NMR studies suggest rapid dynamic conformational interconversions between two C_2 enantiomers (with a low activation barrier) and a slower C_2 - D_3 interconversion (with a relatively high barrier).

Table of Contents

<i>Abbreviations</i>	7
<i>1) Introduction: Self assembly and self-organisation in natural and synthetic systems</i>	9
1.1) Self-assembled systems	9
1.2) The design of hydrogen bonding motifs	13
1.3) Supramolecular polymers	16
1.4) Reversible binding for sensing applications	20
1.5) Dendritic self-assembled systems.....	21
1.6) Self organised systems: Discotic liquid crystals.....	23
1.6.1) <i>Definition</i>	23
1.6.2) <i>Types of columnar packing</i>	24
1.6.3) <i>Properties of the hexagonal columnar phase required for novel applications</i>	25
1.6.4) <i>Designation of phase and alignment by microscopy</i>	26
1.6.5) <i>Theories on the growth of aligned domains in columnar mesophases</i>	27
1.7) Supramolecular Columnar Liquid Crystals	28
1.7.1) <i>Exploiting complimentary hydrogen bonding interactions</i>	28
1.7.2) <i>Thermal decomposition of supramolecular liquid crystals</i>	31
1.7.3) <i>Other types of supramolecular columnar liquid crystals</i>	32
1.8) From Self-Assembled Discotics to Functional Nanoporous Membranes.....	33
1.9) Fabrication of Nanoporous Scaffold.....	35
<i>2) Towards the Synthesis of an Entirely New Supramolecular Discotic Mesogen</i>	38
2.1) Aims and strategy	38
2.2) Design of benzoic acid corona units for supramolecular discotic liquid crystal ...	40
2.3) Design of core for supramolecular discotic liquid crystal	40
2.4) Retrosynthetic analysis	41
2.4.1) <i>Dimethylbenzoic acid derived corona 6</i>	41
2.4.2) <i>Propane-1,3-diol derived corona 8</i>	42
2.4.3) <i>Tris(imidazolyl)triazine cores 5 and 7</i>	43
2.4.4) <i>Triimide supramolecular synthon 9</i>	44

2.5) Results and Discussion	45
2.5.1) Towards dimethylbenzoic acid derived corona 6	45
2.5.2) Towards propane-1,3-diol derived corona 8	46
2.5.3 Towards trisimidazolyl triazine core 5	47
2.5.4) Towards solublised triazine core 7	48
2.5.5) Towards the synthesis of triimide 9	49
2.6) Conclusions.....	49
3) The Synthesis and Novel Application of a Supramolecular Discotic Liquid Crystal ..50	
3.1) Aims and Strategy.....	50
3.2) Molecular Design.....	51
3.3) Synthetic Results and Discussion	52
3.3.1) Synthesis of benzotri(imidazole) core 47	52
3.3.2) Syntheses of coronas 1 and 48	53
3.4) Bulk properties of methacrylate complex 48.47	54
3.4.1) ¹ H NMR showing formation of supramolecular complex between corona 48 and core 47.....	54
3.4.2) DSC showing phase behaviour of methacrylate complex 48.47.....	55
3.4.3) Polarised optical microscopy of thick films of methacrylate complex 48.47	57
3.4.4) Polymerisation in the presence of initiators	57
3.5) Application of methacrylate complex 48.47 on surfaces.....	60
3.5.1) Polarised optical microscopy of thin films	60
3.5.2) Attempted alignment in the presence of initiator	60
3.5.3) Verification of effect of initiator and inhibitor on phase behaviour by DSC	61
3.6) Bulk properties of acrylate complex 1.47	61
3.6.1) ¹ H NMR showing formation of supramolecular complex between corona 1 and core 47.....	62
3.6.2) DSC showing phase behaviour of acrylate complex 1.47	63
3.6.3) Polarised optical microscopy of thick films.....	64
3.6.3) Polymerisation of acrylate complex 1.47	64
3.6.4) X-ray scattering studies	65

3.7) Application of acrylate complex 1.47 on surfaces.....	66
3.7.1) <i>Polarised optical microscopy of thin films</i>	66
3.7.2) <i>Attempted alignment, polymerisation and etching on gold</i>	67
3.8) Conclusions to studies of complex 48.47 and 1.47.....	67
4) <i>Synthesis and properties of a novel distorted triphenylene</i>	68
4.1) Introduction.....	68
<i>Disclaimer</i>	68
4.2) Background to Twisted Molecules	68
4.3) Examination of the NMR Traits of 36	71
4.4) X-Ray Crystallographic Studies of 36	73
4.5) Molecular Modelling of Compound 36	76
4.6) Conformational Analyses of Hindered Triphenylenes 1-4.	81
4.7) Fluorescence Spectroscopy of 36	84
4.8) Electrochemical Investigation of 36	86
4.9) Conclusions.....	89
5) <i>Future Work</i>	89
5.1) New liquid crystalline complexes.....	89
5.2) Alignment of liquid crystal complexes.....	89
5.3) Polymerisation of aligned films.....	90
5.4) Formation of Nanoporous Arrays	90
5.5) Further Extensions	90
<i>Acknowledgements</i>	91
<i>Experimental section:</i>	92
<i>Bibliography</i>	148

Abbreviations

FGI	Functional group interconversion
eq	equivalents
conc.	Concentrated
TLC	Thin layer chromatography
DMAP	4-(<i>N,N</i> -dimethylamino)pyridine
NBS	<i>N</i> -Bromosuccinimide
TIPS	Triisopropylsilyl
NEt ₃	Triethylamine
EtOAc	Ethyl acetate
Et ₂ O	Diethyl Ether
DCM	Dichloromethane
THF	Tetrahydrofuran
DMF	Dimethylformamide
CDCl ₃	Deuterated chloroform
DMSO-d ₆	Deuterated dimethyl sulphoxide
NMR	Nuclear magnetic resonance
ITO	Indium tin oxide
DMPA	2,2-dimethoxy-2-phenylacetophenone
TMBPO	Diphenyl-2,4,6-trimethylbenzoylphosphine oxide
MEHQ	methyl hydroquinone or 4-methoxyphenol
POM	Polarised optical microscopy
XPS	X-ray photoelectron spectroscopy
FTIR	Fourier transform infrared spectroscopy
Str	In IR assignments – stretch

In NMR spectral assignments:

br	Broad NMR signal
s	Singlet
d	Doublet
dd	Doublet of doublets
t	triplet
q	quartet
m	multiplet

1) Introduction: Self assembly and self-organisation in natural and synthetic systems

1.1) Self-assembled systems

The elegance and specificity of reversible binding between DNA base pairs¹ has inspired scientists to attempt to mimic nature in synthetic systems.² Much attention has been focused upon understanding and making use of the interactions within these natural architectures. This field is known as molecular self assembly - the spontaneous association of molecules, under equilibrium conditions, into structurally well-defined and stable complexes held together by non-covalent bonds.³ As will be described, the properties of self-assembled complexes make them amenable to a wide range of applications including: further advances in medicine⁴, new or miniaturised computer components,¹ novel nanostructured materials,⁵ and “smart” or recyclable plastics.⁶

Another celebrated example of a self-assembled complex, bound in equilibrium conditions, is the tobacco mosaic virus (TMV) (Figure 1). Elucidated by Butler and Klug,⁷ the virus is made up of RNA strand coated by a cylinder of stacked protein units. It remarkably reassembles into fully working virus following disassembly experiments. The virus is, in effect, the thermodynamic product of the reaction.

i Many companies thrive upon researching organic electronics, e.g. Plastic logic - www.plasticlogic.com;
Cambridge display technology - www.cdtltd.co.uk.

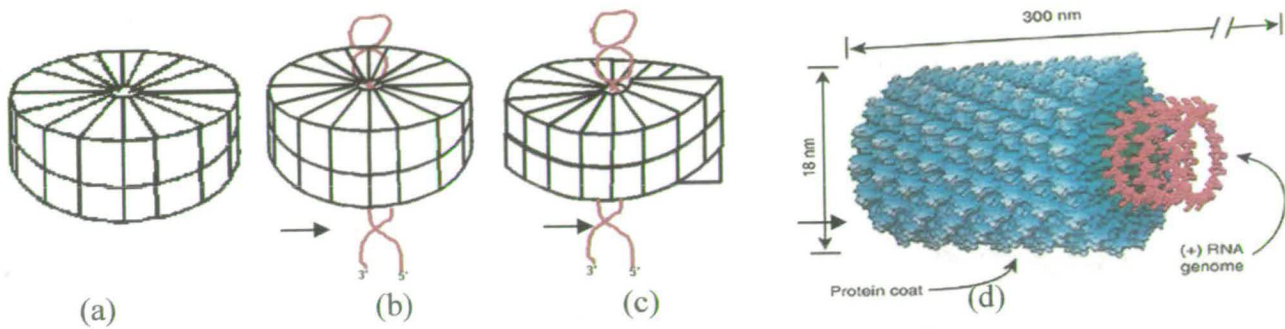


Figure 1: The process of virus assembly can be shown as 4 stages: (a) Assembly of 34 protein units into a two layer disc; (b) binding of a RNA hairpin in between the two layers of the disc causing; (c) a change in configuration to form a short helix; (d) the short helix now presents the RNA in an appropriate orientation for further discs to be bound.⁸

Each identical protein unit possesses a simple set of binding sites which bind initially to the other units in the disc then to the other units in the stack. The viral protein initially (Figure 1) assembles into discs, which successively perform two functions: Firstly recognition of the viral RNA; secondly the, otherwise entropically difficult, assembly of the helical structure.⁹

Binding leads to decrease in degrees of translational, vibrational and rotational freedom of the proteins involved. This leads to a decrease in entropy which is offset slightly by the increase in entropy arising from liberation of water molecules. This positive ($-T\Delta S$) term must be overcome by the exothermic enthalpy of binding (ΔH) for binding to take place. The 4 stages of viral assembly have equilibria associated with them. One single binding event in the formation of a protein disc may have an unfavourable free energy associated with it. However, when all 34 protein segments that make up a disc have associated, the free energy is lower overall for the reasons explained above. Thus each intermediate acts as a thermodynamic sink i.e. enough binding events have taken place to make the intermediates shown in (Figure 1a, b, c, d) stable. The consequence of the thermodynamic nature of binding is that errors are corrected, and assembly is effectively an all or nothing process.

The folding of proteins into their tertiary structure and binding with other proteins and co-factors into their quaternary structure relies upon a number of types of reversible interactions.¹ These include: hydrogen bonds, electrostatic interactions (with or without full charges), solvophobic effects, aromatic π -stacking, van der Waals contacts and disulphide bridges (covalent bonds which are formed reversibly). Avadin is a glycoprotein of unknown function bound into a tetramer by hydrogen bonds, van der Waals forces, and hydrophobic interactions as shown in (Figure 2).

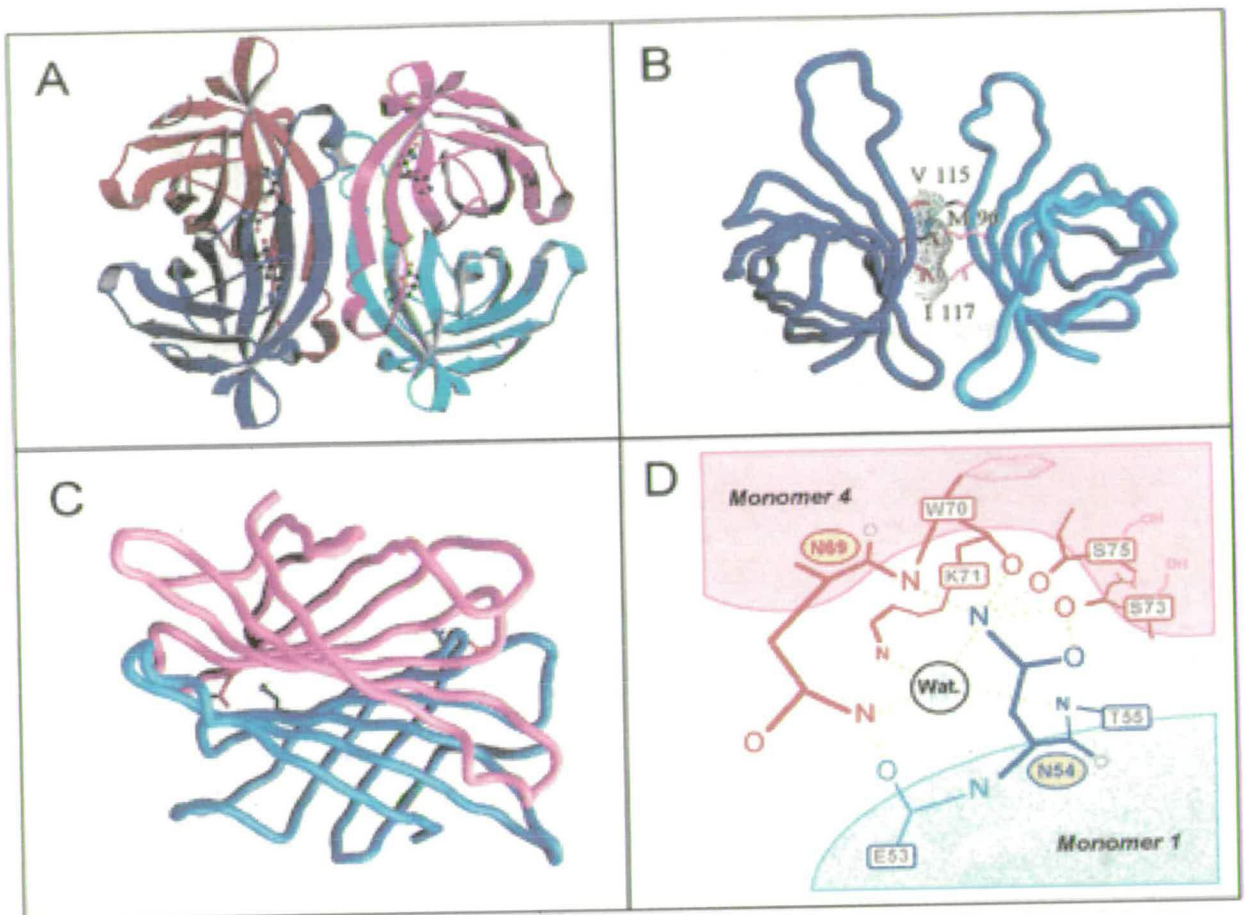


Figure 2: (A) Ribbon diagram of the avidin tetramer. The monomers are colour-coded as follows: 1, light blue; 2, red; 3, dark blue; and 4, magenta. (B), interface between monomers 1 and 3 (the 1-3 interface), consisting of hydrophobic interactions between three identical residues from each monomer indicated by the white mesh. (C) The 1-4 interface emphasizing the large interface between them. Colour-coded side chains of residues Asn-54 (monomer 1, blue) and Asn-69 (monomer 4, red) bind by the hydrogen bonding network including a conserved water molecule shown in (D). The same interaction is duplicated between residues Asn-54 (*Monomer 4*) and Asn-69 (*Monomer 1*) on the other side of the dimer interface.¹⁰

Firstly, the protein is held together by the hydrogen bonding interactions involving glutamic acid, asparagine, threonine, tryptophan, serine and lysine (Figure 2 D). Secondly it is joined by a hydrophobic interaction between the valine, isoleucine and methionine residues shown (Figure 2 B).¹⁰ This example demonstrates the complex hydrogen bonding arrays in proteins and the close control exerted by natural systems upon the positioning of water molecules in hydrogen bonding arrays. Synthetic chemists are only beginning to harness hydrogen bonding in aqueous systems, however the systematic design of hydrogen bonded systems in low polarity solvents is an established field.¹¹

The directionality and specificity of hydrogen bonds as well as types of reversible covalent bond (co-ordinate bonds to boron, metal-ligand interactions) has made them obvious targets in the design of synthetic self-assembling complexes.¹¹ Latterly, hydrophobic effects, aromatic π -stacking and van der Waals contacts have been explored in specifically designed complexes. The development of synthetic enzyme systems containing hydrophobic centres which can allow reactions not usually possible in aqueous media remains a significant challenge for supramolecular chemists.

1.2) The design of hydrogen bonding motifs

The hydrogen bonding surface of a molecule can be described in terms of donor and acceptor sites. The donor sites (D) present a hydrogen atom with partial positive charge to the acceptor site (A) which consists of a lone pair on oxygen, nitrogen or fluorine. The complementary DAD.ADA binding of uracil and 2,6-diaminopyridine exemplifies the principle (Figure 3).

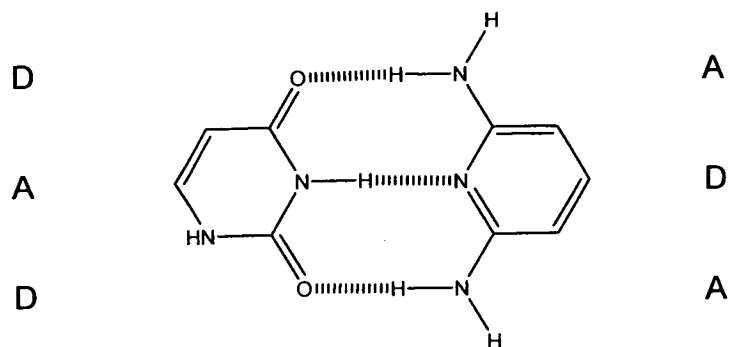


Figure 3: The complementary DAD.ADA binding of uracil and 2,6-diaminopyridine

The binding sites of DNA base pairs and many synthetic analogues are pre-organised similarly to the above uracil - 2,6-diaminopyridine system. This pre-organisation is achieved by the planarity and size matched nature of the molecules. Jorgensen and co-workers¹² hypothesised that the strength of hydrogen bonding between a triply hydrogen bonded complex could be predicted, all other dimensions being equal, by the arrangement of donor and acceptors. The binding of guanine and cytosine (ADD.DAA) and of uracil and 2,6-diaminopyridine (ADA.DAD) were modelled on the basis of their secondary electrostatic interactions as shown in (Figure 4). Experimental discoveries supporting this theory were made by Zimmerman *et al.*¹³

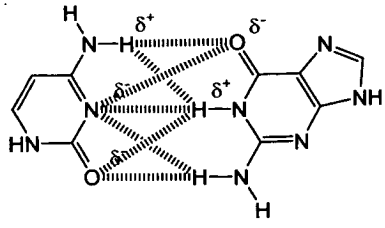
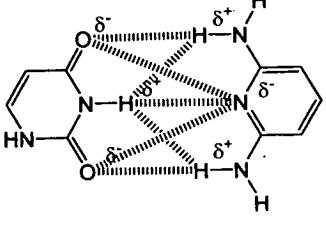
	(a)	(b)
		
Total primary hydrogen bonding interactions	3	3
Total repulsive secondary electrostatic interactions	2	4
Total attractive secondary interactions	2	0
Net effect of secondary electrostatic interactions	neutral	repulsive

Figure 4: A comparison of the binding interactions of (a) guanine with cytosine and (b) uracil with 2,6-diaminopyridine. Negatively polarised hydrogen bond donor atoms are shown with δ^- and positively polarised hydrogen bond accepting protons as δ^+ . The secondary electrostatic interactions are colour coded as shown.

The net effect of the secondary electrostatic interactions is neutral for guanine/ cytosine and repulsive for uracil/ 2,6-diaminopyridine. The guanine/ cytosine base pair is indeed found to have a higher binding constant than that of uracil/ 2,6-diaminopyridine. Similar hydrogen bonded systems have been applied initially to form bimolecular solids such as the cyanuric acid – melamine lattice. Lately much attention has focussed upon polymers formed by or containing hydrogen bonding groups.

1.3) Supramolecular polymers

Supramolecular polymers can be defined as polymers where the individual subunits are connected by non-covalent bonds. There has been much interest in this area as the polymerisation of such materials is, in principle, reversible. Early attempts, by the groups of Griffin and Lehn,¹¹ relied upon 3-centred hydrogen bonds as shown above. Long chain molecules only formed upon controlled crystallisation of the materials. A breakthrough was achieved by Sijbesma, Meijer, and co-workers¹⁴ when they developed a quadruple H-bonded motif based on the dimerisation of 2-ureido-4-pyrimidones.

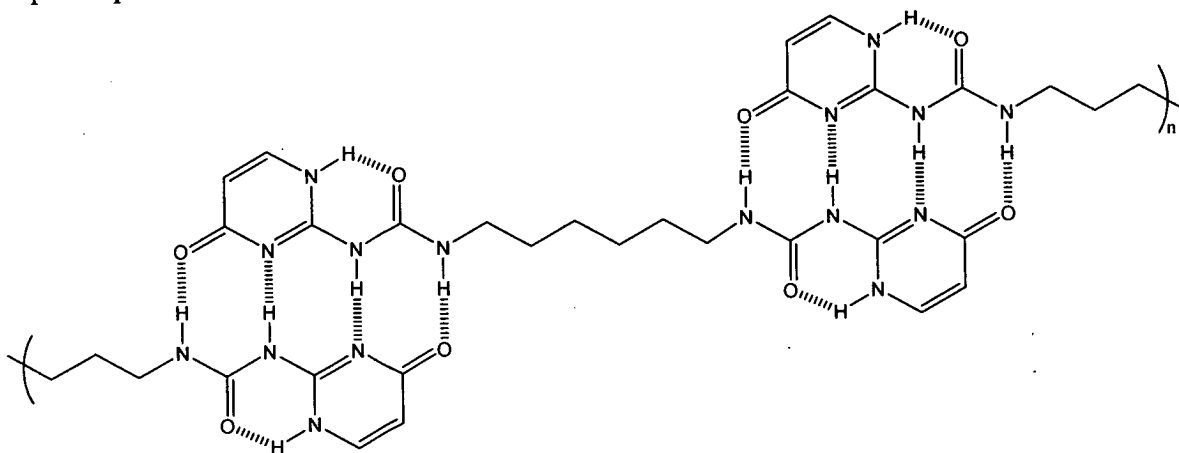


Figure 5: Dimerisation molecules with two 2-ureido-4-pyrimidone units form a supramolecular polymer. The molecules cannot self-associate into macrocycles due to the short length of the alkyl spacer.

The unidirectional design of the binding sites means that only linear polymers are formed by the molecule shown, network polymers have also been demonstrated using trifunctional monomers. As temperature increases or polar solvent is added, chain length decreases which in turn causes a decrease in viscosity. Composition of polymer mixtures is also easily tuneable in a way not possible with covalent polymers. One of the most attractive features of supramolecular polymers is that they can be entirely recyclable without the changes in physical properties observed for covalent polymers. Supramolecular polymers also have self-healing properties.¹⁵

Meijer has subsequently functionalised supramolecular polymers with (*p*-phenylene)vinylene oligomers¹⁶ for use as an electron transport material in solar cells. The well defined nature of oligomers gives them specific electronic and physical properties making them attractive candidates for electronic devices. Polymeric materials, on the other hand offer improved processability and copolymerisation allows material properties to be tuned. The supramolecular polymer allows the properties of oligomers and polymers to be exploited simultaneously.

Ghadiri *et al.*¹⁷ synthesised the supramolecular oligomers shown below. Peptide macrocycles with alternating amino acid stereochemistry interact by way of eight C=O---H-N hydrogen bonds forming supramolecular nanotubes as shown in (Figure 6).

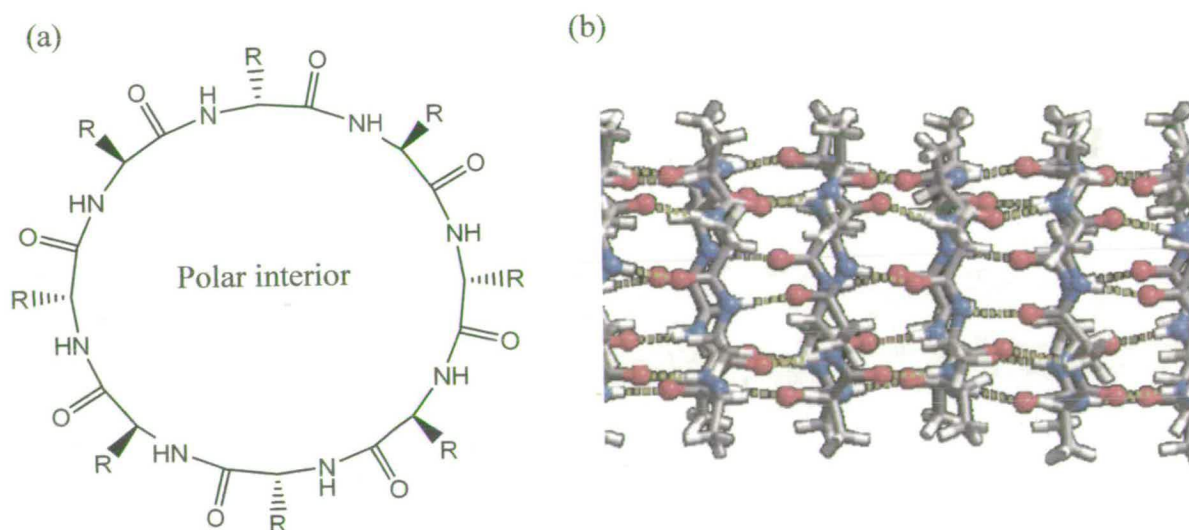


Figure 6 (a): The 12 membered cyclic peptide with alternating amino acid stereochemistry developed by Ghadiri and co-workers. **(b)** The peptide macrocycles form nanotubular assemblies due to C=O---H-N hydrogen bonds. Nitrogen is blue, oxygen red, carbon grey and hydrogen white.

The self-assembled hollow superstructures assemble through the cell membranes of bacterial cells preferentially to those of mammalian cells (Figure 7) causing cell death. If specificity for bacterial cells is improved further, they may find application in antibiotics^{18,19}

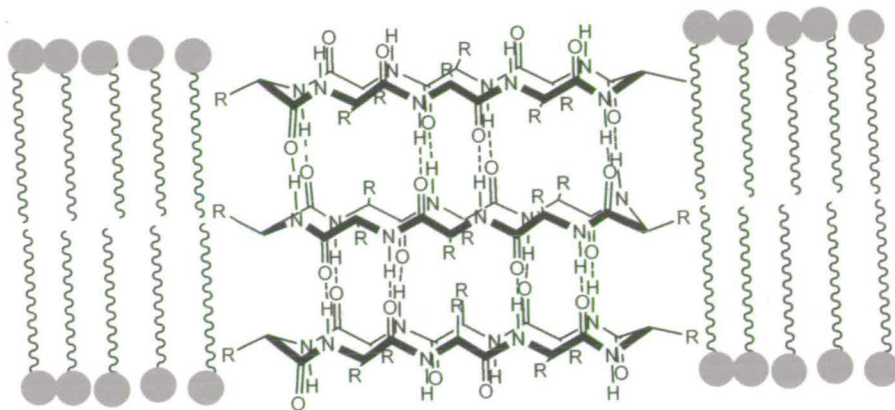


Figure 7: The peptide nanotube intercalates the lipid bilayer which makes up the bacterial cell membrane (polar head groups shown as black circles, hydrophobic chains shown as wavy lines).

Analogously to the self-assembly of TMV, the thermodynamic nature of the binding of Ghadiri's peptide antibiotic has a number of advantages over more traditional membrane-disrupting agents. The nanotubes have been shown to form in a number of different configurations and to pierce the cell membrane in different orientations due to the dynamics of self-assembly. This makes it very difficult for bacteria to become resistant given the number of possibilities the peptide has for attack. The process of peptide self-assembly is intrinsically error checking, as poorly formed nanotubes will not template tube extension as effectively as well formed ones.

The Ghadiri peptide was designed with slightly different factors in mind to the previous hydrogen bonding groups described. In the configuration shown in Figure 7, the peptide macrocycle is presenting a DADADADA surface downwards and could be said to present an ADADADAD surface upwards. The amino acid side chains point outwards adopting equatorial positions to reduce 1,4 diaxial interactions (Figure 8). This allows the peptides to adopt the correct orientation to bind due to their alternating stereochemistry. Additionally, if a second amino acid residue is bound to either the C=O or N-H of a certain amino acid residue this will increase the strength of the next binding interaction that particular residue makes on the unbound side (the N-H or C=O

respectively). This cooperativity effect is due to the electrostatic and organisational effect of the hydrogen bonds formed.

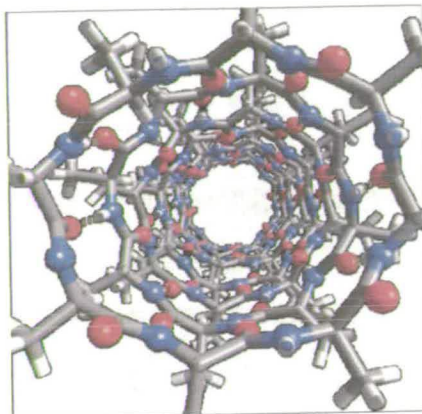


Figure 8: Molecular model showing the octa(alanine) form of the cyclic peptide; the alternating stereochemistry causing the methyl side chains to point outwards in equatorial positions.

Biesalski²⁰ has demonstrated that the Ghadiri peptide nanotubes can be taken from the dynamic equilibrium environment and frozen by polymerisation as macromolecular nanotubes (Figure 9). Polymerisation of self-organised structures, formed under thermodynamic control, under a particular set of conditions is a technique common in many areas of organic materials chemistry. It allows a structure to be kinetically trapped to increase durability of the material within a device or application or allow further processing steps to take place. In this case the peptide nanotubes are continually dissociating and re-forming in solution, polymerisation gives them the robustness required for applications such as drug delivery devices.

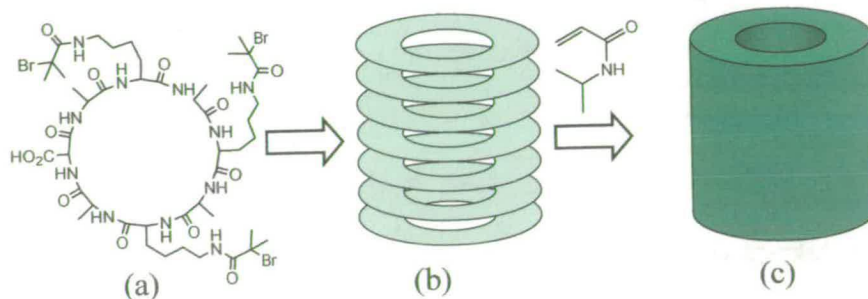


Figure 9 (a) The modified peptide macrocycle forms self-assembled nanotubes **(b)**, represented as green rings. These are functionalised with initiating groups such that addition of *N*-Isopropylacrylamide in aqueous dispersion causes polymerisation to form **(c)** a novel class of macromolecule (depicted as a green cylinder).

The hybrid peptide-polymer nanotubes (Figure 9c) can be tailored in their surface properties by use of different polymer side chains and R groups. The interior of the tubes could be tailored to accommodate pharmaceutical agents. The slow metabolism of the nanotube *in vivo* would release the drug in a controlled fashion. This has the potential to allow lower doses, a reduction in side effects and improved treatment.¹⁸

1.4) Reversible binding for sensing applications

Bertozzi *et al.* have formed sensing polymers with diacetylene molecules, functionalised with two long alkyl chains, one bearing a terminal carboxylate group and the other a peptide group.²¹ The molecules are self-assembled by dissolution in aqueous NaCl solution followed by cooling. The supramolecular aggregates formed (by hydrophobic, electrostatic and hydrogen bonding interactions) are irradiated with UV light to induce polymerisation. The resulting unsaturated polymer has a UV spectrum related to its coordination length: i.e. the higher the average number of vinylene units in one plane, the lower the absorption frequency. Changes in conditions (temperature, pH, bound biomolecules etc.) lead to changes in polymer morphology and co-ordination length, which is expressed as a colour change. This makes the materials applicable to biological sensing applications.

Higgins *et al.* demonstrated a similar effect with a conducting polyalkylthiophene grafted with biotin molecules²². In tetrameric glycoprotein avidin¹⁰ (Figure 2), each subunit bears a non-covalent binding site for biotin (Figure 10) with an exceedingly high association constant $K_a = 10^{15} \text{ M}^{-1}$. Binding of avidin to the polymer side chains leads to changes in polymer morphology and co-ordination length. This was detected as a change in electrochemical behaviour and resistance in the polymer, and has been extended to solid state devices. The strength of the binding is dictated by the large number of hydrogen bonding interactions between biotin and the residues shown (Figure 10).

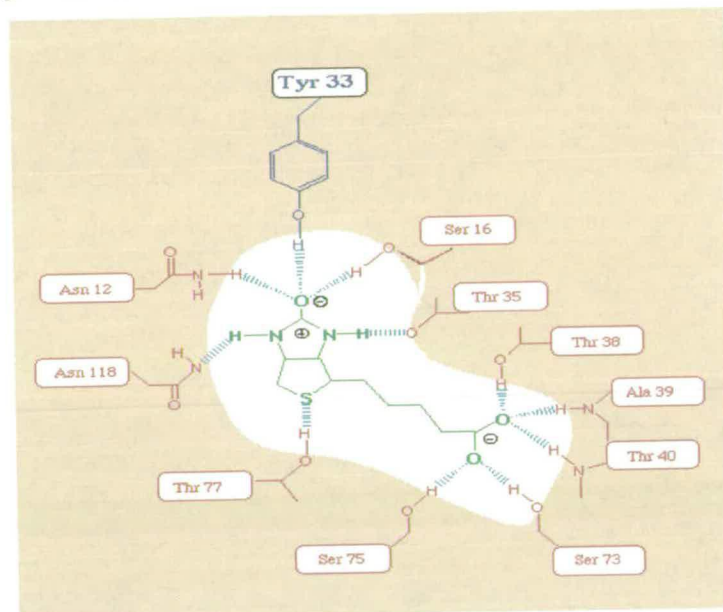


Figure 10: The binding site of biotin in avidin

1.5) Dendritic self-assembled systems

A dendrimer is a macromolecule with a regular branched structure, they are often characterised according to the number of generations of repeating branch unit employed. Cyclic dendrimers with high orders of symmetry are somewhat difficult to prepare given the large number of bonds which have to be formed from a cyclic core. Zimmerman *et al.*²³ have shown how hydrogen bonding recognition units can be used to access libraries of interesting centrosymmetric dendrimers.

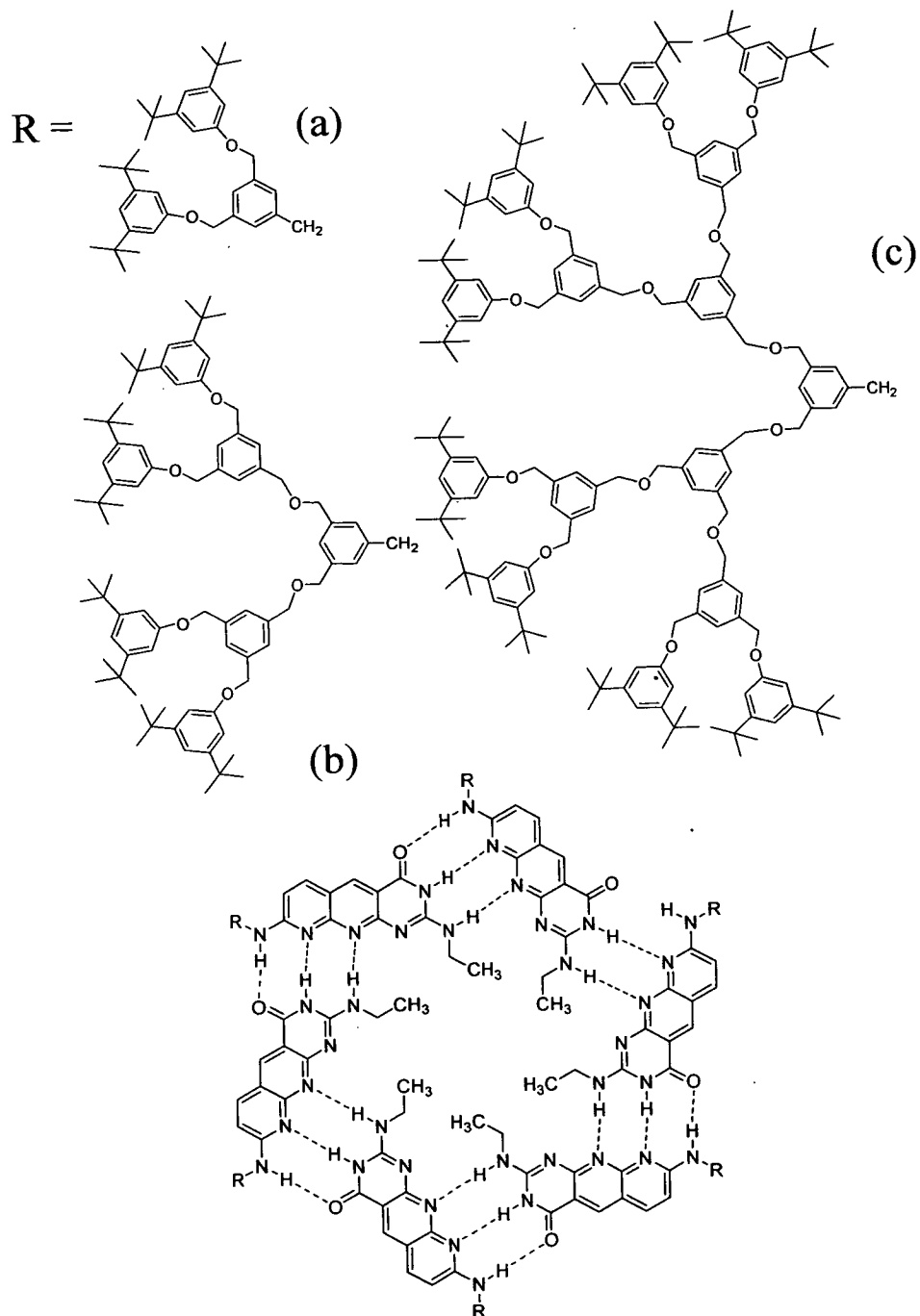


Figure 11: The naphthyridine derivative (below) forms a C_6 symmetric planar aggregate bearing dendron R groups a, b, or c (above).²³

The hydrogen bonded assembly (Figure 11) brings together six dendron groups chosen from (a)-(d). Much of the work on such compounds consists of a search for novel properties and macroscopic organisation. In this context it is interesting to note that the formation of monodisperse dendrimers containing mixed dendrons can be achieved in some cases. Steric effects dictate that when a 1:1 mixture of naphthyridine derivatised with R groups (a) and (c) respectively is allowed to equilibrate in solution; the main product consists of a hexameric dendrimer with alternating large and small dendrons with C_3 symmetry. These directing effects could be used to create libraries of dendrimer formulations to test for novel properties.

1.6) Self organised systems: Discotic liquid crystals

1.6.1) Definition

Thermotropic liquid crystals are defined as organic materials exhibiting states of molecular order intermediate between a liquid and a solid over a specific temperature range. Discotic liquid crystals are a sub-class of these materials, composed of disc-like molecules.²⁴ Molecules forming discotic liquid crystalline phases have radial anisotropy: i.e. the centres of the molecules have different properties to the peripheries, as shown by the three examples (Figure 12). Other shapes of molecules can also form columnar phases, including shuttlecocks,²⁵ bananas²⁶, wedges.²⁷

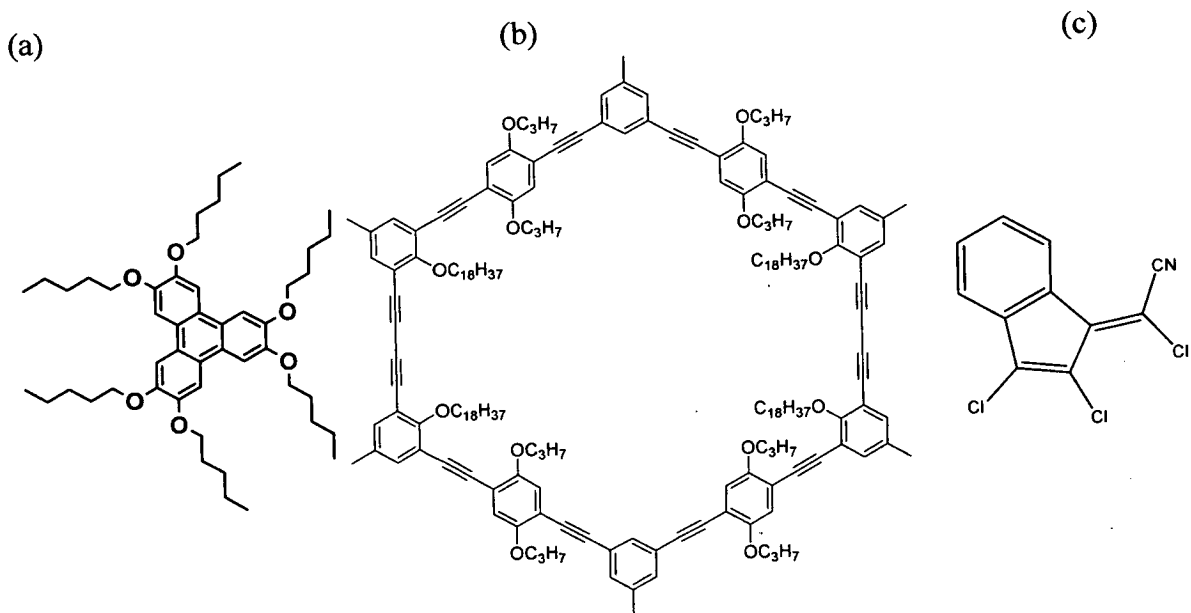


Figure 12: Three molecules which form discotic liquid crystal phases²⁸ (a) The classical aromatic core with aliphatic corona; (b) A shape-persistent macrocyclic corona filled with aliphatic chains;²⁹ (c) It was suggested that the soft polarisable chlorine and cyanide moieties act in a similar way to the soft aliphatic components of more conventional discotics. Hence a discotic phase is formed as the interactions between these parts of the molecule loosen upon heating before the π -stacking interactions between the aromatic rings.³⁰

1.6.2) Types of columnar packing

Molecules with planar sometimes polar cores and flexible aliphatic coronas (Figure 12a) were discovered first have been researched most thoroughly.³¹ The common mesophases exhibited by discotic liquid crystals are shown below (Figure 13). The nematic phase consists of molecules with similar orientation but no order in the other two dimensions. This phase is not easily obtained but has been applied to give dramatic improvements in the non-linear optical coatings on flat-panel displays, allowing obtuse viewing angles.³²

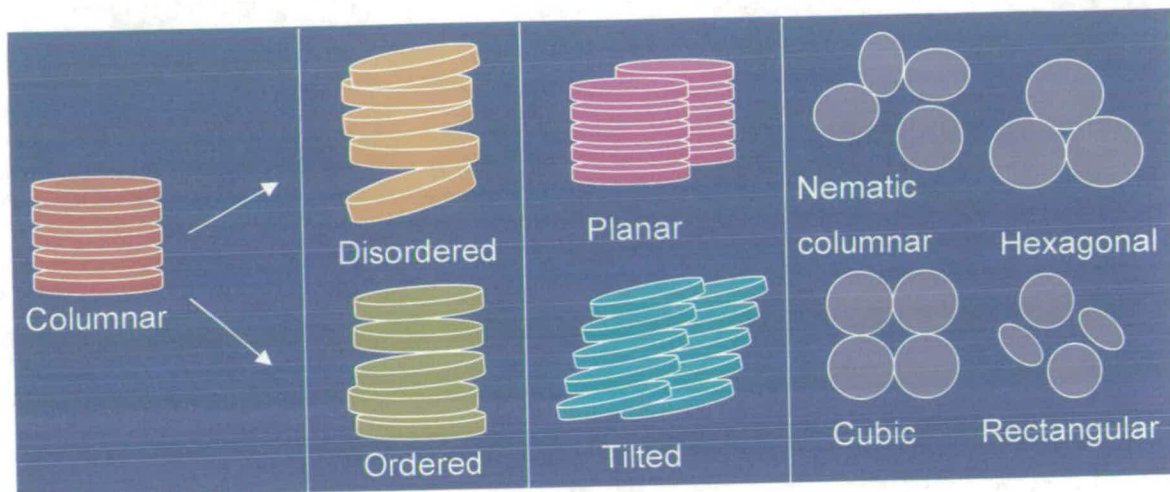


Figure 13: Schematic representation of the common columnar mesophases displayed by liquid crystals. The table is read from left to right, columns can be either disordered or ordered and tilted or planar. The columns can then pack into various arrays including those shown.

Disc-like molecules shown as coloured cylinders (Figure 13) stack into columnar phases as shown. Order in columnar discotic liquid crystal phases refers to the degree of planarity of a layer of molecules. When the centre of mass of a molecule is, on average, in a layer for more time than it is not, the columnar phase is described as ordered.²⁸ The columnar hexagonal ordered or disordered phases are very common and had not been considered to have applications, until the burgeoning interest in nanostructured materials came about.^{5, 33}

1.6.3) Properties of the hexagonal columnar phase required for novel applications

Key to the application of discotic liquid crystals in optoelectronic devices is their alignment on surfaces.³⁴ Ordered hexagonal arrays can be formed, which could transport electrons or store data in a vertical sense. Alternatively alignment perpendicular to the surface could lead to conduction across a surface for application in thin film transistors. Discotic liquid crystals of extended aromatic molecules such as the hexabenzocoronene derivative (Figure 14) can actually show greater π -orbital overlap than their crystalline counterparts. Müllen *et al.*, have systematically tailored the properties of these extended

aromatic systems to allow facile alignment on surfaces.³⁵ Surprisingly, compared to *n*-octanyl side chains, 3,7-dimethyloctanyl side chains cause marked changes in properties liquid crystal properties. Solubility increased and melting points decreased markedly allowing processing at easily accessible temperatures.

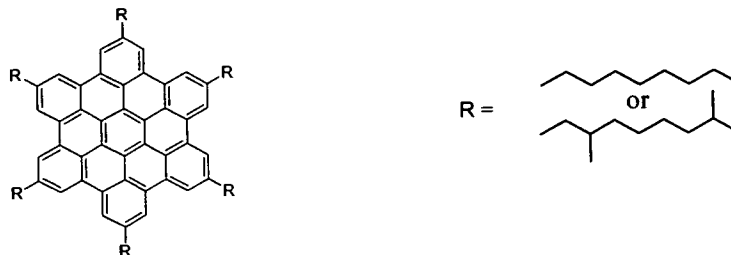


Figure 14: The hexabenzocoronene derivatives developed by Müllen *et al.* The 3-methyl substituent was, in some cases introduced as a single enantiomer.

Various design features and deposition techniques have been developed,³⁶ aiming for alignment of discotic liquid crystals parallel or perpendicular to the surface. Parallel or homeotopic alignment is reviewed here as it is more relevant to the research project.

1.6.4) Designation of phase and alignment by microscopy

The most common method for observation of the alignment behaviour of liquid crystals is polarised optical microscopy.²⁸ Liquid crystals generally exhibit birefringence i.e. the plane of plane polarised light is rotated when passing through the sample. This rotation is caused by one component of the light wave experiencing a different refractive index to the other, as it passes through the sample. This optical anisotropy is common to all crystals and liquid crystals which do not belong to a particular set of high symmetry space groups. If the light passes parallel or perpendicular to the optical axis of the material (with often corresponds to the direction of the stacks of discs) no birefringence is observed. The material then appears dark under crossed polarisers. A dendritic texture in these dark areas is characteristic of aligned columnar phases. If the dendritic domains are hexagonal in shape, this is a manifestation of hexagonal columnar packing.³⁷

1.6.5) Theories on the growth of aligned domains in columnar mesophases

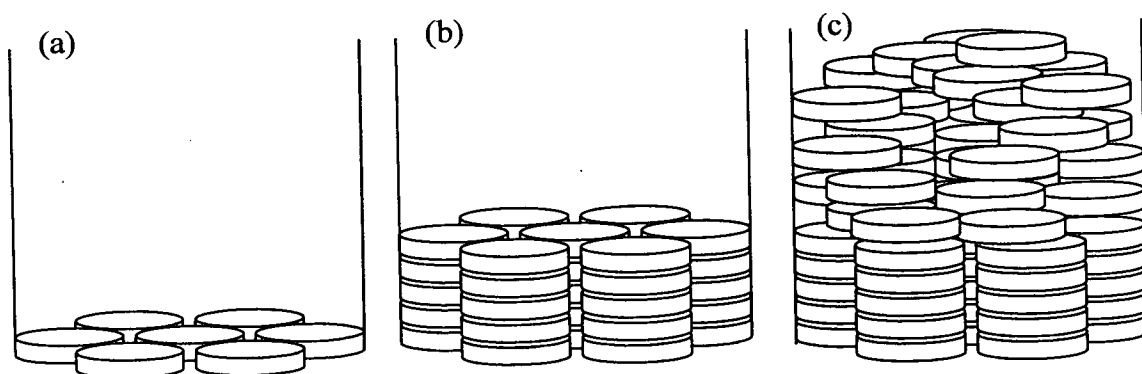


Figure 15: The first layer of discotic mesogens can assemble parallel to the surface (a). This can then assemble a thin layer of homeotropically aligned discs (b). A point arises (c) whereby no further alignment of the film takes place.

The alignment of the initial monolayer (Figure 15 a) on polar oxide surfaces can be made more likely by connecting the periphery of the core unit with heteroatoms. These interact with substrates such as indium tin oxide (ITO) and silica, holding the molecule to the surface.³⁸ Indium tin oxide is a useful material as it is both conducting and transparent and has been applied successfully in many types of electro-optical device.³⁹ Most work on liquid crystal alignment uses thick films sheered by pressure from a second glass slide.⁴⁰

Kato has demonstrated a similar surface anchoring principle for a type of columnar ionic liquid crystal sandwiched between ITO-coated slides. Initial results⁴¹ suggest that the ionic liquid crystal aligned heterogeneously (with domains pointing in all directions except the desired vertical). Functionalisation of the ITO surface with (3-aminopropyl)triethoxysilane led to a change in the orientation of alignment to homeotropic.⁴²

It has been shown that, in sufficiently thin films, a range of discotic columns can be made to stack vertically, parallel to the surface, by cooling directly from the liquid phase on carbon⁴³ or silicon⁴⁴ substrates. This observation suggests that the first layer of

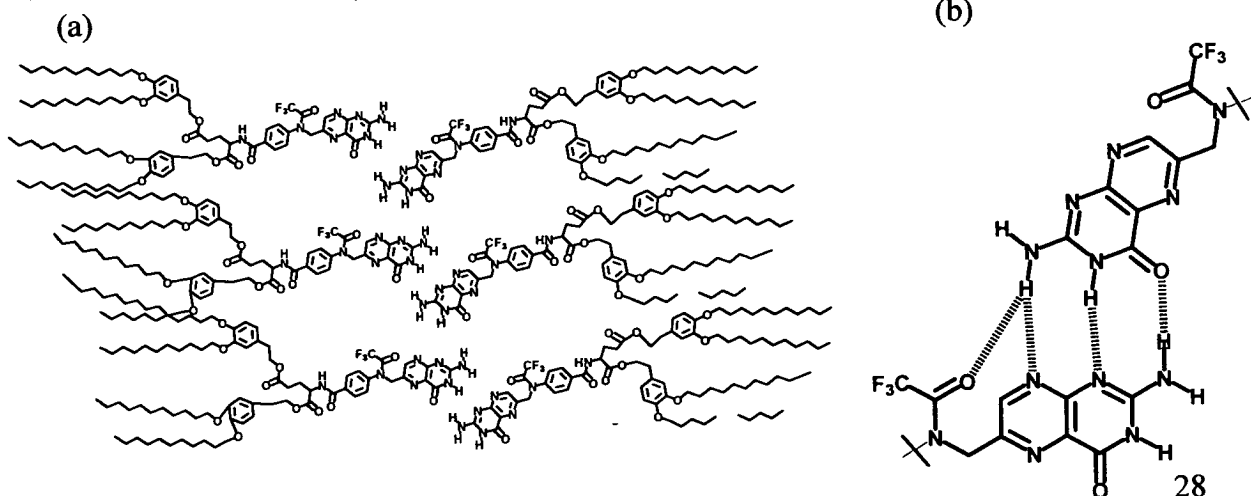
molecules templates the assembly of each stack (Figure 15a). Random nucleation at the air interface produces defects in thicker films (Figure 15c). Bock and co-workers modelled this process and found that for each material there was an optimal film thickness and cooling rate to allow homeotropic domains to grow.⁴⁴ However other research groups have indicated that the air interface hinders this process, Bushby and co-workers have even used the surface of a discotic film as a gas sensor.⁴⁵ It was recently demonstrated that thin films could be sandwiched in a cell uniformly to aid alignment, as for thick films, this research is reviewed in the future work section.⁴⁶

Many interesting charge transport materials are accessible from the covalent discotic liquid crystals described above using the bulk properties of the phase.⁴⁷ It is however difficult to use the ordered arrays formed by traditional discotic liquid crystals to template arrays of species for other applications. Were the core segment of the liquid crystal removable by some means, this would template a nanoporous scaffold. Such a scaffold could, for example, be decorated with nanoscale sensing apparatus.

1.7) Supramolecular Columnar Liquid Crystals

1.7.1) Exploiting complimentary hydrogen bonding interactions

Supramolecular discotic liquid crystals are a relatively new class of materials whereby the disc-shaped molecule to form the liquid crystal phase is made up of self-assembled components.⁴⁸ The following example, (Figure 16) developed by Kato,⁴⁹ displays the dynamic nature of a hydrogen bonded liquid crystal, analogous to the aforementioned Zimmerman dendrimer system.



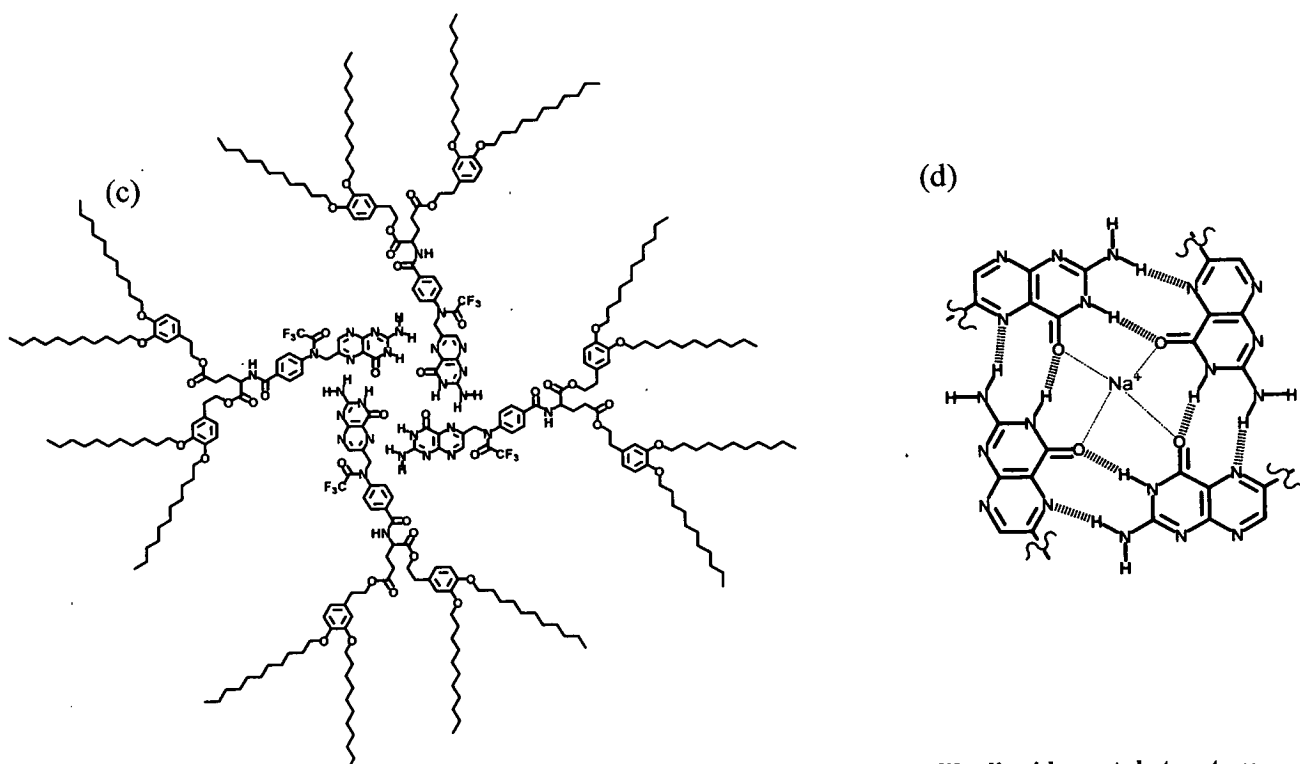
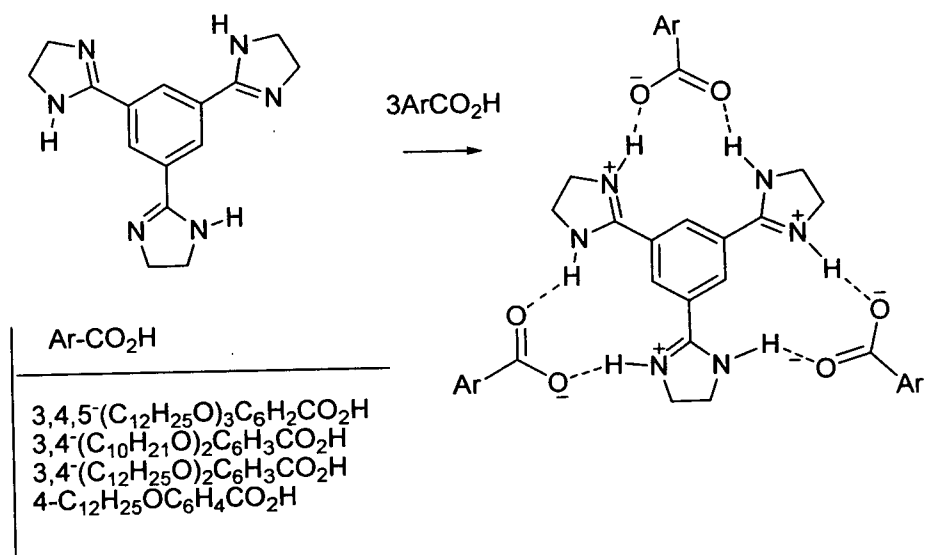


Figure 16: The folic acid derivative shown normally exhibits the ribbon-like liquid crystal structure shown (a) bound by the complementary hydrogen bonding array shown (b). On addition of a nonpolar solvent or of inorganic salt $\text{NaOSO}_2\text{CF}_3$ the hydrogen bonding pattern changes to (d) - a cyclic tetramer which forms a disc-like assembly (c). When $\text{NaOSO}_2\text{CF}_3$ is added to the liquid crystal, Na^+ is bound in a coordination sphere at the centre of the stack.

The folic acid derivatives (Figure 16a) normally exist as a ribbon-like liquid crystalline phase, due to the two strong DDDA.AAD hydrogen bonding interactions (Figure 16 b) by which each molecule is bound. Solvophobic effects or ion complexation drive the polar hydrogen bonding headgroups to become enclosed into the macrocycle shown (Figure 16c). In this configuration each molecule is bound by two weaker complementary DD.AA hydrogen bonding interactions (Figure 16d).

Kraft *et al*⁵⁰ have reported a core template and have prepared a variety of benzoic acid derivatives which bind to it in a 1:3 ratio. The structure-property relationships of the discotic liquid crystals formed have then been tested.



Scheme 1: The supramolecular discotic liquid crystals reported by Kraft and co-workers. Benzoic acid derivatives with three, two and one dodecyloxy substituents respectively, as well as one bearing two decyloxy chains were prepared as shown in the table.

Corona segments bearing one, two and three alkyl chains (Scheme 1:) were formed into liquid crystalline complexes. It was found that at least two alkyl chains were required for hexagonal phase formation. The mesophase with the lowest enthalpy change with respect to the crystalline phase was the one with three alkyl chains. This indicates that the trialkoxy benzoic acid corona likely forms the most ordered mesophase.²⁸ This measure also indicates that, for this system, decyl chains form more ordered liquid crystals than dodecyl ones.

The complex containing 3,4-didecyloxybenzoic acid formed dendritic domains upon cooling from the isotropic liquid. This indicates homeotropic alignment as discussed in section 1.6.

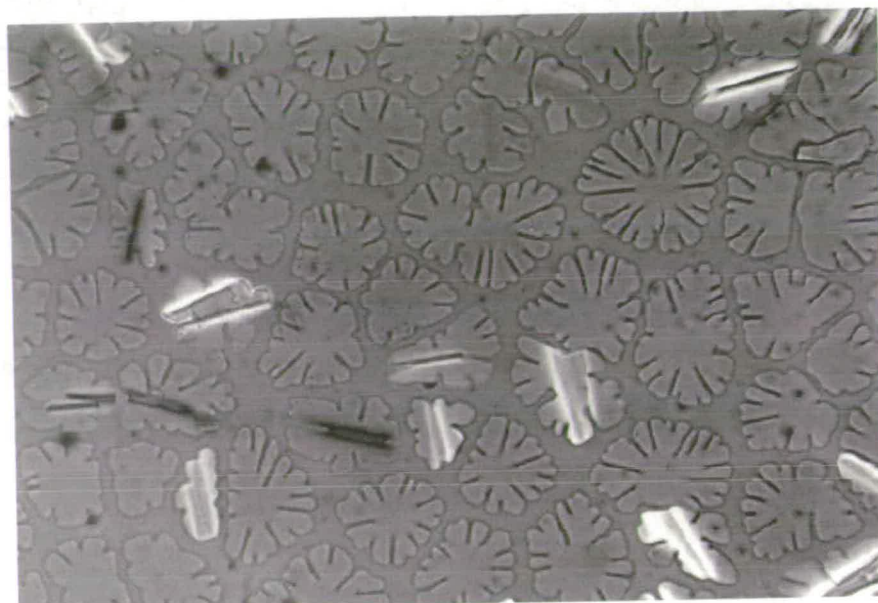


Figure 17: Reproduced from reference 50, dendritic homeotropic domains formed by the supramolecular discotic liquid crystals synthesised by Kraft and co-workers (Scheme 1). Under near to crossed polarisers, no scale given.

1.7.2) Thermal decomposition of supramolecular liquid crystals

Jho and co-workers⁵¹ synthesised series of discotic liquid crystals formed by simple hydrogen bonding between phloroglucinol core and alkoxy stilbazole peripheral units. Interestingly, they demonstrated the decomposition of the hydrogen bonds upon heating in the isotropic phase by following the disappearance of a band in the IR spectrum. This indicated that the liquid crystal phase was helping to stabilise the hydrogen bonds. If this holds true for all such self-assembled systems, the discs must re-associate before a mesophase can develop.

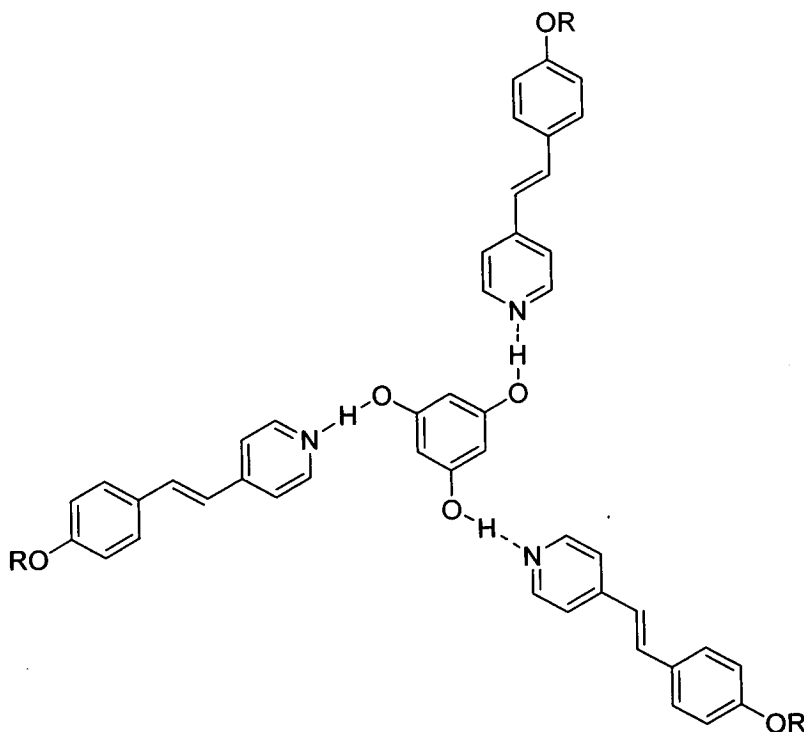


Figure 18: Phloroglucinol core and alkoxy stilbazole peripheral units developed by Bruce and co-workers.

Reinhoudt and co-workers have recently demonstrated a very thermally stable supramolecular mesogen. This double-rosette molecular box made use of the strong, three centred, binding between melamine moieties and barbituric or cyanuric acid residues.⁵²

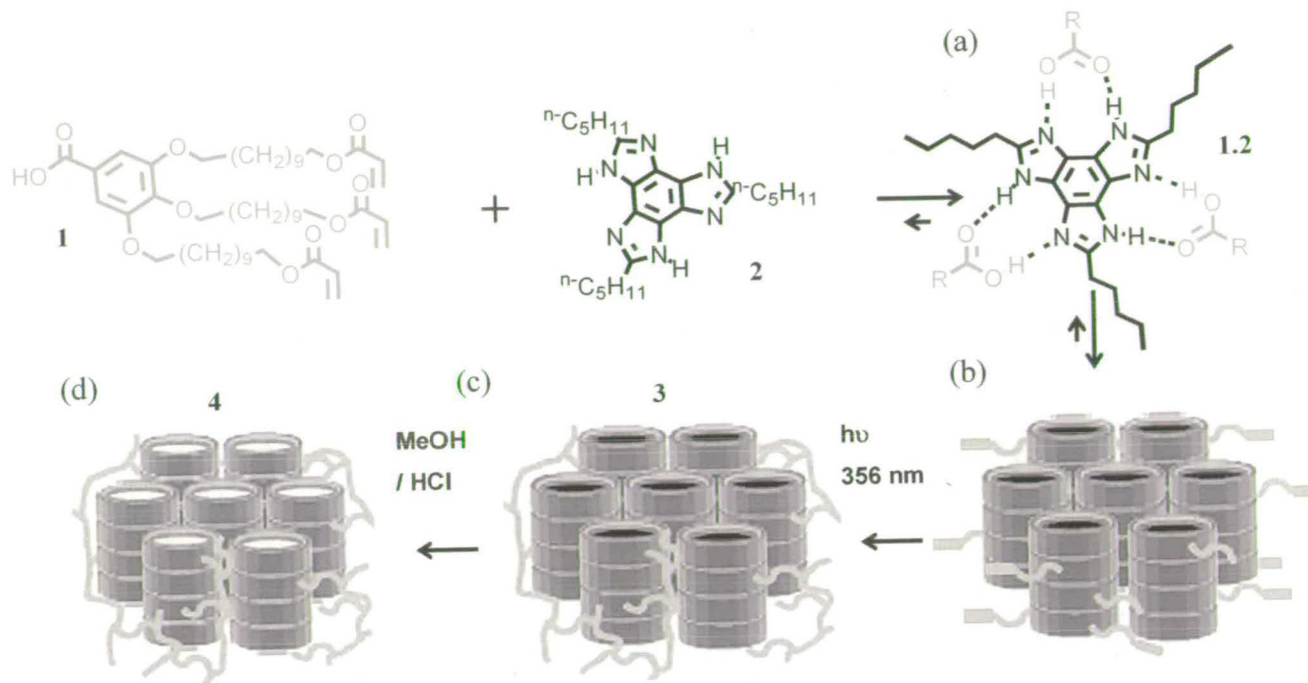
1.7.3) Other types of supramolecular columnar liquid crystals

The interactions exploited for the construction of such liquid crystalline disks are not limited to complimentary hydrogen bonds. Sessler and co-workers⁵³ have demonstrated that an expanded porphyrin salt forms discotic liquid crystals, only after absorbing electron deficient aromatic molecules such as trinitrotoluene. The small aromatic molecule sits at the centre of the porphyrin, held in place by a combination of donor-acceptor interactions and weak hydrogen bonds to sulphate anions. Percec has demonstrated that fluorophobic effects can be used to form highly ordered columnar phases.^{27, 54} “Halogen bonding” between an aromatic iodide and a pyridine residue has recently been exploited by Xu, He and co-workers for the construction of a smectic liquid crystalline complex.⁵⁵

1.8) From Self-Assembled Discotics to Functional Nanoporous Membranes

Kim and co-workers⁵⁶ first introduced one of the paradigms upon which this project is based. This involves the assembly of a discotic liquid crystal, around a central core unit using reversible hydrogen bonds (Scheme 2). A 1:3 mixture of the benzotri(imidazole) core **2** and trialkoxybenzoic acid derivative **1** is dissolved in chloroform, stirred and evaporated twice to yield the liquid crystalline complex **1.2** (Scheme 2) in quantitative yield. This is then annealed between glass plates to forming a hexagonal columnar liquid crystalline phase .

Analogously to Biesalski's polymeric modification of Ghadiri's peptide nanotubes (Figure 9), it is possible to lock the discotic liquid crystal in its ordered mesophase by polymerisation to form **3**. Initiators are commonly used to polymerise acrylate-functionalised liquid crystals. Kim chose however to crosslink complex **1.2** without the presence of initiator, presumably to avoid possible effects upon supramolecular binding or liquid crystal formation. Following polymerisation, core segment **2** can be washed away from polymer **3** by overcoming the hydrogen bonding interactions with a polar solvent and acidic condition, providing the nanoporous membrane **4**. Polymer **3** is insoluble not due to its composition but because it is a highly crosslinked network polymer.



Scheme 2: The formation of a nanoporous polymer array is described. (a) The assembly of three trialkoxybenzoic acid derivatives (1) around a benzotri(imidazole) core 2. (b) A columnar hexagonal phase is formed by complex 1.2 as in Figure 15. (c) The liquid crystal assembly is irradiated with U.V. light, activating the polymerising groups to form polymer matrix 3. The polymerised sheet is then peeled from the substrate for the next stage. (d) The basic core segments are washed away by protonation with acid and use of a hydrogen-bonding competitive solvent such as methanol to form nanoporous polymer 4.

The material was characterised by powder X-ray diffraction using synchrotron radiation showing [100] and [110] reflections with the appropriate reciprocal spacing ratio for a hexagonal lattice.

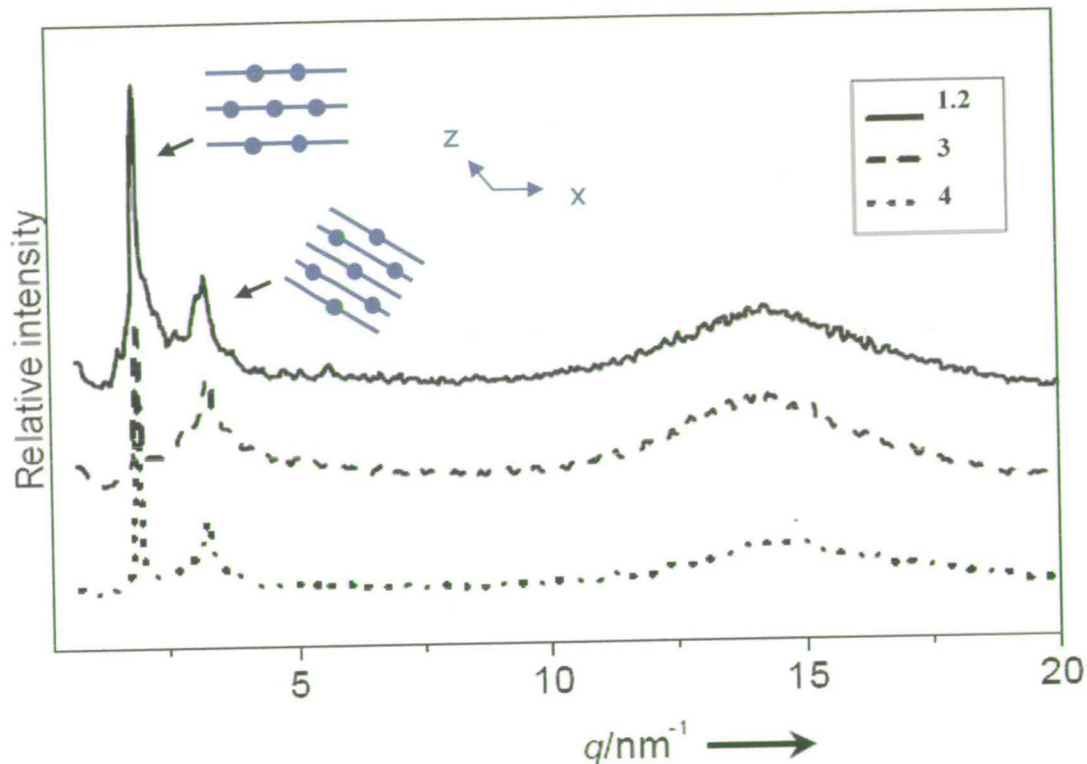


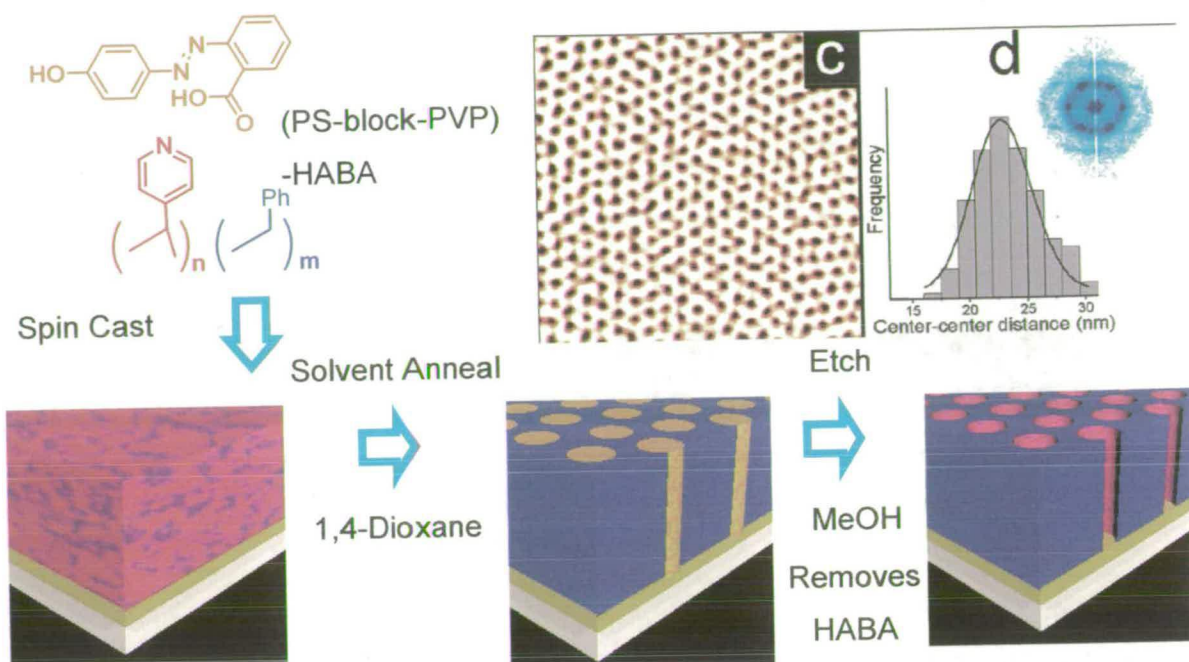
Figure 19: X-ray data for complex 1.2, polymer 3 and membrane 4 taken from reference 56

A similar functional nanoporous membrane was powderised to create a heterogeneous acidic catalyst and showed superior turnover numbers to comparable resins.⁵⁷ This is due to high density of carboxylate groups and the high porosity of the polymer. 4

1.9) Fabrication of Nanoporous Scaffold

Amphiphilic copolymers polymers can be applied to the formation of nanoporous scaffolds A scaffold in this context is distinguished from the membranes synthesised by Kim and co-workers⁵⁶ in that it is on a surface.

In the recent example (Scheme 3), Minko and co-workers⁵⁸ used a polystyrene-polyvinylpyridine co-polymer swelled with a hydrogen bonding donor, hydroxyazobenzoic acid (HABA).



Scheme 3: Formation of nanoporous scaffold from a Polystyrene-Polyvinylpyridine copolymer, doped with the azo dye hydrogen bonding donor shown. The mixture is spin cast and subjected to solvent annealing. Etching with a non-polar solvent reveals pores of 8 nm diameter (see AFM labelled C, width scale = 500 nm). Fast fourier transform plot of the AFM is labelled d shown with a histogram of centre to centre distances, reproduced from reference⁵⁸.

The nanoporous scaffold formed was applied as a template for the formation of nickel nanodots by electrodeposition. Data storage had previously been demonstrated by Russell and co-workers by electrodeposition of cobalt in a similar block-copolymer system.⁵⁹ Dai and co-workers have additionally demonstrated the carbonisation of a nanoporous film formed similarly.⁶⁰

Lee and co-workers⁶¹ showed that pentaphenylene rods connected via an ester linkage to a poly(propylene oxide) chain formed a supramolecular crystalline sheet with an ordered nanopore array, the pores being filled with the phase-separated polar polymer chain. The water soluble polymer is removable by base mediated ester hydrolysis, leaving the crystalline nanoporous sheet now bearing carboxylate groups.

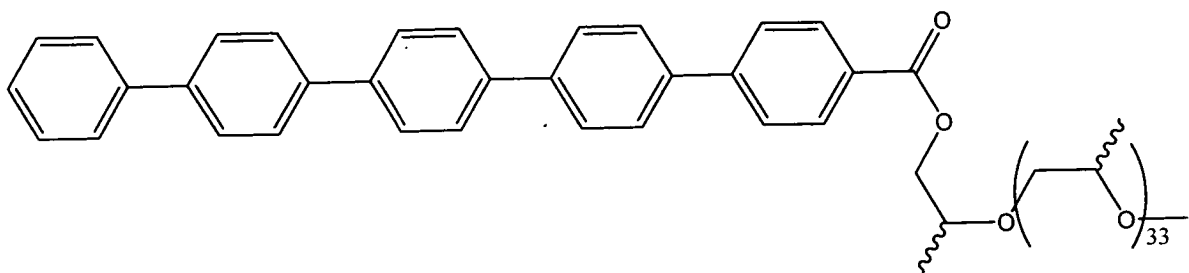


Figure 20: The rod (left) and coil (right) molecule designed by Lee and co-workers

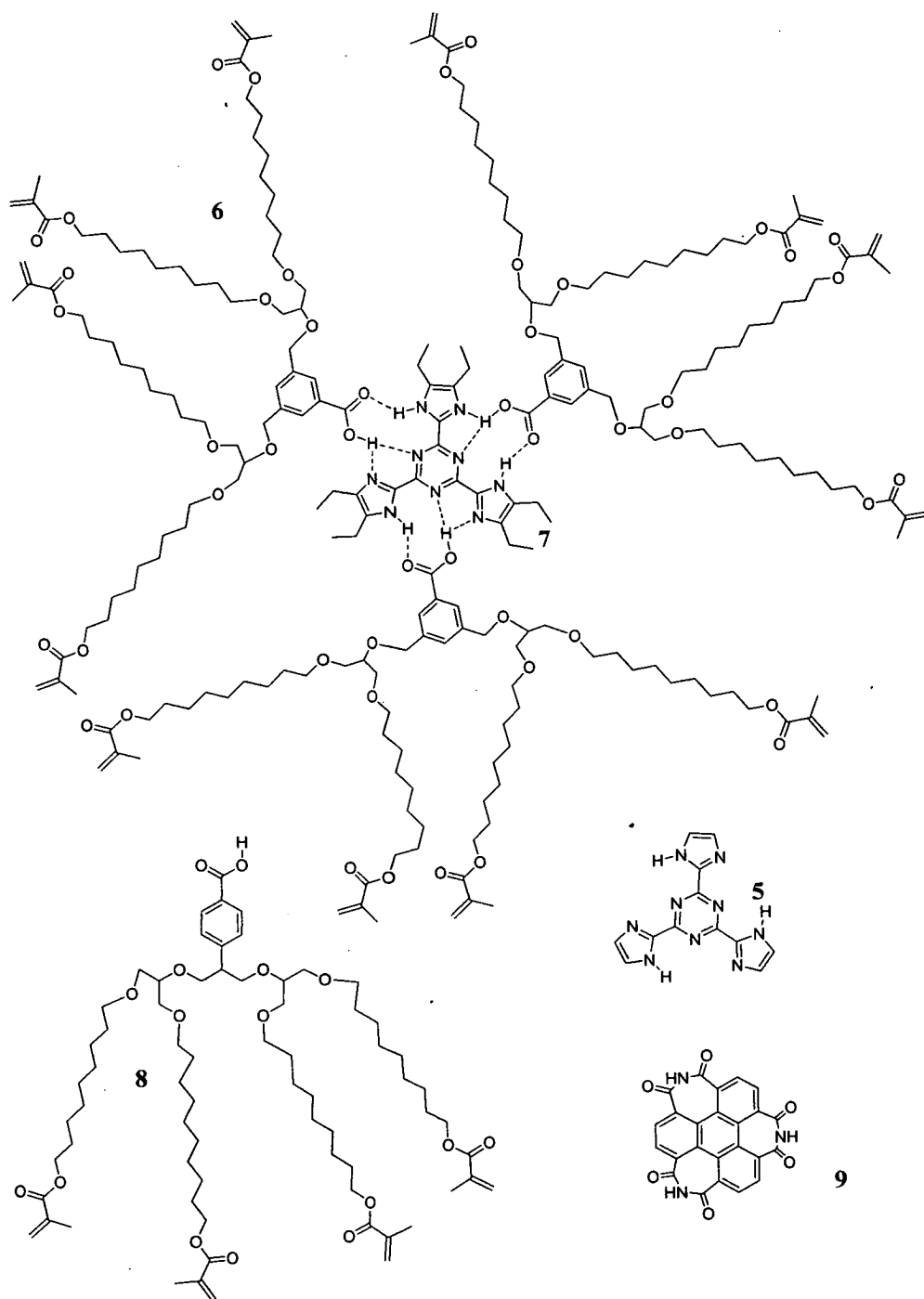
Block-copolymer lithography gives access pore sizes from 8 nm.⁶² The application of supramolecular discotic liquid crystals in these porous templates will fill a gap in the sizes of pore possible (1-5 nm).

2) Towards the Synthesis of an Entirely New Supramolecular Discotic Mesogen

2.1) Aims and strategy

The initial of this project was the synthesis of an entirely new supramolecular discotic liquid crystal mesogen. To increase liquid crystalline order, the number of aliphatic chains per corona unit was increased from 3 to 4 (comparing to complex 1.2). To increase binding strength and robustness, new binding motifs were envisaged. The polymerisable group was also changed to form a more robust polymer matrix. In order to realise a supramolecular liquid crystal with the required characteristics, novel architectures were carefully designed.

The cores and coronas designed are shown in (Scheme 4) below. In the first design C_3 symmetric trisimidazolyltriazine core **5** or **7** is surrounded by 3 equivalents of benzoic acid derivatives **6** or **8** with novel substitution patterns. Secondly, triimide supramolecular synthon **9** was designed, incorporating an ADA hydrogen bonding motif inspired by uracil (Figure 3, p 14).



Scheme 4: Diagram showing the proposed supramolecules. Benzoic acid derived corona 6 is shown binding to tris(imidazolyl)triazine core 7 by hydrogen bonding interactions. This interaction would be replicated for any 1:3 complex of the cores 5 and 7 with coronas 6 and 8 shown. Tri-imide core 9 was investigated as a separate synthon for supramolecular liquid crystals.

2.2) Design of benzoic acid corona units for supramolecular discotic liquid crystal

Benzoic acid groups present DA hydrogen bonding site upon one, uncomplicated and versatile functional group. They have the added advantage of a possible co-operative effect whereby the basic hydrogen bond donor site on the core unit is protonated by the acid. The positively charged heterocycle now effectively acts as a DD site, complementary to the negatively charged AA site of the carboxylate group. This motif is depicted for the Kraft system (Scheme 1: p 30). As well as reducing secondary repulsive interactions (as explained in Figure 4, p 15) there is an electrostatic attraction between the positive and negative charges on core and corona.

Kraft showed that increasing the number of aliphatic chains increased order in the liquid crystalline phase. We therefore designed novel systems with four aliphatic chains in the belief that this would further stabilise the liquid crystalline phase. The polymer formed should be robust as four methacrylate groups are employed as opposed to three acrylate groups. We aim to synthesise Coronas **6** and **8** to study the effect of divergence between side chains upon the liquid crystalline properties.

The side chains on the corona need to be of sufficient length to force the formation of discotic liquid crystals but not overly long as to reduce order. Given that the ether branching units in each corona add length, the designs of Coronas **6** and **8** incorporate a C₉ spacer unit as opposed to the longer chains used in previous examples.^{56, 50}

2.3) Design of core for supramolecular discotic liquid crystal

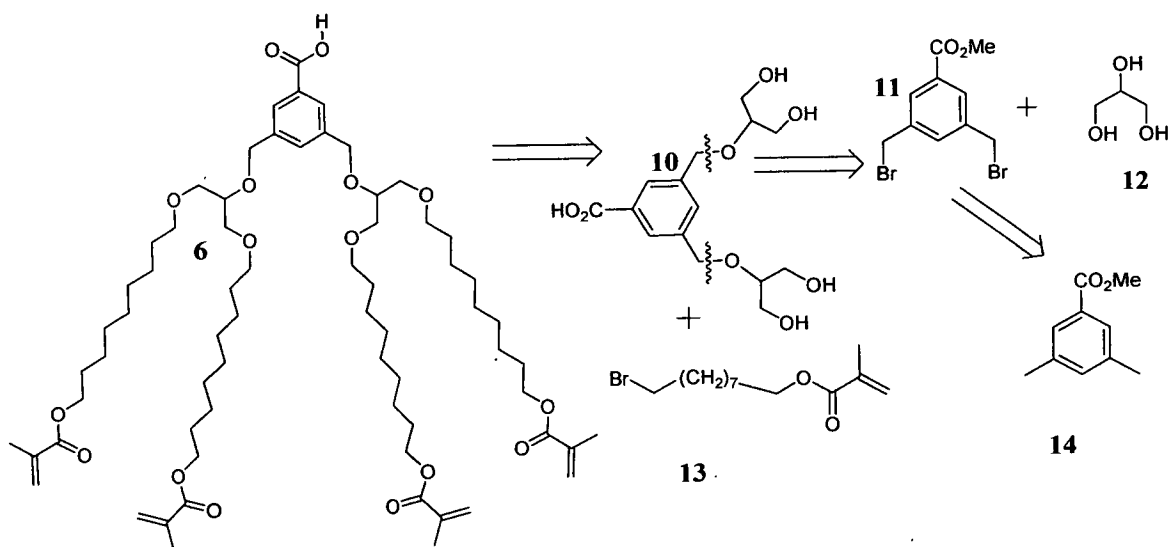
The C₃ symmetric triazine derived heterocycles **5** and **7** will provide an AAD hydrogen bonding surface to the benzoic acid moieties of the corona units **6** and **8**. This three-centred unit should impart more structural integrity upon the supramolecular system than achieved in previous examples^{49,50} which employed a simple DA system. Due to

synthetic considerations the design of core 5 was modified to incorporate six alkyl chains to give core 7.

Core 9 is investigated as an entirely different supramolecular synthon, it was intended to bind to strongly to diaminopyridine systems (Figure 3, p14). Were these systems functionalised appropriately with aliphatic chains, discotic liquid crystals should be formed. The design and synthesis of such a system was to be attempted were 9 successfully synthesised.

2.4) Retrosynthetic analysis

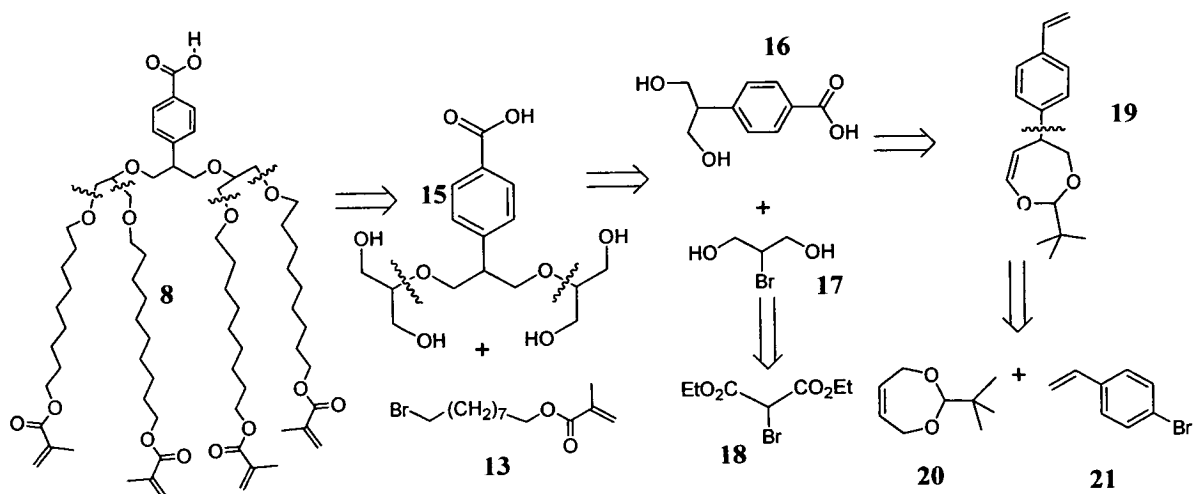
2.4.1) Dimethylbenzoic acid derived corona 6



Scheme 5: Retrosynthesis of dimethylbenzoic acid derived corona 6

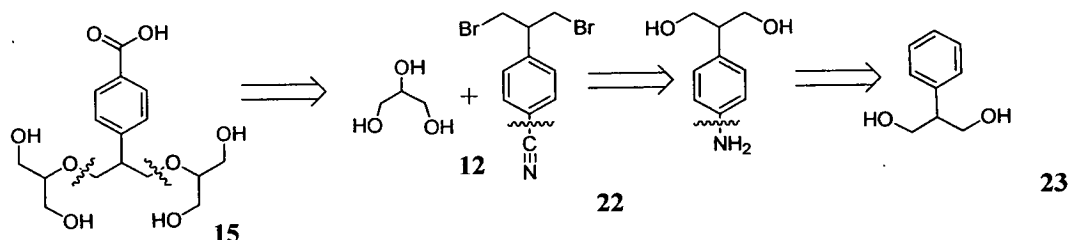
C-O disconnections of Corona 6 (Scheme 5) reveal tetra-ol building block 10 and long chain bromo-ester 13, as synthetic intermediates. Further retrosynthesis of tetra-ol 10 leads to glycerol 12 and benzoic acid 14, as cheap commercially available starting materials.

2.4.2) Propane-1,3-diol derived corona 8



Scheme 6: Propane-1,3-diol derived corona - initial retrosynthesis

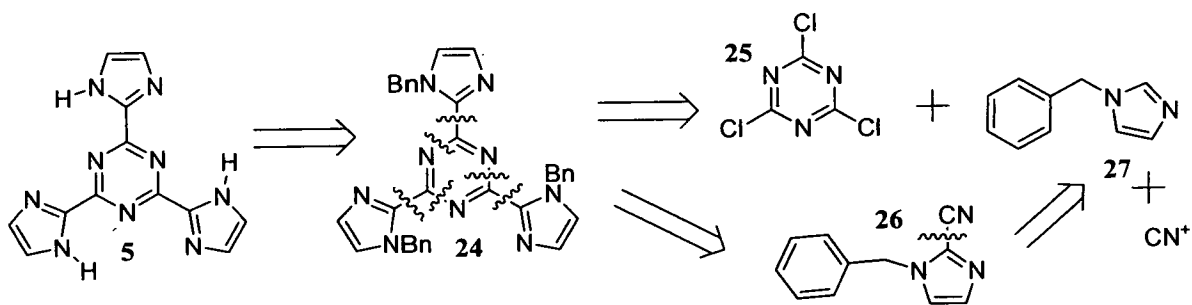
C-O disconnections of Corona 8 provide tetra-ol 15 and long chain bromo-ester 13 as synthetic targets. Further C-O disconnections of benzoic acid derivative 15 lead to propanediol 16 and commercially available diethyl bromomalonate 18. Styryl oxepin 19 is disconnected at the bond shown with a simultaneous hydrogen shift via a Heck reaction. This leads to commercially available 4-bromostyrene 21 and an acetal of 2-butene-1,4-diol 20.



Scheme 7: Revised retrosynthesis deriving from Corona 8

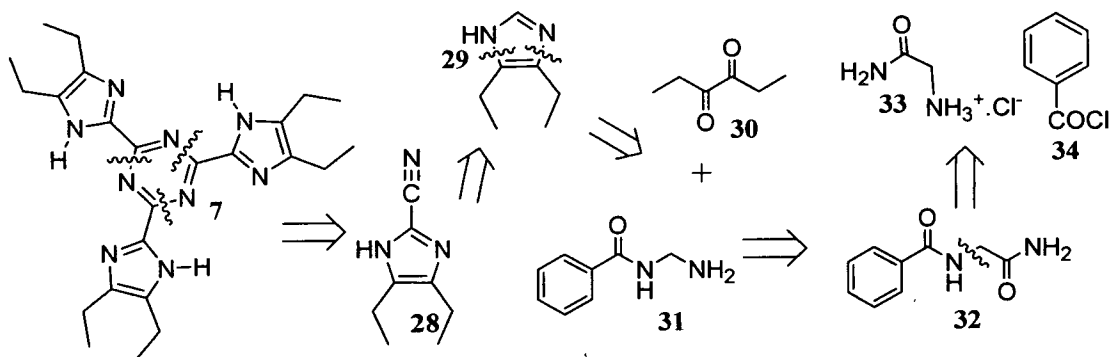
Tetra-ol 15 is disconnected through the two C-O bonds shown (Scheme 7). This leads to glycerol 12 and dibrominated benzonitrile 22. Functional group interconversions⁶³ lead to commercially available 2-phenylpropane-1,3-diol 23.

2.4.3) Tris(imidazolyl)triazine cores 5 and 7



Scheme 8: Tris(imidazolyl)triazine core 5 retrosynthesis

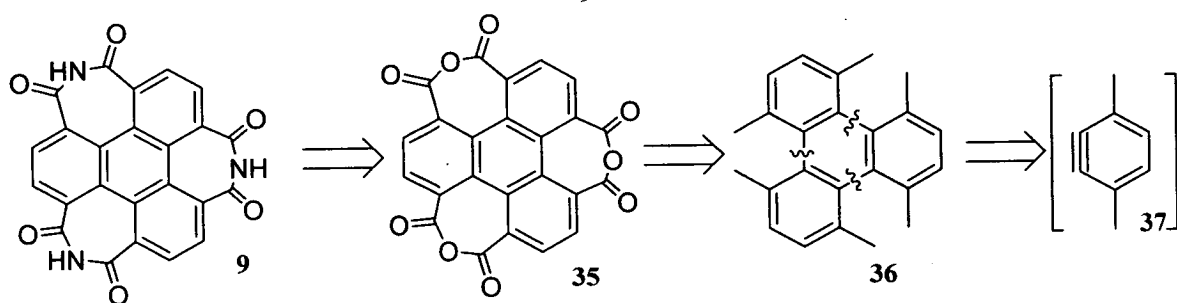
Tris(imidazolyl)triazine **5** affords intermediate **24** (Scheme 8). The 3 C-C disconnections marked in blue give direct access to cheap commercially available starting materials cyanuric chloride **25** and *N*-benzylimidazole **27**. Alternatively the triple disconnection marked in red leads to 1-benzyl-2-cyanoimidazole **26**, which itself can be disconnected via an electrophilic addition to give commercially available *N*-benzylimidazole **27** and a source of CN^+ .



Scheme 9: Solublised tris(imidazolyl)triazine core 7 retrosynthesis

Solublised core unit **7** is disconnected directly to cyanoimidazole **28**. Further retrosynthesis leads to key 4,5-dialkylimidazole building block **29**. FGI of **29** leads to available dione **30** and protected methylene diamine **31**. FGI of amine **31** gives diamide **32** via a modified Hoffmann rearrangement. Further disconnection leads to available starting materials glycine hydrochloride **33** and benzoyl chloride **34**.

2.4.4) Triimide supramolecular synthon 9

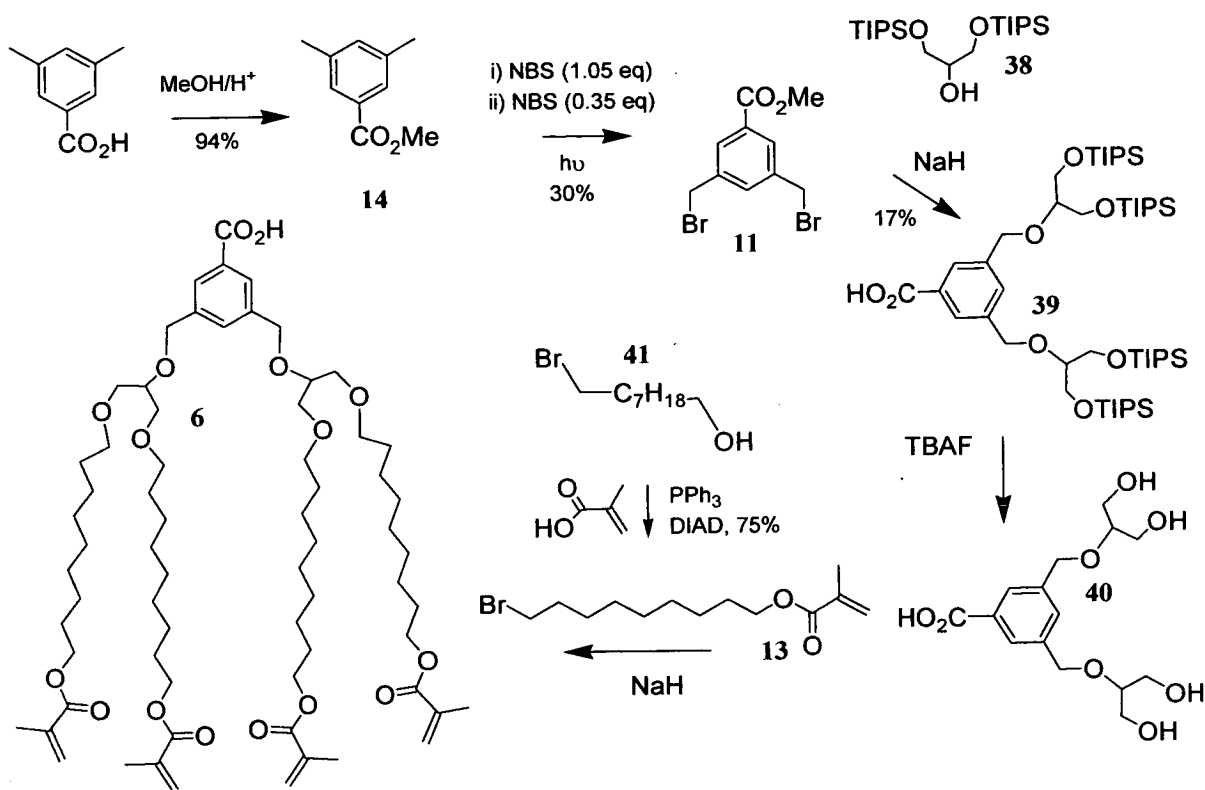


Scheme 10: Retrosynthesis of triimide supramolecular synthon 9

FGI of triimide 9 gives trianhydride 35 which can be derived from novel hexamethyltriphenylene 36 via selective oxidation with basic $\text{Na}_2\text{Cr}_2\text{O}_7$.⁶⁴ Hexamethyltriphenylene 36 can then be disconnected to benzyne 37. Further retrosyntheses and synthetic attempts for triimide 9 form the basis of reference 65.

2.5) Results and Discussion

2.5.1) Towards dimethylbenzoic acid derived corona 6

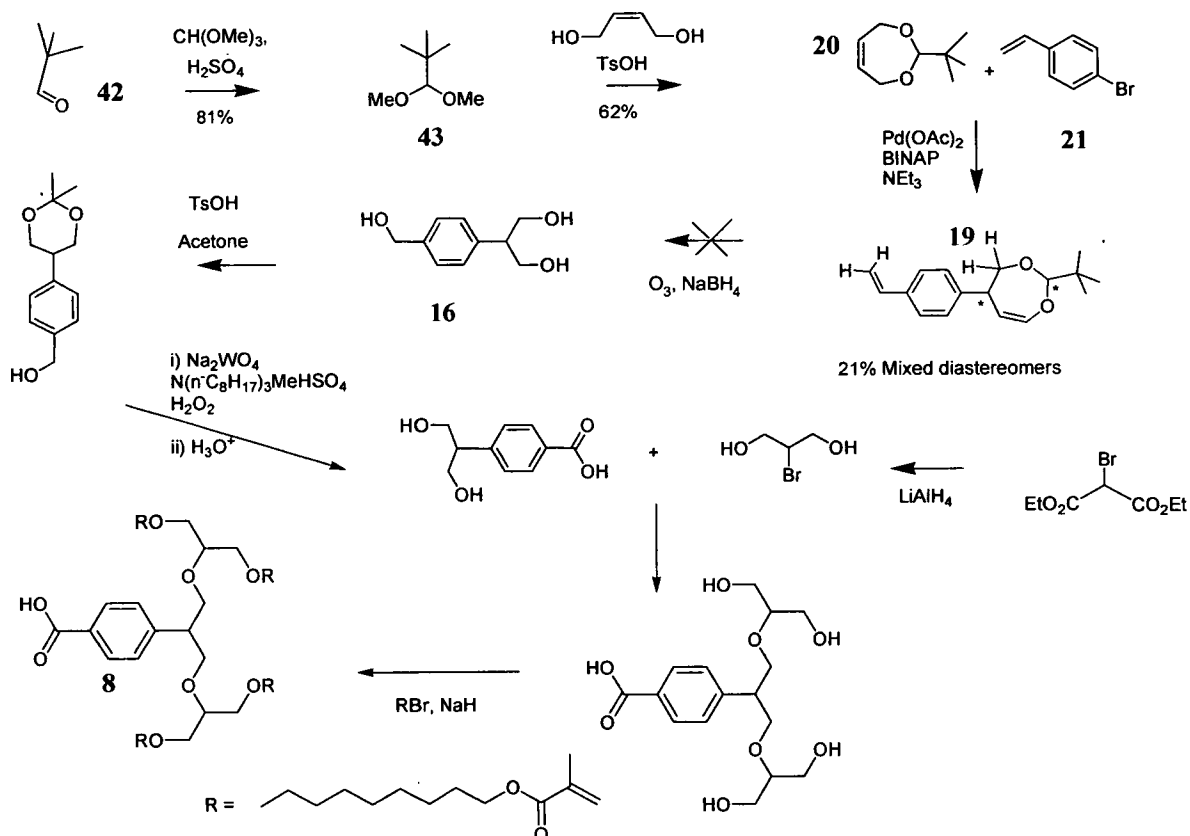


Scheme 11: Corona 6 synthesis – a corona with a wide angle between alkyl units

Silyl protected glycerol **38** (88%) and methyl ester **14** were synthesised in excellent yield by standard procedures (Scheme 11). The dibrominated product **11** was synthesised by NBS bromination of methyl ester **14**. The transformation was completed in two steps to avoid the formation of tribrominated product. Dibrominated ester **11** was then subjected to a Williamson ether synthesis and the methyl ester was shown to be partially labile to the reaction conditions, forming acid **39** in poor yield. Isolation of the highly polar tetrahydroxy benzoic acid **40** was not realised. Ester **13** proved surprisingly difficult to synthesise: Addition of alcohol **41** to methacryloyl chloride and ester couplings with DCC and EDCI failed to produce ester **13** in high purity. Furthermore reaction of alcohol **41** with activated ester perfluorophenyl methacrylate, or methacrylic acid in the presence of TBTU and HOBT produced no detectable product. However long chain

brominated ester **13** was synthesised in good yield by a Mitsunobu esterification. Although compound **40** was not synthesised, an attempt was made to apply long chain bromo-ester **13** in a Williamson ether synthesis. Unfortunately this led to polymerisation.

2.5.2) Towards propane-1,3-diol derived corona **8**

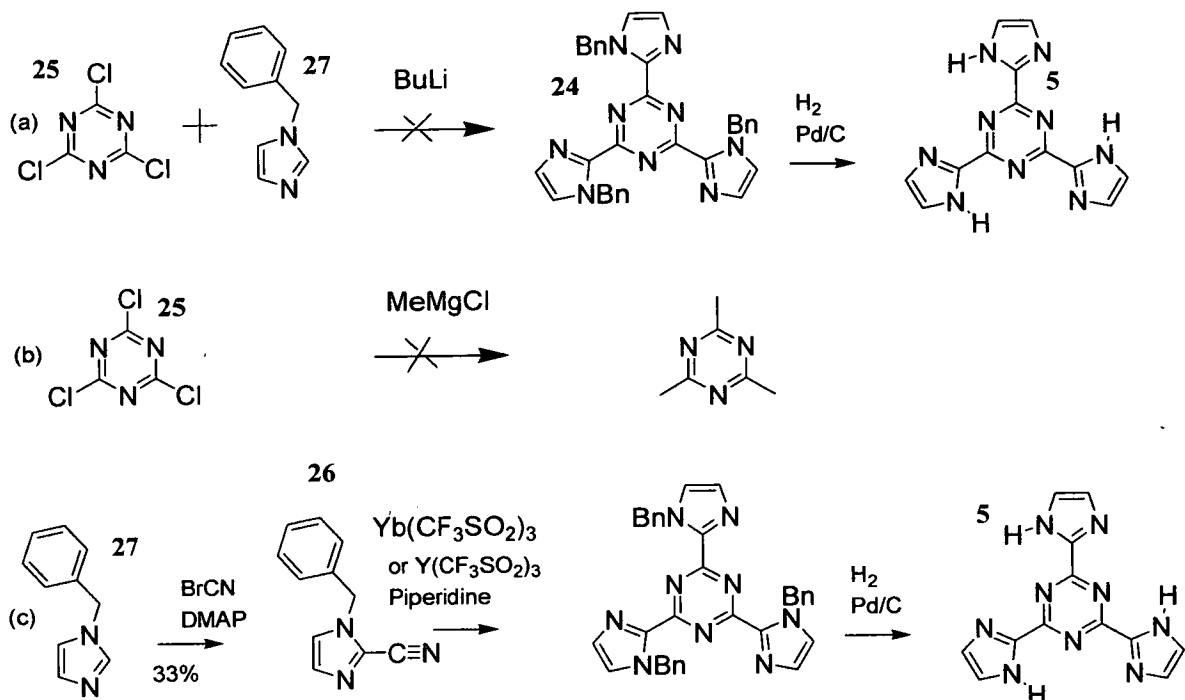


Scheme 12: First attempted synthesis of Corona **8 - corona unit which branches with a narrow angle.**

Styryl dioxepin **19** was targeted initially as a key intermediate for the 1,3 diol moiety required for benzyl alcohol **16**.⁶⁶ Dioxycycloheptene derivative **20** was synthesised by two standard acetal forming reactions in good yield⁶⁷ as direct reaction of pivaldehyde **42** with 1,4-butanediol gave equilibria lying well to the left. Despite several optimisation attempts using solution and microwave chemistry, styryl oxepin **19** was synthesised in low yield via a Heck coupling⁶⁸ between 4-bromostyrene **21** and dioxycycloheptene

derivative **20**. After the work-up difficulties encountered with the formation of **16**, a more efficient route to Corona **8** was envisaged as shown on page 42.

2.5.3 Towards trisimidazolyl triazine core **5**

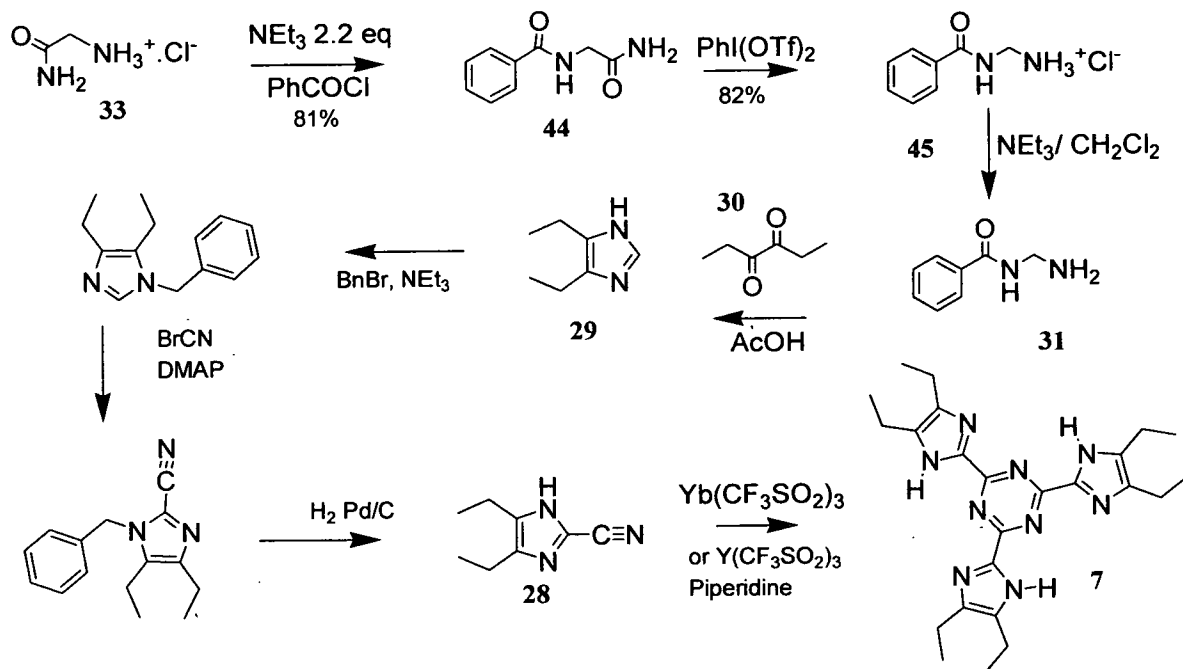


Scheme 13: Three strategies tested towards the synthesis of the imidazole-functionalised triazine core unit **5 designed to bind three benzoic acid derived corona units. (a) Substitution of an alkyl lithium for a chloride, (b) substitution of a Grignard nucleophile for a chloride, and (c) cyclotrimerisation of cyanoimidazoles with and without protection.**

The initial approach to the core unit **5** was by nucleophilic aromatic substitution. As reported for similar systems,⁶⁹ it was found that carbon nucleophiles (Scheme 13 a & b), reacted poorly with cyanuric chloride **25**. The second approach to the imidazole functionalised triazine **5** was via cyclotrimerisation of cyano-substituted imidazoles by lanthanide catalysis. Benzyl protected cyano imidazole **26** was synthesised utilising the DMAP adduct of cyanogen bromide,⁷⁰ a useful source of electrophilic cyanide. Direct cyclotrimerisation of **26** was not effective. This may have been due to steric hindrance adjacent to the cyano group. 2-cyanoimidazole was therefore targeted as a cyclotrimerisation substrate with reduced steric hindrance. Unfortunately it proved very

difficult to purify and work with due to high polarity, therefore a new route was proposed. Decoration of the imidazole with solubilising alkyl groups would give access to 4,5-dialkyl-2-cyanoimidazole intermediate **28** with increased solubility and reduced steric hindrance.

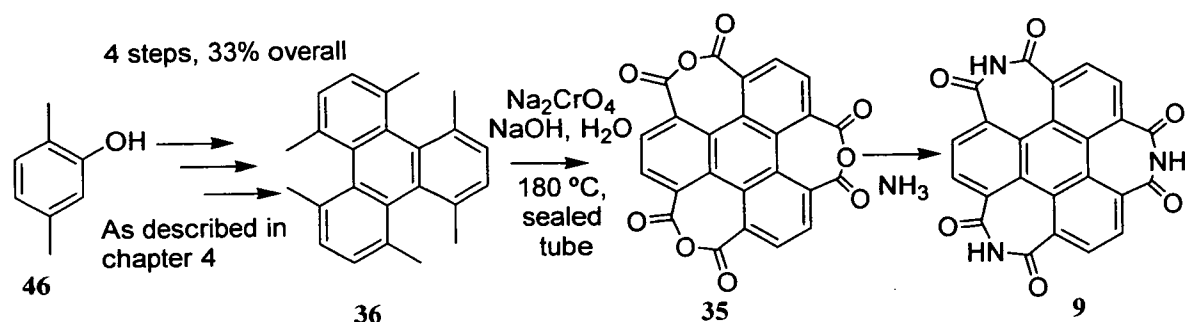
2.5.4) Towards solubilised triazine core **7**.



Scheme 14: Core II - Soluble triazine derivative **7 to be synthesised from 4,5-dialkylimidazole building block **29**.**

The synthesis of 4,5-diethylimidazole **29** was attempted from a literature procedure.⁷¹ The amine precursor **45** was synthesised by a benzoylation reaction followed by a modified Hoffmann rearrangement.⁷² The free amine **31**, although unstable to silica was isolated by reaction of hydrochloride salt **45** with triethylamine and filtration through basic alumina. Unfortunately the condensation reaction of amine **31** with hexane-1,6-dione **30** was unsuccessful. Synthesis of 4,5-dialkylimidazole building blocks was eventually accomplished within the group, however the required functionalisation at the 2-position to form analogues of **28** did not succeed.

2.5.5) Towards the synthesis of triimide **9**



Scheme 15: Work towards the synthesis of triimide **9**

Hexamethyltriphenylene intermediate **36** was successfully synthesised from phenol **46** as described in Chapter 4. Methyl groups on triphenylenes and other polycyclic aromatic hydrocarbons can be selectively oxidised to yield carboxylic acids or cyclic anhydrides.⁶⁴ For triphenylene **36** however, this reaction is not expected to yield the desired trianhydride **35**. A product originating from the relief of steric strain is more likely, as explained in section 4.8. Therefore the synthesis of triimide **9** has yet to be realised.

2.6) Conclusions

Our initial designs of novel supramolecular mesogens were perhaps overly complex, leading to inefficient synthetic routes. The following chapter describes the synthesis and application of a simpler material. Although triimide **9** was not pursued further, the novel properties of hexamethyltriphenylene intermediate **36** were investigated and form the basis of chapter 4.

3) The Synthesis and Novel Application of a Supramolecular Discotic Liquid Crystal

3.1) Aims and Strategy

The revised aim of this project was to synthesise a known liquid crystal system and explore its utility in novel applications. The symmetrical core surrounded by corona units, first synthesised by Kim and co-workers (Scheme 3, p36), gives access to functional nanoporous scaffolds. We aim to tailor various surfaces, e.g. gold, ITO, with these nanoporous materials and work toward their application in magnetic data storage and electrochemical sensing (Figure 21).⁷³

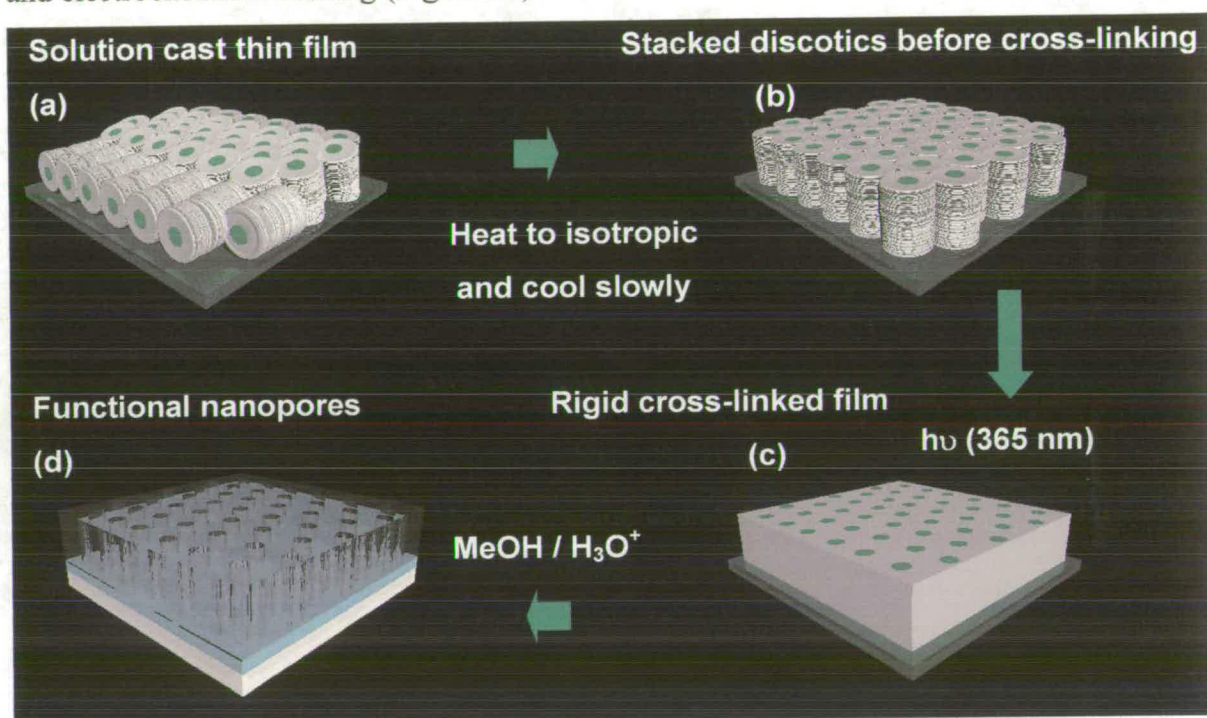


Figure 21: (a) The discotic liquid crystals formed from a core (green) and a corona (white). Spin casting produces a film containing molecular columns of random orientation. (b) The columns are aligned by slow cooling from the isotropic liquid. (c) The molecules are then cross-linked by irradiation with U.V. light. (d) Functional nanopores are uncovered by reversal of the hydrogen bonding interactions with a polar solvent and acid.

Thin films will be formed by spin casting, annealing should align the molecules as required (Figure 21b). Following this, a nanoporous scaffold will be formed if the aligned film can be polymerised and etched as shown. The films need to be thin such that the aspect ratio of the 1 nm diameter pores (Figure 21d) is not so large as to preclude applications.⁵⁹ Glass slides allow the direct observation of phase changes, the alignment protocol can then be switched to a conducting substrate such as ITO, or gold on silicon.

3.2) Molecular Design

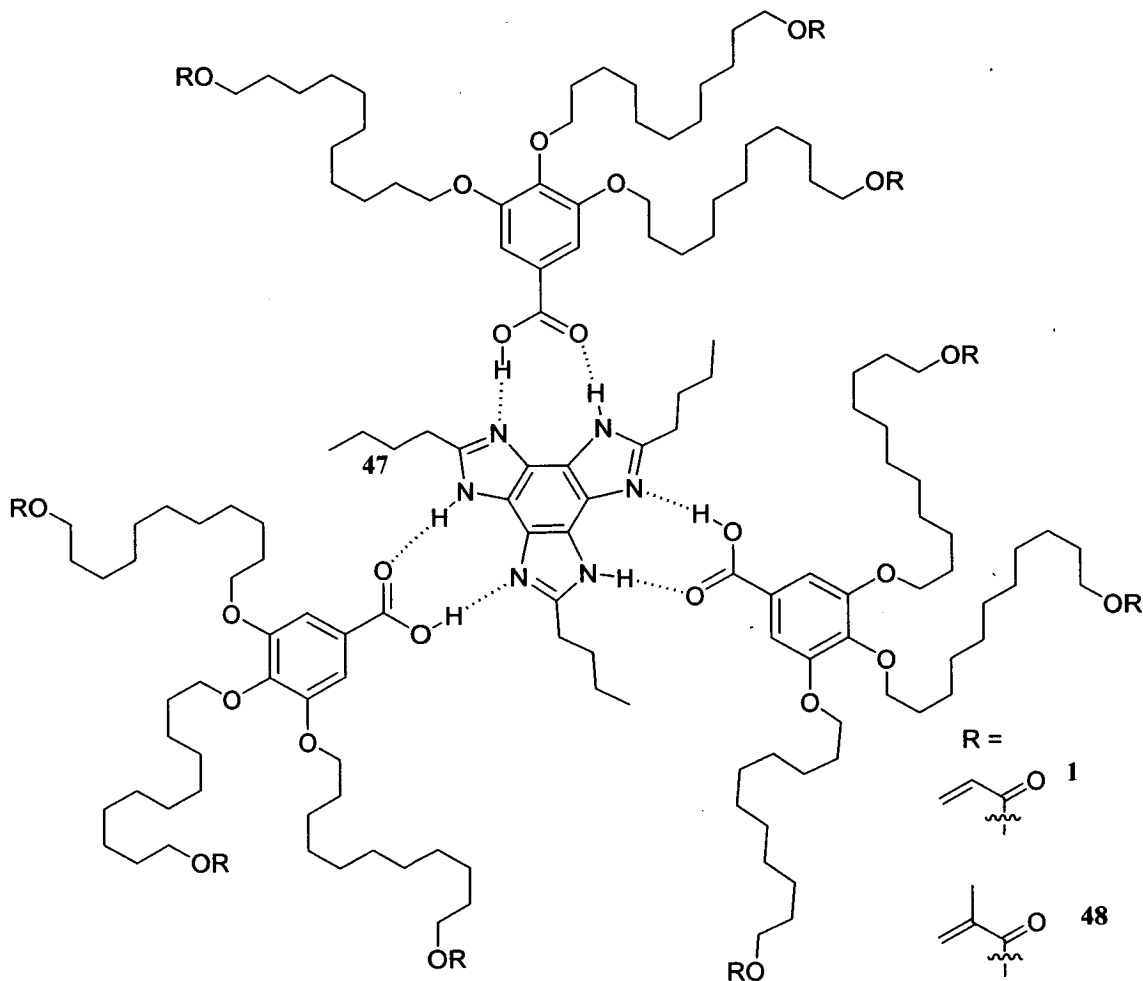


Figure 22: Adapted designs for supramolecular liquid crystals to be investigated in chapter 3.

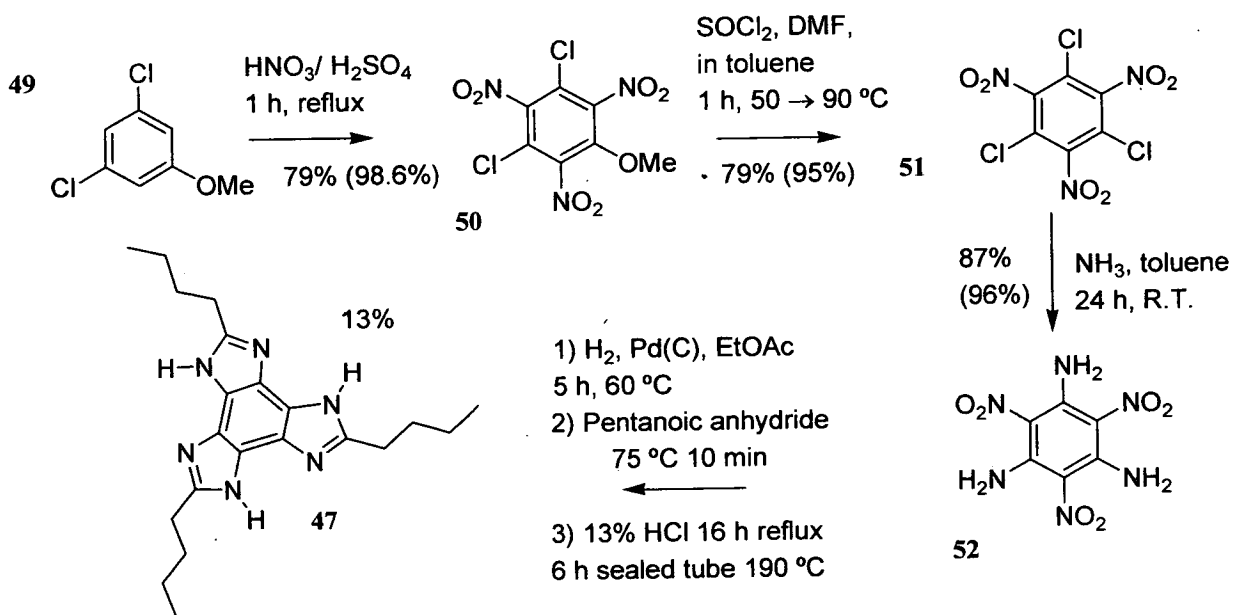
The original design by Kim and co-workers⁵⁶ was adapted slightly (Figure 22). Pentyl-derivatised bezotri(imidazole) 2 is replaced by butyl-derivatised core 47. The alkyl chain



was shortened in an attempt to increase the efficiency of the etching step (Figure 21c and d). The efficacy of methacrylate as a polymerisable group is also tested by the synthesis of methacrylate derivative **48** in addition to the resynthesis of acrylate derivative **1**.

3.3) Synthetic Results and Discussion

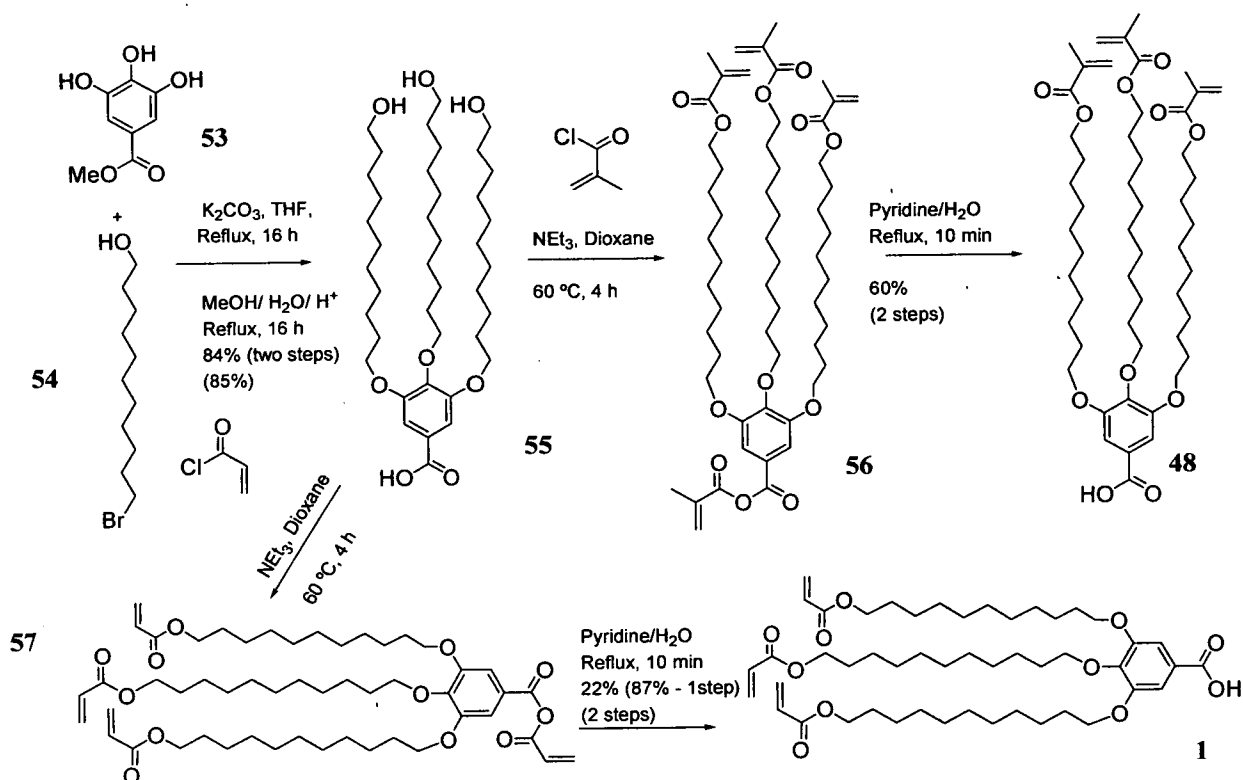
3.3.1) Synthesis of benzotri(imidazole) core **47**



Scheme 16: The synthesis of benzotri(imidazole) **47**, a close derivative of the pentyl-substituted **2** (Scheme 2, p 30), literature yields are shown in parentheses.

Activated dichloroanisole **49** was nitrated to form trinitro compound **50**. Stoichiometric thionyl chloride and DMF provided a Lewis acid and organic chloride to convert a methoxy group into chloride and forms trichloro compound **51**, now highly activated towards nucleophilic aromatic substitution. Reaction with ammonia afforded explosive compound trinitrotriaminobenzene in excellent yield. Yields towards this intermediate did not reach the values quoted in the patent, perhaps due to smaller scales employed, or less efficient stirring. The nitro groups were reduced *in situ* to form the unstable hexaminobenzene. Reaction with pentanoic anhydride and cyclisation in aqueous acid afforded the final benzotri(imidazole) **47** in acceptable yield.

3.3.2) Syntheses of coronas 1 and 48



Scheme 17: The syntheses of new methacrylate-derived gallic acid derivative 48 and known acrylate derivative 1 (Scheme 2, p 30), literature yields are shown in parentheses.

A well known Williamson ether synthesis and hydrolysis led acid triol **55** in the literature yield. The synthesis of the new gallic acid **48** was attempted by a protocol developed by Ziessel and co-workers.⁷⁴ The synthesis of this derivative was challenging as the final product was neither stable to chromatography nor amenable to recrystallisation. It was accomplished by careful work-up of the mixed ester anhydride species **56**. The synthesis of **1** has yet to be optimised; some material appeared to be lost due to copolymerisation with excess acrylic acid during work-up. We had difficulty obtaining pure product from the 1 step conditions reported by Gin and co-workers⁷⁵ and it is interesting to note that Kato went via a mixed ester anhydride species to synthesise other derivatives of **1**.⁴¹

3.4) Bulk properties of methacrylate complex 48.47

3.4.1) ^1H NMR showing formation of supramolecular complex between corona 48 and core 47

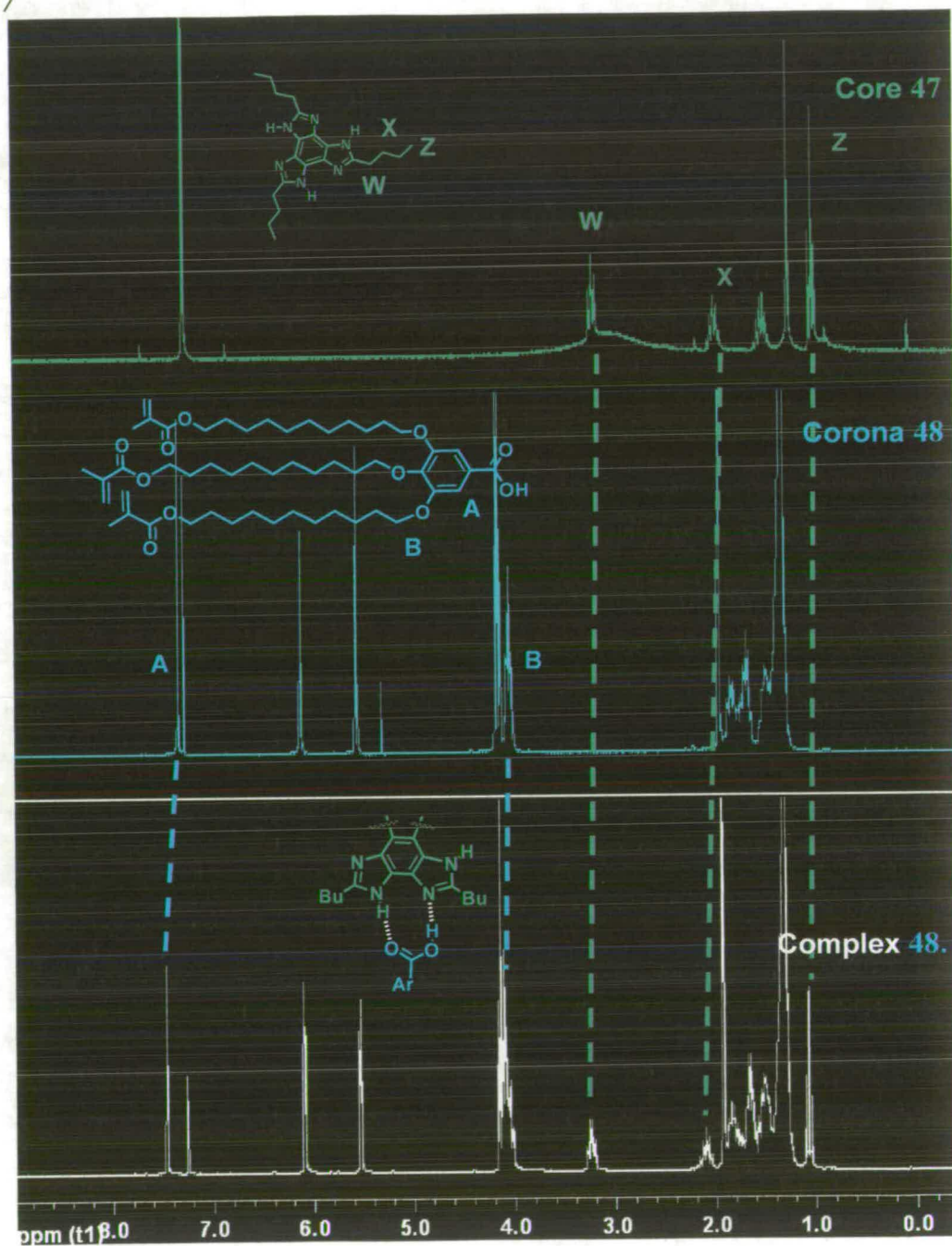


Figure 23: ^1H NMR spectra showing the synthesis of complex 48.47. Protons in close proximity to the complex show an increase in chemical shift, characteristic of complexation.

Complex **48.47** was formed in the non-polar solvent chloroform by the method developed by Kim and co-workers.⁵⁶ The NMR resonances of the protons close to the site of complexation show the expected movement to higher chemical shift (Figure 23).

3.4.2) DSC showing phase behaviour of methacrylate complex **48.47**

Complex **48.47** formed liquid crystals as desired. Differential scanning calorimetry (DSC) showed highly reversible phase changes as shown.

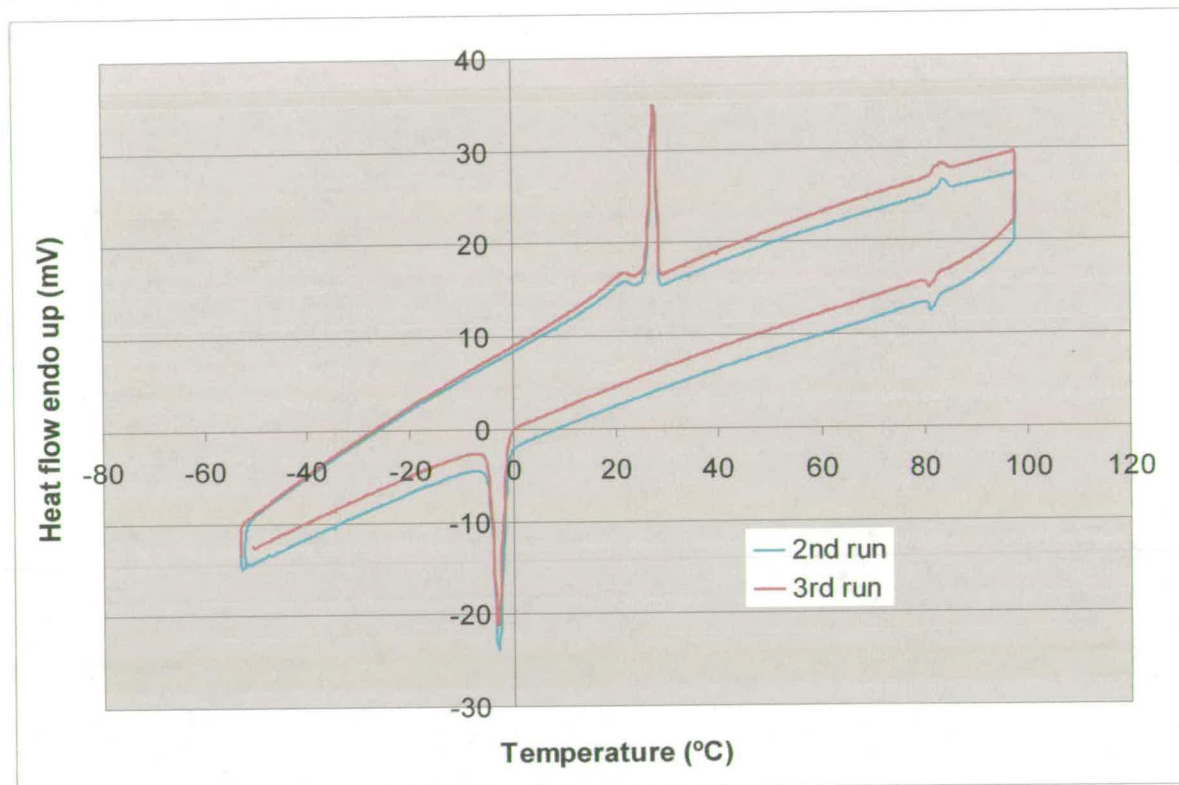


Figure 24: DSC trace of Complex **48.47** showing phase behaviour.

The working hypothesis from the DSC trace is that the large phase change at 27 °C (30 J/g on 1st run, 29.6 on 2nd, 25.6 J/g on 3rd) represents the melting of the crystalline phase. A second melting of lower enthalpy (2.1, 1.7 and 1.7 J/g respectively) occurs at 84.5 °C. The phase changes occur in reverse upon cooling with some supercooling. The general behaviour of the two samples analysed, (a) and (b) is similar. The disparities (Table 1) likely stem partly from the two-component nature of the complex (weighing error) and additionally from the fact that the small, broad peaks are close to the detection limits of

the machine. The enthalpies are lower than those reported by Kraft and co-workers for a similar complex,⁵⁰ however Kim did not publish results for complex 1.2 so no direct comparison can be made.

Experiment			(a)	(b)
Scan 1 Heat	K → Col	Onset (°C)	18.9	14.0
		Peak (°C)	27.6	26.5
		ΔH (J/g)	30.0	35.6
	Col → I	Onset (°C)	81.5	73.5
		Peak (°C)	84.5	76.0
		ΔH (J/g)	2.1	1.7
Scan 1 Cool	I → Col	Onset (°C)	83.1	73.0
		Peak (°C)	81.4	71.0
		ΔH (J/g)	-1.4	-0.8
	Col → K	Onset (°C)	0.8	3.8
		Peak (°C)	-2.9	0.0
		ΔH (J/g)	-32.7	-40.0
Scan 2 Heat	K → Col	Onset (°C)	18.9	14.0
		Peak (°C)	27.6	26.8
		ΔH (J/g)	29.6	33.7
	Col → I	Onset (°C)	81.2	72.2
		Peak (°C)	83.9	74.3
		ΔH (J/g)	1.7	1.0
Scan 2 Cool	I → Col	Onset (°C)	83.1	73.0
		Peak (°C)	81.4	72.5
		ΔH (J/g)	-1.5	-0.8
	Col → K	Onset (°C)	0.8	3.6
		Peak (°C)	-2.9	-0.3
		ΔH (J/g)	-32.4	-38.9
Scan 3 Heat	K → Col	Onset (°C)	24.6	15.5
		Peak (°C)	27.6	27.7
		ΔH (J/g)	25.9	34.8
	Col → I	Onset (°C)	81.1	71.1
		Peak(s) (°C)	83.9	71.4
		ΔH (J/g)	1.7	0.8

Table 1: DSC results for a and b samples of complex 48. 47 a more comprehensive table is given in the experimental section.

3.4.3) Polarised optical microscopy of thick films of methacrylate complex 48.47

Polarised optical microscopy allows the identification of the phases present. Textures of the crystalline phase and the liquid crystalline phase upon heating (not generally repeatable) are included in the experimental section. The sample of complex 48.47 melts to the isotropic at 97 °C, slow cooling provides textures characteristic of the hexagonal columnar phase. As predicted by DSC, the crystalline phase does not appear to re-form at room temperature.

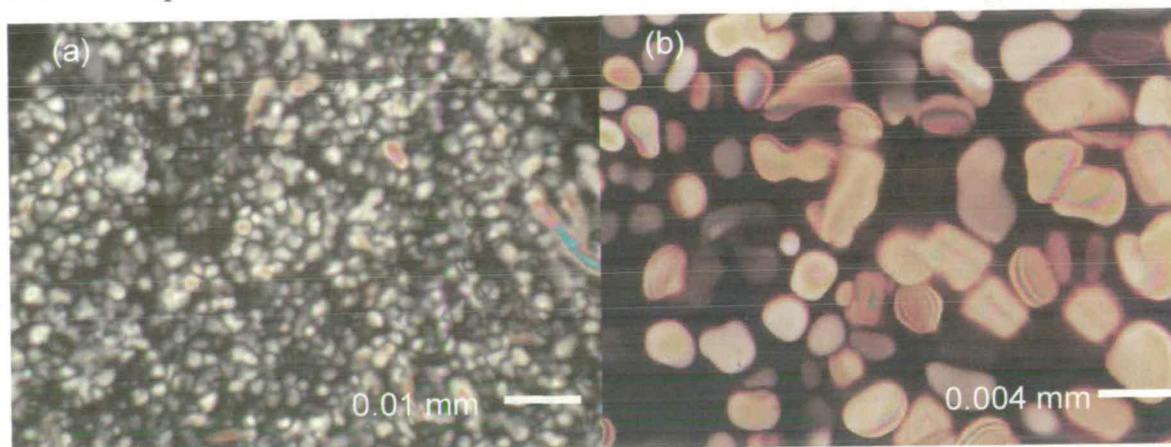


Figure 25: a) Texture of columnar hexagonal phase of complex 48.47, texture of same phase in a well characterised literature material.⁷⁶

Figure 25 indicates that the hexagonal columnar phase has been formed; the phase changes found by DSC can now be tentatively assigned.

Heating	Cooling
Cr 27.0 → Col _h 84.5 → I	I 81.0 → Col _h -3.1 → Cr

3.4.4) Polymerisation in the presence of initiators

Polymerisation of the complex was attempted using UV light, it was discovered however that methacrylate esters require initiation for UV polymerisation using non-laser radiation sources. This is due to competition between polymerisation and decomposition when wavelengths < 320 nm are used.⁷⁷ The incorporation of small amounts of

polymerisation initiator was therefore attempted. The extent of polymerisation was measured by the disappearance of the methacrylate C=C stretch IR band at 1638 cm^{-1} . Two different initiators were studied, looking for maximum polymerisation with minimum weight fraction of initiator. In initial experiments the bulk IR spectrum of polymer was compared qualitatively to that of monomer. It was found that relatively high weight fractions ($> 2.5\%$ w/w) of the common initiator 2,2-dimethoxy-2-phenylacetophenone (DMPA) were required. As these large quantities interfered with the phase behaviour of the material, the polymerisation was also attempted with diphenyl-2,4,6-trimethylbenzoylphosphine oxide (TMBPO) as lower concentrations were required⁷⁸. To avoid thermal polymerisation, methyl hydroquinone (MEHQ), an inhibitor was also incorporated.⁷⁸ This should stop thermal polymerisation within the timescales used, but will be consumed quickly when UV polymerisation is commenced. Samples were prepared by drop casting the formulation on a KBr disc and annealing at $97\text{ }^{\circ}\text{C}$ for 1 hour. In IR spectroscopy, given an isotropic sample, absorbance is proportional to sample length and concentration. In this case, sample orientation and length are not expected to change as the film is quite uniform. Therefore the degree of polymerisation is determined either from the decrease in absolute or relative absorbance at 1638 cm^{-1} .

Experiment	Irradiation Time (min)	% methacrylate conversion by ratio method	% methacrylate conversion by direct method
Methacrylate complex 48.47 0.8% w/w TMBPO 0.1% w/w MEHQ	10	71.9	67.9
	60	89.7	91.1
Methacrylate complex 48.47 0.4% w/w TMBPO 0.1% MEHQ	60	59.9	69.0
Methacrylate complex 48.47 0.5% w/w DMPA 0.1% MEHQ	60	36.3	41.6

Table 2: Samples were irradiated at 365 nm for the times shown. Degrees of conversion were found by comparison with the unpolymerised sample, either directly or by the ratio of the methacrylate absorbance to that of the C=C aromatic stretch peak at 1586 cm⁻¹.

The phosphine-based initiator TMBPO was found to be highly effective even at relatively low concentrations. The formulations could now be tested for alignment on surfaces.

3.5) Application of methacrylate complex 48.47 on surfaces

3.5.1) Polarised optical microscopy of thin films

Thin films of complex were formed by spin casting. It was found that a 2.25% w/v solution in chloroform, cast at 3000 rpm gave films ~ 125 nm thick, films thinner than these were not stable to annealing. The films were annealed just above the isotropisation temperature for a time and cooled slowly to form aligned homeotropic domains as shown (Figure 26).

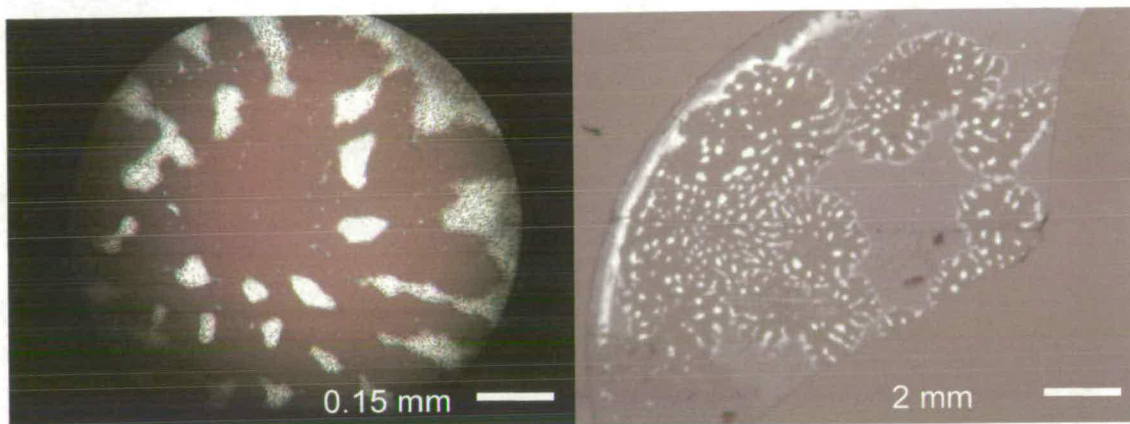


Figure 26: Homeotropic domains formed upon cooling pure complex 48.47 from the isotropic.

An attempt to improve alignment by functionalisation of the surface with aminopropylsilane proved unsuccessful, actually having the opposite effect of preventing homeotropic alignment. The differences in architecture and chemistry between Kato's ionic liquid crystals and this supramolecular complex were obviously too great. The next requirement was to lock-in the organisation of the molecules by polymerisation.

3.5.2) Attempted alignment in the presence of initiator

The incorporation of the required initiators and inhibitors led to difficulties obtaining an aligned sample. In the case of 2.5% or 1% DMPA + 0.1% MEHQ the textures appeared normal but alignment never occurred. This retardation was common to any trace impurities in our liquid crystal phase. In the case of 0.4% or 0.8% TMBPO + 0.1%

MEHQ the temperature of isotropisation appeared to be greatly reduced and the textures observed changed markedly.

3.5.3) Verification of effect of initiator and inhibitor on phase behaviour by DSC

A formulation containing only TMBPO appeared to polymerise thermally. None of the liquid crystalline phase melting peaks observed for unadulterated complex **48.47** were present for a sample containing 0.4% w/w TMBPO + 0.1% w/w MEHQ or for a sample containing 0.1% w/w MEHQ alone. These results therefore support the evidence from microscopy, indicating that the presence of initiator fatally disrupts the alignment of complex **48.47**.

3.6) Bulk properties of acrylate complex 1.47

Due to the lack of success incorporating initiator into complex **48.47**, the alignment procedure was attempted with the acrylate-derived gallic acid derivative **1**, developed by Kim and co-workers, despite reservations over the thermal stability of this material.

3.6.1) ^1H NMR showing formation of supramolecular complex between corona 1 and core 47

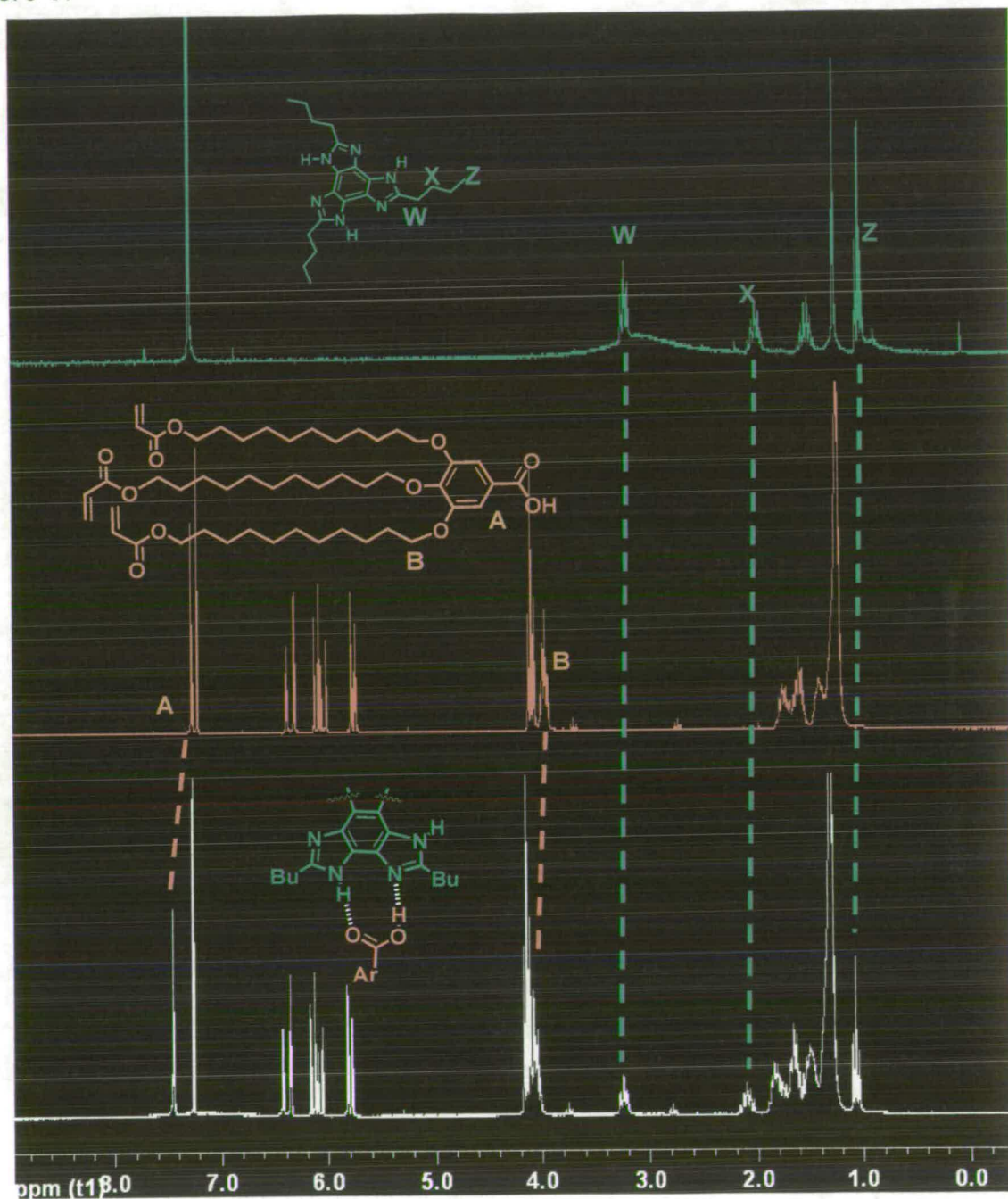


Figure 27: NMR spectra showing the synthesis of complex. Protons in close proximity to the complex show an increase in chemical shift, characteristic of complexation.

The NMR spectra show formation of complex **1.47** analogously to complex **48.47**.

3.6.2) DSC showing phase behaviour of acrylate complex **1.47**

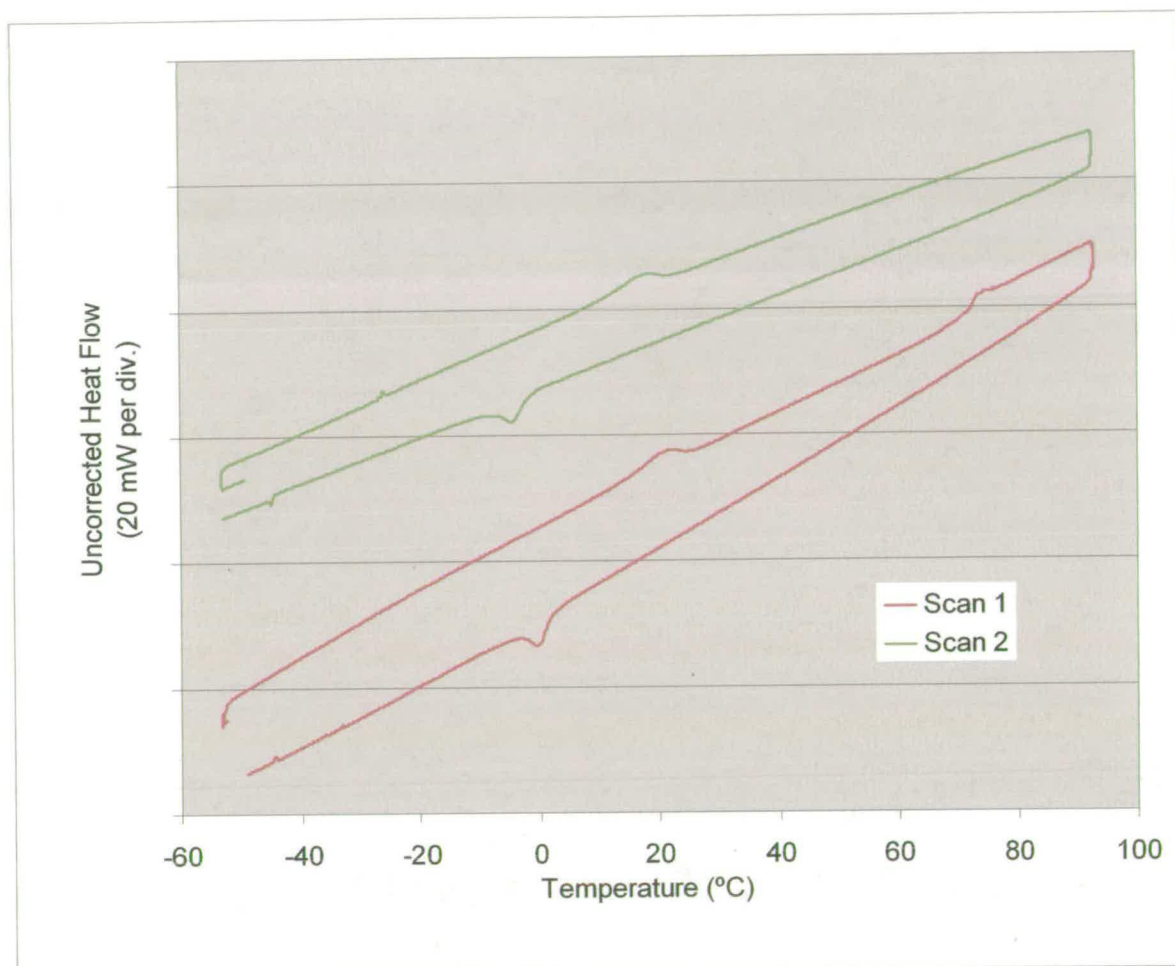


Figure 28: DSC trace of complex **1.47**

The phase behaviour of complex **1.47** appears analogous to that of complex **1.2**, reported by Kim and co-workers.⁵⁶ Namely, a liquid crystalline phase appears only upon heating, with a mesophase range of 21.9 to 74.9 °C. The isotropic phase does not appear to change back into the liquid crystal phase upon cooling. An attempt is made to integrate the peaks in the experimental, however broadness makes it difficult to draw firm conclusions. X-ray characterisation was used to provide more information.

3.6.3) Polarised optical microscopy of thick films

Approximately 400 nm thick films of complex **1.47** were formed by spin casting on glass and were melted into the isotropic phase momentarily then allowed to cool quickly. This technique had been used previously by Gin and co-workers⁷⁵ for a lyotropic liquid crystalline formulation of a derivative of gallic acid **1**. A superficial texture appeared on the surface of the film but the base of the film appeared aligned. Upon pressing with a second glass slide, the areas in contact with the slide aligned as shown in the micrograph.

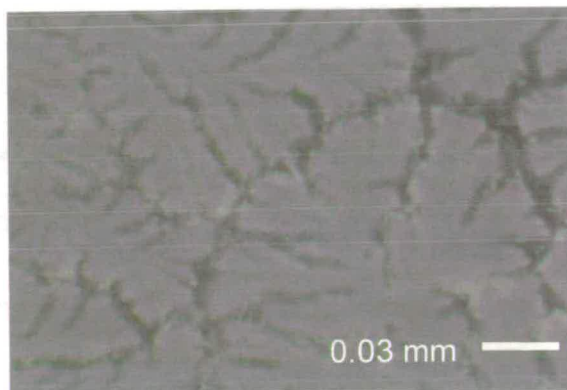


Figure 29: Homeotropic domains formed in thick films of complex **1.47** upon momentary heating to the isotropic, cooling to 50 °C, pressing with a second glass slide and slow cooling to R.T. Viewed under crossed polarisers.

This technique is not suitable for any type of device fabrication as the pressure is not applied with nanometre precision. A new technique is suggested in the future work section to overcome the problems caused by the air interface.

3.6.3) Polymerisation of acrylate complex **1.47**

Complex **1.47** was polymerised, following annealing, without initiation as reported by Kim and co-workers.⁵⁶ The degree of polymerisation was determined by IR spectroscopy with the same method as applied to complex **48.47**. The acrylate C=C stretch band occurs at 1636 cm⁻¹, it was compared with the aromatic C=C stretch at 1585 cm⁻¹ to show 49% conversion after 15 minutes. By directly comparing absorbances for the same film sample on KBr before and after polymerisation the conversion value obtained was 60%.

3.6.4) X-ray scattering studies

Polymerised complex **1.47** was characterised in an X-ray powder diffractometer at $\text{CuK}\alpha$ (1.54 Å).

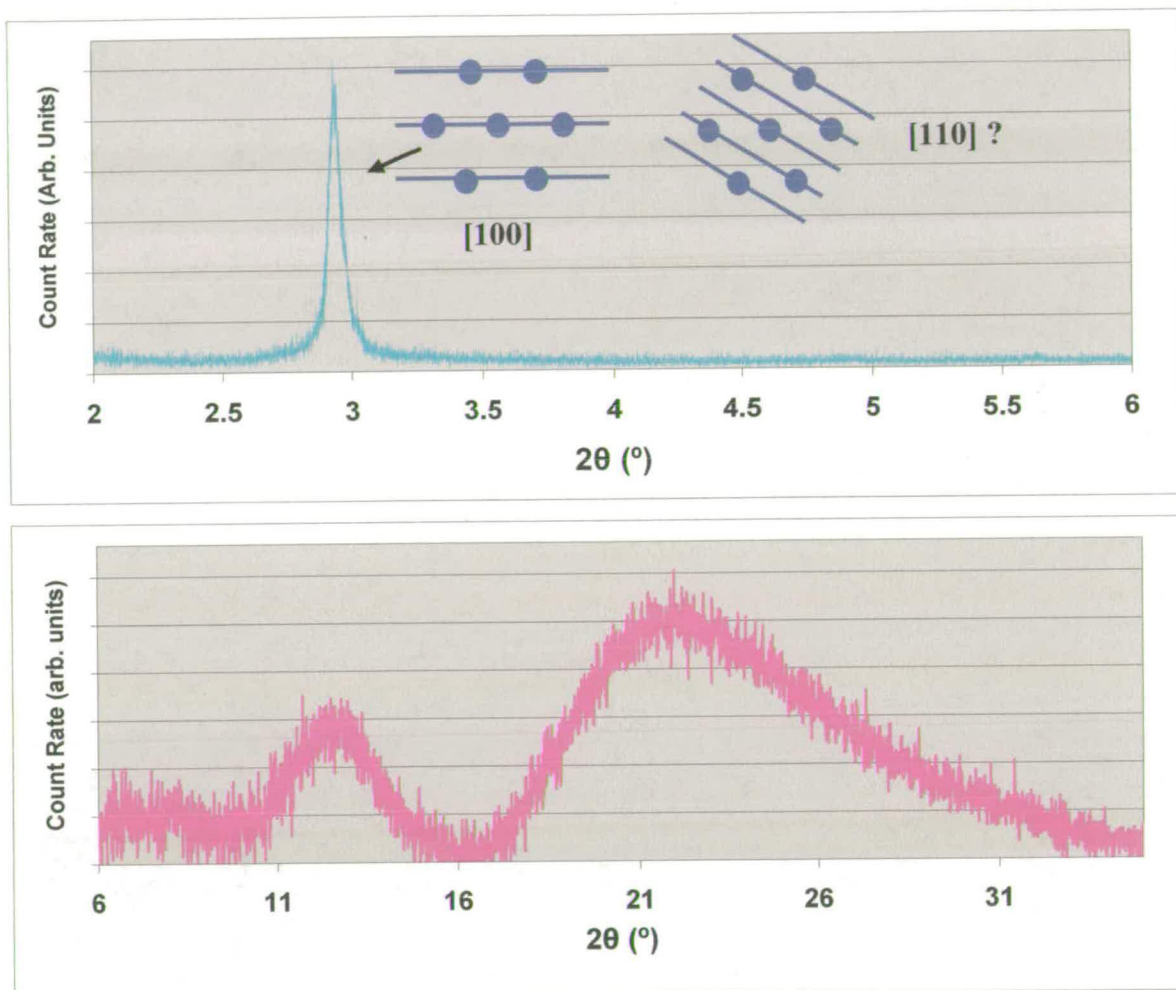


Figure 30: X-ray scattering was performed in two separate experiments using the scintillation counter detector for low angles (above) and the PSD detector for wide angles (below).

Peaks were detected at $2\theta = 2.9, 13$ and 22° , corresponding to distances of 30.1, 6.9, and 4.1 Å respectively. The peak at 30.1 Å corresponds to [100] lateral reflections between close-packed columns as shown by the inset. In order to define the lattice as hexagonal, a second reflection [110] should be present. This is most likely hidden by noise. The reflection might be observed using a synchrotron X-ray source or improved

experimental conditions. The wide angle reflection at 4.1 Å correspond to reflections between the close packed alkyl chains, the reflection at 6.9 Å may correspond to the second harmonic of π -stacking reflections (i.e. 2×3.45 Å).

The structural data gathered, although consistent with those for Kim's complex **1.2** do not yet allow unequivocal designation of the phase behaviour or lattice parameter of acrylate complex **1.47**.

3.7) Application of acrylate complex **1.47** on surfaces

3.7.1) Polarised optical microscopy of thin films

Kim and co-workers chose to anneal complex **1.2** at 30 °C between glass plates before polymerisation. No mention is made in their work of alignment occurring although the diagrams presented appear to suggest this. We attempted to align thin films (~125 nm) of our acrylate complex **1.47** by long term annealing within the liquid crystalline range. Some domains grew as shown in Figure 31.

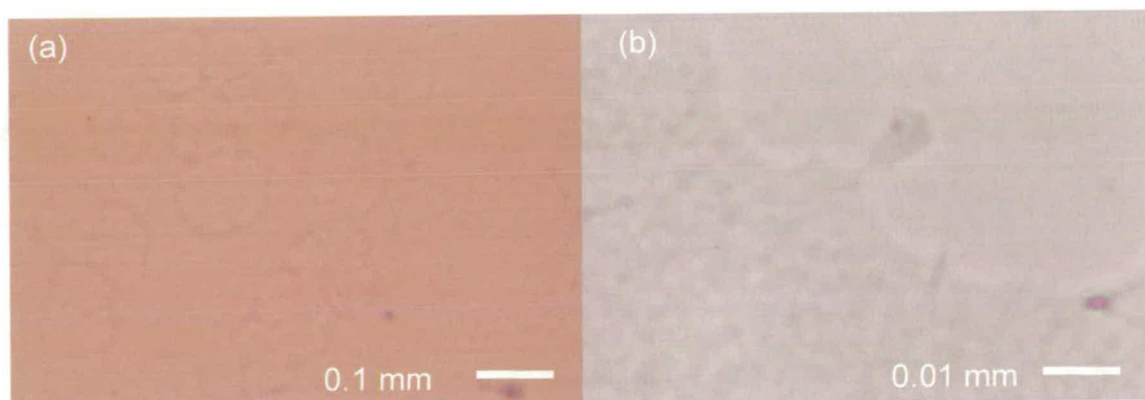


Figure 31: a) Texture of complex **1.47** under crossed polarisers after heating for 12 h at 40 °C. Aligned area at high magnification. Note that the contrast is low due to the thinness of the film and the field is light due to compensation by the camera.

Smoother substrates have been suggested to improve the homotropic alignment of thin films.⁴⁴ Complex **1.47** was therefore applied to gold coated silicon [111] substrates.

3.7.2) Attempted alignment, polymerisation and etching on gold

Complex **1.47** was spin cast in thin films on to gold coated silicon [111] substrates. Following annealing at 40 °C for 12 h the films were polymerised by irradiation with UV light at 365 nm. Etching was attempted by the procedure of Kim and co-workers. The films were stable to sonication in a 1:1 mixture of 3N aqueous HCl and methanol. XPS characterisation of the films is in progress; this technique gives elemental analysis on a surface, which should allow the disappearance of the nitrogen-rich core **47** to be monitored.

3.8) Conclusions to studies of complex **48.47 and **1.47****

We have designed and synthesised two variants of a supramolecular discotic liquid crystal developed by Kim and co-workers. Shortening of the alkyl chains of Kim's pentyl-derivatised benzotri(imidazole) core **2** to butyl derivatised benzotri(imidazole) **47** did not appear to have a great effect upon the liquid crystalline properties. The effect upon etching efficiency has yet to be determined. The complexes **1.47** and **1.2** have mesophase ranges of 21.9 to 74.9 °C and 23.0 to 74.7 °C respectively and both complexes exhibit the same lack of reversibility by DSC. Replacement of acrylate corona **1** with methacrylate **48** induced more reversibility and therefore eased the alignment process. Unfortunately polymerisation has not yet been successfully combined with alignment for complex **48.47**. Observing literature reports of crosslinking in columnar liquid crystals, it becomes apparent that initiators can be successfully incorporated into dendron-based systems where the number of wedges in a column is not precisely defined.^{75,38} On the other hand, classical discotic systems appear a lot more sensitive with reports of phase behaviour being disrupted by initiators.⁷⁹

4) Synthesis and properties of a novel distorted triphenylene

4.1) Introduction

The attempted synthesis of new hydrogen bonding receptors led to the discovery of 1,4,5,8,9,12-hexamethyltriphenylene - a molecule with a 'flipping twist'.

Disclaimer

The work detailed here is published as:

"1,4,5,8,9,12-hexamethyltriphenylene- a molecule with a 'flipping twist'" by Yi Wang, Andrew D Stretton, Mark C McConnell, Peter A. Wood, Simon Parsons, John B Henry, Andrew R Mount, and Trent H Galow. *J. Am. Chem. Soc.* 2007, 129, 13193-13200.

I, Andrew Stretton was personally responsible for the initial idea behind the paper (as an intermediate to triimide **9**), preparation of synthetic procedures, and vital optimisation of the synthetic steps. The remainder of the work was completed by the co-authors, as acknowledged on page 91. Note that American spellings are used in this chapter due to the location of publication.

4.2) Background to Twisted Molecules

Molecules that present functional groups in an atypical fashion, for example distorted from their preferred geometry, are intriguing targets for synthesis. Examples of systems previously examined include twisted amides⁸⁰ and nitro substituents⁸¹, and the highly distorted aromatic rings found in several triphenylenes, naphthalenes and pentacene cores.⁸²⁻⁸⁶ These systems are inherently higher in energy than their non-strained cousins and can be far more reactive - the reactivity being driven by release of steric strain.^{80,83}

Overcrowded “ D_{3h} ” symmetricⁱⁱ polycyclic aromatic hydrocarbons (PAHs) can adopt either a C_2 or D_3 (propeller-like) conformation.⁸⁷ The C_2 versus D_3 question is part of a wider issue regarding the driving forces underlying the conformational preference, i.e. sterics versus electronics, and considerable effort has been devoted towards resolving this point. Triphenylenes are a family that fit under the “ D_{3h} ” umbrella. Currently, only the moderately twisted peraryloxytriphenylene **58b**⁸⁸, perfluorotriphenylene **59**^{82,85} and the highly twisted perchlorotriphenylene **60**^{83,84b} molecules have been studied crystallographically, while aryloxy compounds **58a** and **58c**, and perbicyclo[2.2.2]octenetriphenylene **61**⁸⁹ have been synthesized but not characterized by X-ray.⁹⁰ However, Pascal et al. have suggested that halogen substituents may themselves have significant electronic effects which affect the structural characteristics.⁸⁷ As a result they concluded that “the presently available experimental structures are perhaps not the very best examples for an examination of the C_2/D_3 dichotomy”. They suggested and modeled four “ideal” candidates,^{iii,91} one of which was 1,4,5,8,9,12-hexamethyltriphenylene **36**. They predicted that **36** would adopt a C_2 conformation, as opposed to D_3 with the C_2 system being computationally more stable by greater than 7 kcal/mol⁻¹. Therefore, the experimental realization of **36** would provide a model system for investigating many of the key issues, including conformational interconversions – an almost uncharted area of knowledge for these hindered triphenylenes. We report here the synthesis and the complete characterization of compound **36**. This characterization includes X-ray crystallography, variable temperature ¹H NMR (VT-NMR), molecular modeling, fluorescence spectroscopy, and cyclic voltammetry (CV).

ii The D_{3h} symmetry is related to how molecules are drawn on paper. Often, these structures are drawn without ‘wedged bonds’ which is indicative of ‘ D_{3h} ’ symmetry – this can be misleading.

iii The experimental structures investigated were hexabenzotriphenylene, decacyclene, a hexa-*t*-butyldecacyclene, perfluorotriphenylene **58** and perchlorotriphenylene **59**. The three remaining theoretical structures examined, to the best of our knowledge, have not been synthesised. These are a hexamethyldecacyclene, and two isomeric hexafurotriphenylenes.

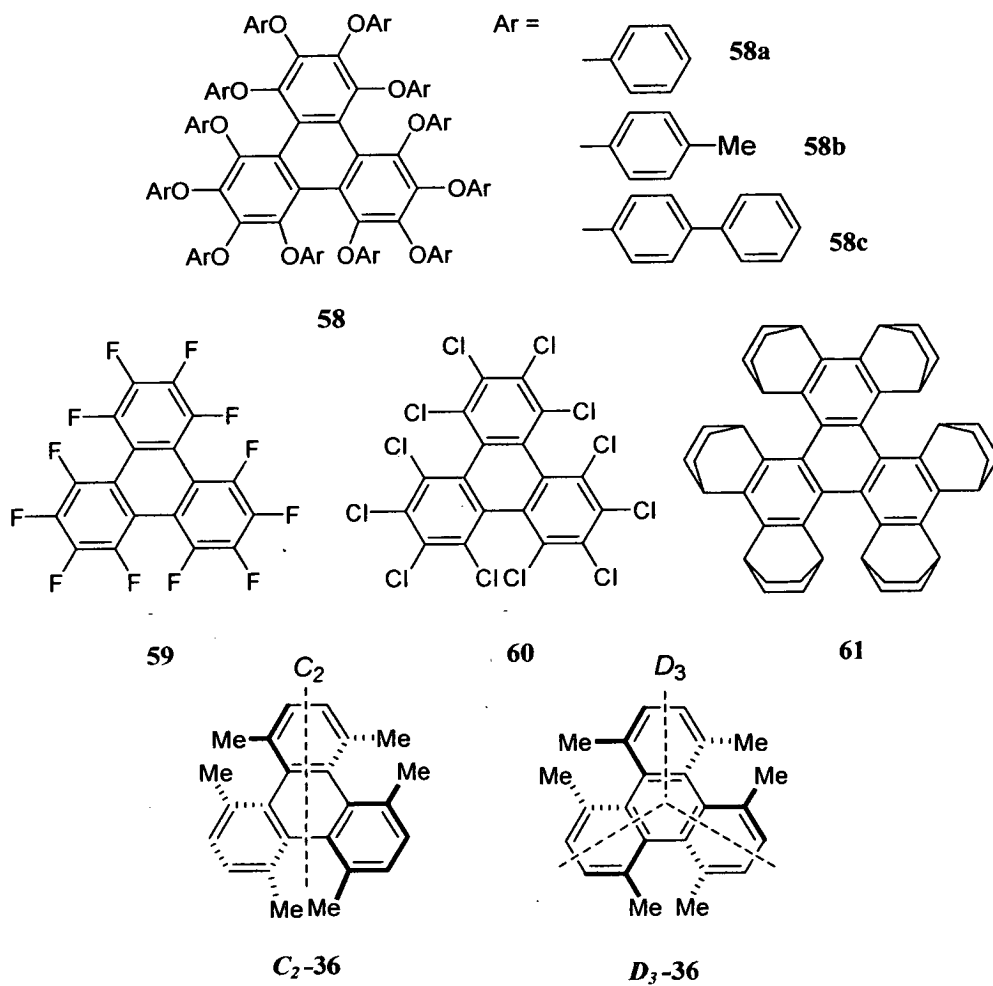
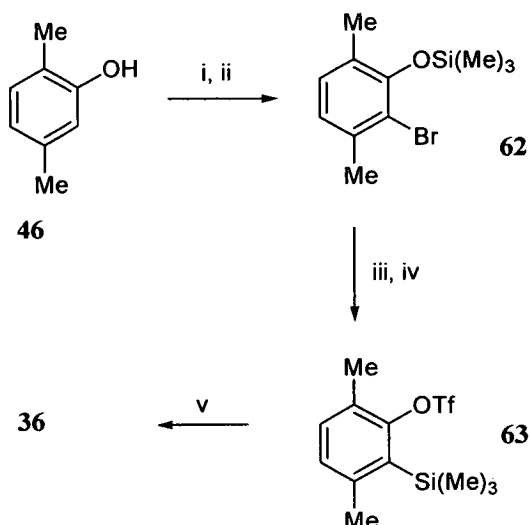


Figure 32: Known distorted triphenylenes containing no additional fused rings, and 1,4,5,8,9,12-hexamethyltriphenylene represented in the two possible conformations, C_2 and D_3

To prepare **36** we exploited the fact that arynes undergo metal-catalyzed cyclotrimerization reactions to afford polycyclic aromatics (Scheme 18).⁹²⁻⁹⁶ Treatment of commercially available 2,5-dimethylphenol **46** with NBS (15 °C) and hexamethyldisilazane (HMDS) afforded bromosilylether **62**. Sequential reactions with butyl lithium (BuLi) at -100 °C and triflic anhydride (-100 °C) provided the key *o*-trimethylsilylaryl triflate **63**. Then cesium fluoride was added in the presence of Pd catalyst to give **36** in 65% yield (33% overall).



Scheme 18: Synthesis of 1,4,5,8,9,12-hexamethyltriphenylene **36**. i. NBS, 15 °C, 78%. ii. HMDS, 80 °C; 98%. iii. BuLi, -100 °C. iv. Tf₂O, -100 °C, 66% (2 steps). v. CsF, Pd(dba)₂, 65%.

4.3) Examination of the NMR Traits of **36**

The ¹H NMR spectrum of **36** at 25 °C (Figure 33) revealed only two sharp peaks, one aromatic singlet (7.18 ppm; 3H) and one methyl singlet (2.45 ppm; 9H). Initially, this was suggestive of *D*₃ symmetry, which was possible given the observation by Guitián et al. and Bennet et al. that the *D*₃ hexabenzotriphenylene product could be formed as the kinetic product^{92,97} under similar mild reaction conditions. However, given Pascal's theoretical prediction that the *C*₂ conformer would be the thermodynamically most stable product, we decided to further characterize **36** using VT-NMR, X-ray crystallography, and computational modeling.

The results of the ¹H VT-NMR experiment are shown in (Figure 33). On decreasing the temperature from 25 to -80 °C, the parent peak associated with the aromatic protons (7.18 ppm; 25 °C) resolved completely into two broad singlets (7.21 and 7.05 ppm; 2H and 1H respectively; -80 °C), with partial resolution of the methyl singlet (2.45 ppm) into two overlapping broad peaks (2.41 and 2.35 ppm). From these data a coalescence temperature (*T*_c) of -55 °C (220 K) was determined, which reveals rapid room

temperature conformational interconversions between two C_2 enantiomers rather than the presence of one D_3 conformer in solution. The activation energy (E_a) associated with this C_2 - C_2 racemization, was calculated using:

$$E_a = \Delta G^\ddagger = RT_c[23 + \ln(T_c/\Delta\nu)]$$

where $T_c = 220$ K and $\Delta\nu = 57.6$ Hz. This gave $E_a = 10.20$ kcal/mol⁻¹, which is a relatively low activation barrier, given the expected magnitude of methyl steric interactions. The rate of this interconversion, k , at T_c , was determined by using the formula:

$$k = \pi\Delta\nu / \sqrt{2}$$

as 128 s⁻¹ iv. From the Arrhenius equation, assuming invariance of the frequency factor with temperature between T_c and 25 °C, this gives an estimate of k at 25 °C of 5.7×10^4 s⁻¹. This high interconversion rate explains the simple ¹H NMR spectrum that was observed at 25 °C.

It is interesting that only two distinct peaks were observed at low temperatures in the ¹H VT-NMR for the aromatic protons in Figure 33, rather than the three expected for this compound with C_2 symmetry. This is due to an accidental isochrony - two different types of proton with the same chemical shift (at 7.21 ppm at -80 °C). However, no accidental isochrony was observed in ¹³C VT-NMR investigations at this temperature (see Supporting Information). In fact the three aromatic peaks (132.900, 130.569, 128.771 (C-H) ppm) and one methyl peak (22.257 ppm) at 25 °C decoalesced into nine aromatic (133.997, 132.950, 132.731, 131.987 (C-H), 131.199, 130.143, 128.975, 128.836 (C-H), and 125.894 (C-H) ppm) and three methyl peaks (21.626, 22.734 and 23.174 ppm) at -80 °C respectively. This provides additional support for a C_2 symmetric conformation in solution.

iv The formula for determining rates is more commonly used for decoalesced peaks of equal intensity. However, the same formula can be applied to peaks of unsymmetrical intensities as seen in our VT NMR studies. Kost, D.; Carlson, E. H.; Raban, M. *Chem. Comm.* **1971**, *66*, 656-657.

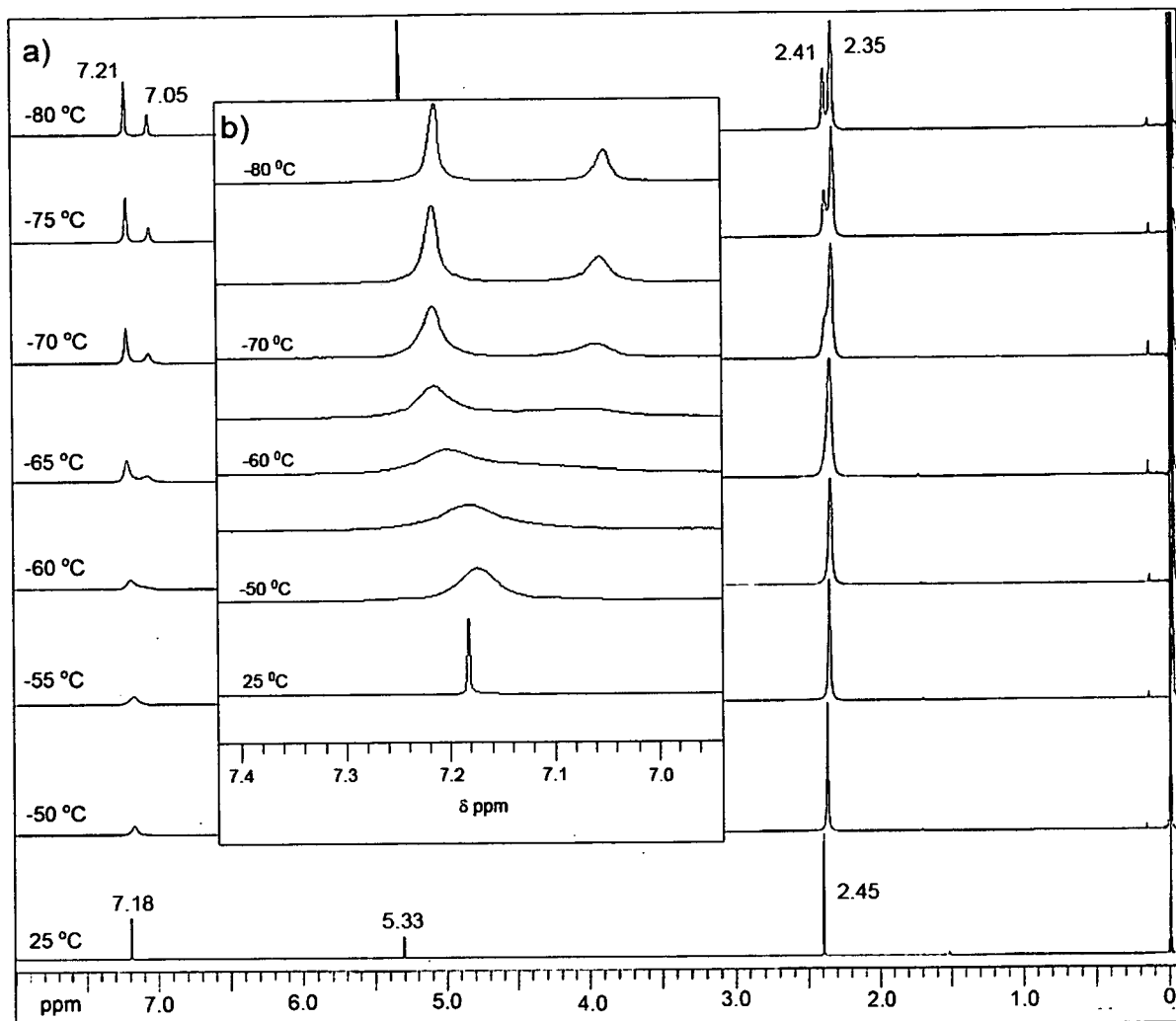


Figure 33: a) ^1H VT-NMR spectra of **36** in 3:1 $\text{CS}_2:\text{CD}_2\text{Cl}_2$ (360 MHz). Temperatures ranged from 25 to -80 $^\circ\text{C}$. The aromatic signal at 7.18 ppm (25 $^\circ\text{C}$) resolved into two new signals – 7.21 and 7.05 ppm (-80 $^\circ\text{C}$) and was concomitant with partial decoalescence of the methyl signal (2.45 ppm) into two overlying peaks – 2.41 and 2.35 ppm. ^1H NMRs calibrated using TMS (0 ppm). Signal at 5.33 ppm is CH_2Cl_2 . Note the ‘simple’ NMR of **36** at 25 $^\circ\text{C}$. b) Inset showing scale-up of the aromatic region.

4.4) X-Ray Crystallographic Studies of **36**

Unlike many other polyaromatic hydrocarbons (PAHs), compound **36** was found to be reasonably soluble in organic solvents. Colorless crystals suitable for X-ray studies were obtained by slow recrystallization of a saturated solution in ethanol. The X-ray structure of **36** is shown in Figure 34 in both framework and corresponding space-filled

representations.^{98,v} The crystal structure revealed a similar conformation to the highly twisted perchloro compound **60** and as a result, there are many parallels between the two systems. First, triphenylene **36** takes on a conformation with C_2 symmetry with very large deviation from planarity. This severe distortion enables alleviation of the 'C:C' non-bonded contacts between adjacent methyl substituents. Even so, the average of nine non-bonded contacts in the crystal structure was 2.976 Å, well within the sum of the van der Waals radii of two carbons (3.4 Å), which indicates significant steric interaction. The $C_{Ar}-CH_3$ radial bonds of **36** are all similar in length (the six radial distances were 1.506, 1.513, 1.510, 1.507, 1.501, 1.525 Å) with mean 1.510 Å. Second, rings B (C: 9-10-12-13-14-16) and C (C: 17-18-20-21-22-24) adopt boat conformations (Figure 2) with distortions approaching those of [8]paracyclophane.^{84b} The remaining naphthalene substructure, rings A and D (C: 24-17-16-9-8-1-2-4-5-6), exhibits a 53° end-to-end twist with the central ring A (C: 24-17-16-9-8-1) and ring D (C: 8-1-2-4-5-6) contributing 35° and 18° respectively to the overall twist. This value is similar to that for **60** in which a 56.6° twist is present⁹⁰. Third, strong bond alternation is seen in the central ring A (Figure 3). The endo bonds have mean length of 1.425 Å while the exo bonds average 1.478 Å. The existence of bond alternation means that **36** can be regarded as three benzene rings (B, C and D) linked together by bonds of low order. Indeed it can be argued that it is the drive for "conservation of aromatization" in B, C and D which induces such close C:C contact between the neighboring methyl groups. This seems to be a common trait in triphenylene compounds, such as triphenylene itself, peraryloxy **58b**, perfluoro **59** and perchloro **60**. These properties lend significant weight to the argument that the geometries of these systems are governed by electronics and not

v (a) The crystal is a pseudo-merohedral twin. Parsons, S. "Introduction to twinning." *Acta Cryst.* **2003**, Section D: Biological Crystallography *D59*, 1995-2003. (b) The crystal structure contains three crystallographically independent molecules. The majority of molecular crystal structures form with one molecule in the asymmetric unit. T. Steiner, "Frequency of *Z'* values in organic and organometallic crystal structures." *Acta Cryst.* **2000**, *B56*, 673-676.

sterics. Further evidence supporting this dictum is provided by the electrostatic potential maps of the C_2 and D_3 conformers of **36** (see Supporting Information).

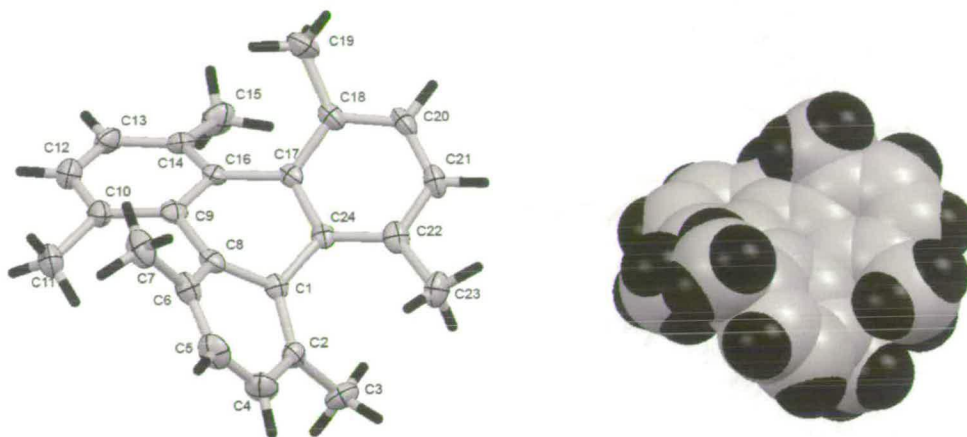


Figure 34: Molecular structure of **36** at 150 K (left) and the corresponding space-filled form (right). Hydrogen atoms shown in black. Thermal ellipsoids have been drawn at 50% probability.

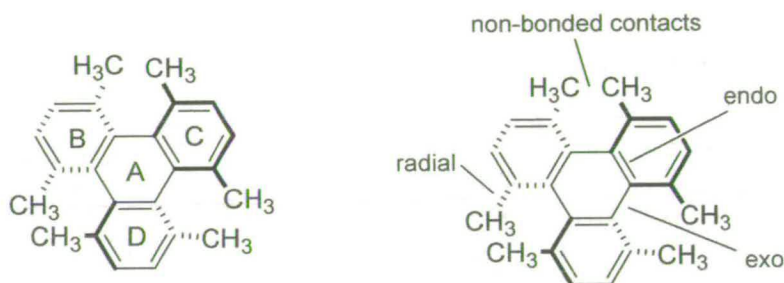


Figure 35: Structures showing ring labels and assignment of bond-types for **36**. The wedge drawings correspond to the conformation present in the crystal structure in Figure 2. Mean bond lengths (Å): endo=1.425; exo=1.478; non-bonded contacts=2.976; radial=1.510.

At first glance, the experimental data seem to fit with Pascal's computational predictions⁹ well. In particular, there are two aspects of the comparison that can be examined more closely. First, the circumference, which is measured as '3 exo + 3 endo bond lengths', arrived at from the computations can provide a good indicator of the actual conformation. It was stated that circumferences greater than 8.6 Å would be associated with C_2 conformations. The predicted circumference was 8.72 Å which matches well with the observed circumference of 8.71 Å and the resulting molecular shape. Second, it was anticipated that strong bond alternation in the central ring A would

exist, typical of a C_2 conformer, and that exo and endo bonds with average lengths of 1.491 Å and 1.417 Å respectively would be seen. These values are reasonably close to the 1.478 Å exo and 1.425 Å endo bonds lengths observed for **36**. The difference appears to be an overestimation of the distortion by these HF/3-21G(*) computations. Since non-bonded contact distances were unavailable and only low level semiempirical (MNDO, AM1, PM3) and ab initio Hartree-Fock (STO-3G, 3-21G(*)) C_2 and D_3 ground state computations without temperature correction were conducted by Pascal for hexamethyl **36**,⁹ we decided to use density functional theory (DFT) computational methods with enhanced basis sets, which were expected to be more accurate, to examine closely the ground states of the C_2 -**36** and D_3 -**36** conformers, and the proposed transition states for C_2 - C_2 racemization and C_2 - D_3 interconversion at 298.15 K.

4.5) Molecular Modelling of Compound **36**

Ground state C_2 and D_3 structures were calculated using the GAUSSIAN 03 program.⁹⁹ These stationary structures were confirmed as energy minima by means of vibrational analysis and the presence of zero imaginary vibrational frequencies. The geometries obtained were fully optimized both using a lower level ab initio HF/6-31G (d,p) calculation, and an extended DFT B3LYP level using the basis sets 6-31G-(d,p) and 6-311G(d,p).^{vi,vii,viii,ix} Concomitant with the ground state studies, the transition states were initially located using semiempirical AM1 calculations implemented in GAUSSIAN 03. These geometries were then fully optimized and confirmed as energy maxima using

vi All calculations were run on the EaStCHEM research computing facility's Edinburgh computer cluster (<http://www.eastchem.ac.uk/rcf>).

vii The structures of all molecules were drawn using the visualization freeware Arguslab.

viii Output was viewed using the Gabedit visualization software freely available from the internet.

ix Images (Figure 4) were rendered using POV-Ray (Persistence of Vision Raytracer) freeware.

HF/6-31G & HF/6-31G (d,p) and B3LYP/6-31G-(d,p) & B3LYP/6-311G(d,p) functionals and basis sets. The fully optimized structures for the C_2 -**36** and D_3 -**36** conformers, and the proposed transition states for C_2 - C_2 racemization (TS-I) and C_2 - D_3 interconversion (TS-II) are represented in Figure 36 together with the corresponding wedge structures which demonstrate both the geometry and symmetry of these systems. The relative disposition of the six methyl groups can be clearly seen.

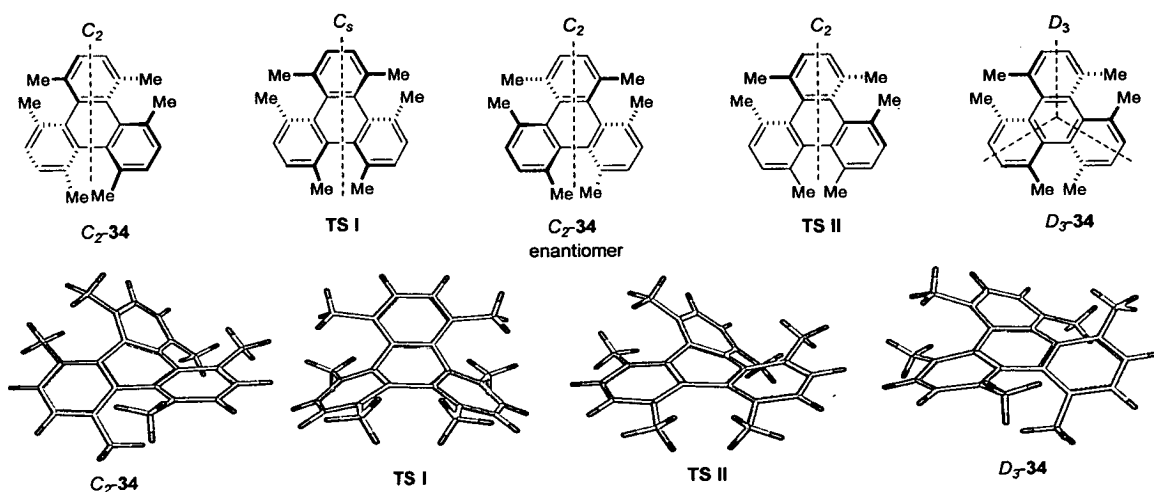


Figure 36: Schematic drawings of the C_2 and D_3 conformations and the transition states of hexamethyltriphenylene **36** (above). Corresponding optimized molecular geometries for the B3LYP/6-311G(d,p) functional and basis set (below).

The two transition states presented in Figure 36, TS-I and TS-II, are shown using the B3LYP/6-311G(d,p) method and basis set; they correspond to the C_2 - C_2 and C_2 - D_3 interconversions respectively. Looking closely at these structures, it can be seen that TS-I presents ‘saddle-shaped’ C_s symmetry which results in a relatively low activation barrier, while TS-II is a more distorted C_2 system and is consistent with a considerably higher barrier to interconversion. The higher free energies calculated for the D_3 conformer (Table 3) explains the formation of the C_2 as the most stable thermodynamic product. To confirm that the C_2 conformer was thermodynamically most stable we heated a small quantity of hexamethyltriphenylene **36** in DMSO- δ_6 at 170 °C for six

hours. A carefully calibrated ^1H NMR verified no change in the spectrum. It is interesting that this synthetic method has always previously given the C_2 conformation as the initially formed product even when this is not the most thermodynamically stable as seen for the formation of the kinetic C_2 hexabenzotriphenylene product.⁹⁷ The formation of the thermodynamic product suggests that these synthesis conditions favor the formation of a molecule with C_2 symmetry, perhaps because the reaction components come together in such a way that the transition state closely resembles the C_2 rather than D_3 structure.

Table 3: Temperature Corrected Calculated Free Energies of Ground States and Barriers to Conformational Interconversions (Activation Energies) in kcal/mol at 298.15 K relative to the C_2 Ground State.

method	D_3 Conformer	C_2 - C_2 <i>TS-I</i>	C_2 - D_3 <i>TS-II</i>
		Exptl: kcal/mol	10.20
AM1	+1.41	+7.84	+23.98
HF/6-31G	+6.44	+11.11	+30.40
HF/6-31G (d,p)	+5.91	+10.93	+29.42
B3LYP/6-31G (d,p)	+4.97	+9.80	+25.42
B3LYP/6-311G(d,p)	+4.97	+9.64	+25.47

Some deviation in the quantitative data in Table 3 is clearly seen, as a result of the differing levels of theory employed for the calculations. Semiempirical AM1 has been shown to be fairly effective at modeling similar barriers observed in hexabenzotriphenylene^{86a} but underestimated the C_2 - C_2 barrier of 36, as is shown by this temperature corrected data. Ab initio Hartree-Fock calculations are known to overestimate energy barriers to conformational interchange, and as expected give greater

values for both C_2-C_2 and C_2-D_3 conformational interchanges than the other methods. The variation of these Hartree-Fock barriers could be the result of neglecting electron correlation effects, which are anticipated to be significant for the conformational interconversions that proceed via greatly distorted transition states.^{97a} The best agreement between the calculated and experimental activation energies (within 0.4 - 0.6 kcal/mol) was achieved by using DFT calculations using the B3LYP functional with two basis sets, 6-31G(d,p) and 6-311G(d,p), consistent with the fact that DFT takes into account electron correlation effects. Such differences are small, and may be due to the effects of solvation (not considered in these calculations). All calculated C_2-D_3 energy barriers were similar and significantly higher than the C_2-C_2 barriers.

To ascertain the degree of fit between the computed C_2 ground state structures and the X-ray structure, root mean square deviations (RMSDs)^x were calculated using the Visual Molecular Dynamics (VMD 1.8.5) program.^{xi} These analyses revealed that all the carbon skeletons of the modeled geometries matched the corresponding backbone of the X-ray structures very well (RMSD range: 0.028-0.056), although some discrepancies were observed. As expected, the B3LYP/6-31G(d,p) & B3LYP/6-311G(d,p) produced C_2 conformers with the best fit (mean 0.040 and 0.042 respectively). Furthermore the non-bonded contacts were best handled by these DFT methods - the average distance for nine contacts in the crystal^{xii} was 2.976 Å, while 2.996 Å (6-31Gd,p) and 3.003 Å (6-311Gd,p) were observed for the DFT structures. The HF/6-31G and HF/6-31G (d,p) geometries (mean 0.045 and 0.047 respectively) showed greater deviation when compared to the DFT methods, which may be due to the lack of electron correlation effects in the calculations.⁹² However, the non-bonded contacts – 3.000 Å (6-31G) and 3.005 Å (6-31Gd,p) - were reasonably close to the experimental value. The AM1 conformer (mean 0.045) seemed to provide a similar overall match to the crystal data as

x Due to the presence of poorly diffracting hydrogen atoms, only the carbon backbones were compared.

xi VMD 1.8.5 program available from internet.

xii All nine distances (Å): 3.007, 2.938, 2.967, 3.005, 2.985, 2.941, 2.955, 2.954, 3.030.

HF, however the non-bonded contacts (2.908 Å) were grossly underestimated – a problem which has been observed prior to this study.⁸⁷ The exo (1.478 Å) and endo (1.425 Å) bonds lengths, seen in the crystal structure, were matched best utilizing the B3LYP/6-31G(d,p) & B3LYP/6-311G(d,p) functionals and basis sets. These gave corresponding mean lengths of 1.481 Å exo and 1.433 Å endo and 1.479 Å exo and 1.431 Å endo. Both of these methods afforded extremely good fits and show the value of employing the DFT calculations for these systems. The HF and AM1 methods gave poorer fits, both underestimating the degree of distortion.

All calculations in Table 3 demonstrated that the C_2 - D_3 energy barrier is substantially higher than the one for the C_2 - C_2 interconversion. An interesting upshot of this high barrier is the implication that methyl flipping, between neighbouring methyl substituents, mostly occurs when the resulting conformer is C_2 , not D_3 . By analysing the conformational dynamics, a complete picture for **36** is provided (Figure 37). Conformer **A** has three possible sites for flipping, the neighbouring methyl substituents at the 1,12-, 4,5-, and 8,9- positions. First, flipping of the 8,9-methyl groups affords **B** which is a D_3 system, so is unfavorable. Second, the 4,5-methyl interchange is favorable as it provides **C** which presents C_2 symmetry. Third, the 1,12-exchange is also favorable providing the C_2 conformer **D**. If this exchange is followed by a 8,9-flip conformer **E** with C_2 symmetry results, meaning that the 8,9-flip is now favorable (*c.f.* **A** to **B**). In a short time, all the methyl groups are rapidly scrambled ($k = 5.7 \times 10^4 \text{ s}^{-1}$), with the flipping mechanism proceeding mainly through low energy C_s transition states; rapid flipping manifests itself as single sharp peaks in the NMR spectrum (Figure 33a).

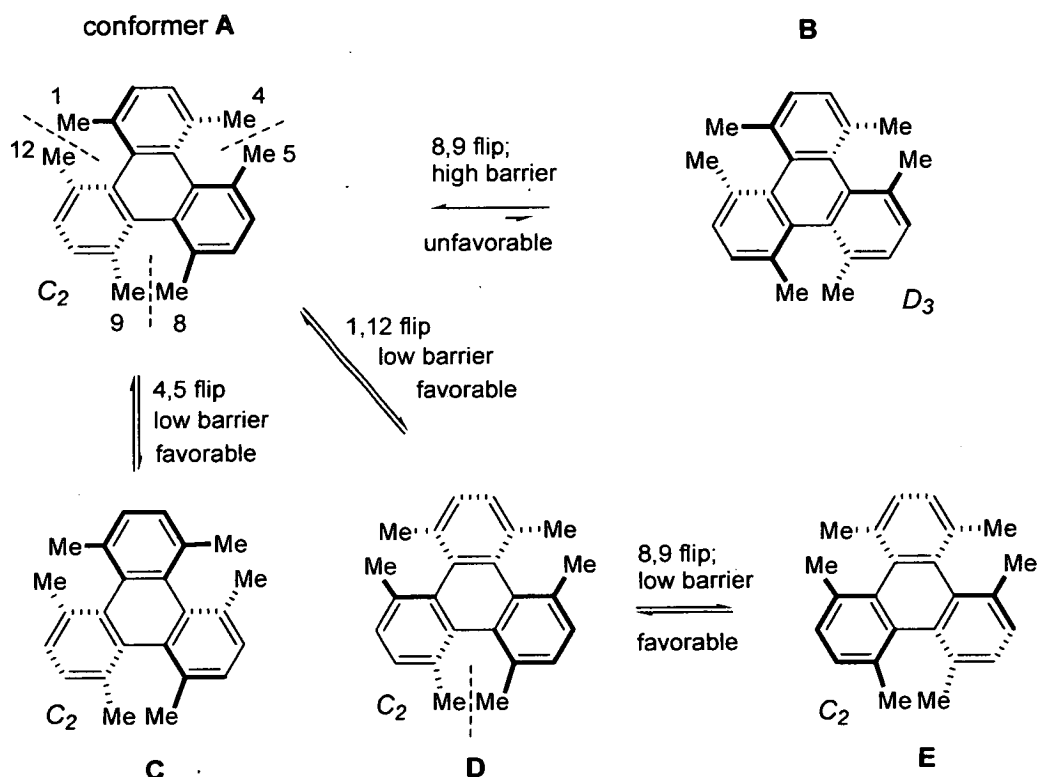


Figure 37: Wedge drawings of **36** illustrating the rapid conformational interconversions that provide averaged ^1H NMR signals. Computations indicate that the mechanism proceeds chiefly through successive low barrier C_2 - C_2 interchanges.

4.6) Conformational Analyses of Hindered Triphenylenes 1-4.

This is the first time that solid evidence has been provided for the dynamic conformational interconversion mechanism for this class of hindered triphenylenes. Pascal's group was the first research group to propose possible dynamic exchange between two enantiomers after synthesizing perchloro **60**.⁸³ Low level AM1 calculations of this system were conducted after failing to resolve the enantiomers by conventional means, and hinted at the possible existence of racemization that progressed via a low energy barrier – where the calculated C_2 - C_2 and C_2 - D_3 barriers were 7.0 and 26.1 kcal/mol respectively. However, due to the physicochemical make-up of **60** it is not possible to validate this. Perfluorotriphenylene **59**, unlike **60**, does have useful NMR active nuclei for investigating the conformational dynamics in solution. ^{19}F NMR was

performed at only 25 and -40 °C with the conclusion that “a propeller-like distortion (D_3) must exist in solution”,^{82,85} even though a C_2 structure was observed in the crystal (the thermodynamic product), and there was no suggestion of conformational interchange. Since we believe an incomplete picture for **59** persists, we performed AM1 and B3LYP/6-311G(d,p) computational studies on this molecule. Similar to our system, perfluorotriphenylene **59** can undergo dynamic conformational interchange, although with a slightly different mechanism. The 6-311G(d,p) C_2 - C_2 and C_2 - D_3 barriers – 1.96 and 6.57 kcal/mol respectively - are *both* low.^{xiii} As a consequence, both the C_2 - C_2 racemization and C_2 - D_3 interconversions can occur very rapidly and easily at room temperature, which gives rise to the appearance of a sharp averaged ‘ D_3 ’ NMR signals in solution, even at -40 °C. Neither the peraryloxytriphenylenes **58a-c** nor perbicyclo[2.2.2]octenetriphenylene **61** were investigated for any type of conformational interchange as no low temperature NMR studies were reported. However, we anticipate that dynamic conformational interconversions do occur for all these systems although to varying degrees. For aryloxy compounds **58b**, the C-O *inner* bond length is 1.377 Å and the van der Waals radius for oxygen is 1.4 Å.⁸⁸ Given that these are slightly longer and larger than the corresponding values for the C-F bonds of **59** (1.330 Å; vdW radius F = 1.35 Å), then it seems reasonable to imagine that dynamic conformational interchange is present and occurs rapidly at room temperature, at a rate somewhere between that observed for **59** and **36**. Supporting evidence is provided by the low-level AM1 calculation on a *mimic* of **58** which suggests that the C_2 - C_2 barrier is approximately 6.08 kcal/mol.^{xiv,xv} For peroctene **61**, the steric demands are expected to be greater than for

xiii The AM1 barriers were 0.82 and 3.45 kcal/mol for the C_2 - C_2 and C_2 - D_3 barriers respectively.

xiv Due to the size and complexity of peraryloxyriphenylene **58b**, a mimic was employed in the modeling calculations. Six phenyl groups were replaced with methyls at the 2,3,6,7,10 and 11 positions. However only the 1,4,5,8,9 and 12 positions are involved in the distortions and were left unchanged. A complete structure of the mimic can be seen in Experimental Section.

perchloro **60** and hexamethyl **36**, since molecular modeling studies predicted a 61° twist, although this not been verified by X-ray characterization. If correct, this implies that that any conformational interconversions are likely to proceed, mechanistically, in a similar manner to **60** and **36**, although with higher activation barriers. A C_2-C_2 transition state was located at the AM1 level and produced a barrier of 7.33 kcal/mol.^{xv} Surprisingly this was very close to that provided for **60** and **36** indicating a rapid interconversion at room temperature.

xv We assume that the underestimation that occurs for the AM1 barriers for hexamethyl **36**, also occurs for **58b** and **61**.

4.7) Fluorescence Spectroscopy of 36

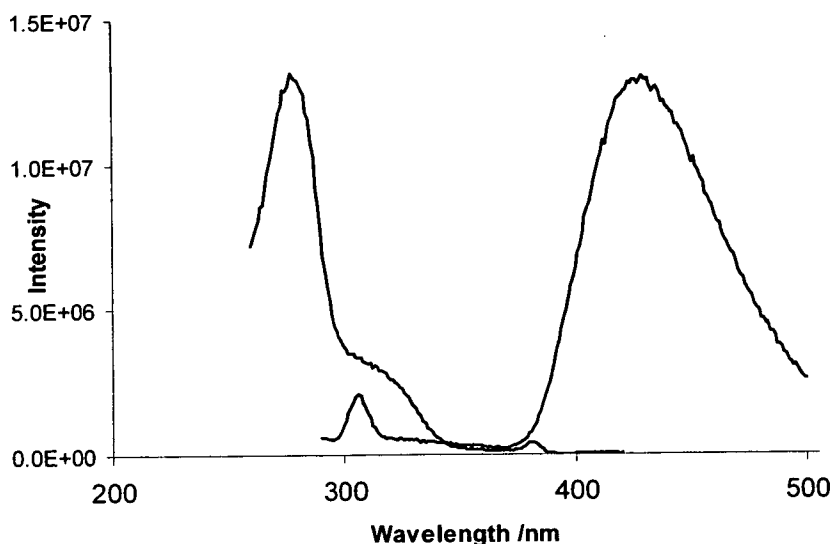


Figure 38: Excitation (at the peak emission wavelength, $\lambda_{em} = 430$ nm, left) and emission (at the peak excitation wavelength $\lambda_{ex} = 280$ nm, right) spectra for 36. $[36] = 1 \times 10^{-6}$ M in ethanol. Quantum yield (ϕ_F) was 7% when measured with comparison to indole ($\phi_F = 0.4$). The emission peak seen near 310 nm and excitation peak near 380 nm are both solvent Raman bands. The quantum yield was estimated by making a comparative measurement using indole as standard, which has a known quantum yield of 40% in ethanol solution¹⁰⁰. Low ($\sim \mu\text{M}$) comparable concentrations of sample and standard were used to ensure that inner filter effects were negligible. For both sample and standard, the quantum efficiency is proportional to the ratio of the integrated emission intensity (the area under the measured emission spectrum) to the integrated absorption intensity (the area under the measured absorption spectrum).

Steady-state fluorescence spectroscopy showed that hexamethyltriphenylene **36** is fluorescent, emitting light in the blue region of the spectrum (Figure 38). Currently the study of this class of compounds is highly desirable due to their potential applications in optoelectronics such as in organic light emitting diodes (OLED).¹⁰¹ A large Stokes shift ($\Delta\lambda = 110$ nm) between the first absorption maximum ($\lambda_{\text{max}} = 320$ nm) and the emission maximum ($\lambda_{\text{max}} = 430$ nm) was observed. This is consistent with a relatively large change in molecular configuration on excitation. This is expected, as excitation should involve a π - π^* electronic transition, resulting in a decrease in π -bonding and an increase in the importance of steric repulsion. The quantum yield for fluorescence (ϕ_F) of **36** was measured as 7% at room temperature. These spectral characteristics are comparable to a dibenzotriphenylene derivative previously studied which also gives blue fluorescence and a similar quantum yield.¹⁰²

4.8) Electrochemical Investigation of 36

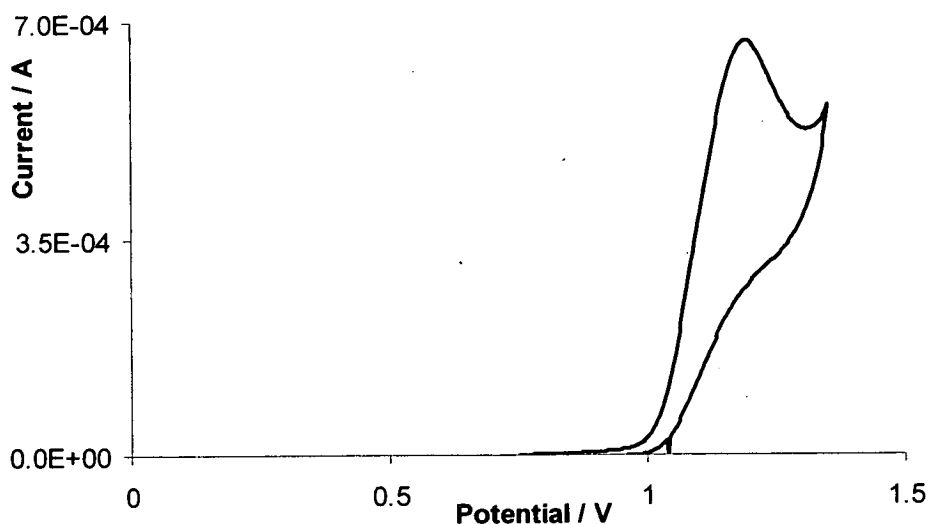


Figure 39: Cyclic voltammogram of 36. [36] = 1 mM in background electrolyte solution of 0.1 M anhydrous LiClO₄ in acetonitrile (dried; distilled). The reference electrode was made in-house and consists of a Ag wire dipped into a solution of AgClO₄ (0.01 M) in background electrolyte solution, with a measured potential of -0.074 V vs the Fc/Fc⁺ couple. The counter electrode was a 2 cm² Pt gauze and the working electrode was a 0.387 cm² Pt rotating-disc electrode. These were controlled by an AUTOLAB PGSTAT30 potentiostat (Eco Chemie B.V) equipped with GPES 4.9 software.

Cyclic voltammetric (CV) analysis of hexamethyltriphenylene **36** (Figure 39) showed an irreversible one-electron oxidation wave ($E_{pa} = 1.10$ V vs Fc/Fc⁺) at all sweep rates studied between 20 mV/s and 500 mV/s. This behavior is analogous to the previously observed irreversible one electron oxidation of the unsubstituted triphenylene ($E_{pa} = 1.50$ V in benzonitrile vs Fc/Fc⁺).⁸⁹ As might be expected, consistent with the electron donating nature of the six methyl substituents, the oxidation peak of **36** was intermediate between unsubstituted triphenylene and proctenetriphenylene **61**, where **61** exhibited a reversible one-electron oxidation wave ($E_{1/2} = 0.44$ V vs Fc/Fc⁺). Komatsu et al. stated that the dramatically decreased oxidation potential of **61** was due to the intrinsic electronic effects of annelation with the bicyclo units which raise the HOMO level of the π -system, through the inductive electron donation and σ - π interactions, coupled with the

additional elevation of the HOMO resulting from the large deviation from planarity. It is possible that the electrochemical reversibility of **61** may be due to the very bulky nature of the bicyclo units, which provide a 'protective shell' (akin to site-isolation) surrounding the oxidized species, preventing it from showing the enhanced reactivity usually seen in these strained systems by undergoing further chemical reaction to form redox inactive species. This would not be the case for **36** and triphenylene, for which rearrangement and/or intramolecular coupling reactions are likely. For this reason it would be intriguing to synthesize and electrochemically characterize a permethylated triphenylene, which would be completely peripherally protected against intramolecular coupling through complete functionalization with twelve methyl substituents.

Calculations of the temperature corrected free energies of **36** and the one electron oxidation product $36^{+\bullet}$, each with C_2 symmetry, along with those for indole (In) and the one electron oxidation product of indole ($In^{+\bullet}$) were carried out using B3LYP/6-311G(d,p) at 298.15 K in acetonitrile, using the polarizable continuum model (PCM)^{xvi}. This resulted in a calculated oxidation potential of **36** as +1.11 V vs Ag/Ag⁺ (0.01 M), compared with the experimentally observed value of +1.14 V. Given that equivalent calculations showed $D_3-36^{+\bullet}$ to be of significantly higher energy than $C_2-36^{+\bullet}$, this good agreement between experimental and calculated oxidation potentials supports the formation of the more thermodynamically stable $C_2-36^{+\bullet}$ as the oxidation product.

xvi It has previously been shown that accurate calculation of absolute values of experimental indole oxidation potentials is possible to within a few tens of millivolts, making this suitable as a reference redox reaction. Calculation of the free energy of the reaction $36^{+\bullet} + In \rightarrow 36 + In^{+\bullet}$ gives the oxidation potential of **36** relative to In. This can then be converted to a calculated oxidation potential on any reference scale by using the experimentally measured value of the indole oxidation potential. Experimental oxidation potentials are obtained from the measured peak potentials, E_p , as $E_p - E_{1/2} = 28.5$ mV for a reversible one electron redox reaction at 298 K, and the half-wave potential $E_{1/2}$ can be considered equal to the standard redox potential (the oxidation potential) when reactants and products have similar diffusion coefficients in solution. Kettle, L.J.; Bates, S.P.; Mount, A.R.; *Phys. Chem. Chem. Phys.* **2000**, *2*, 195-201.

The calculated structure of C_2 -**36**⁺ (Figure 40) shows an increased twist in the naphthalene substructure, with rings A and D (C: 24-17-16-9-8-1-2-4-5-6), exhibiting a 60° end-to-end twist. This is consistent with the calculated increase in the methyl separations (C: 3-23 and C: 7-11) from 2.99 Å to 3.02 Å, and can be attributed to an increase in the importance of steric repulsion due to the reduction in aromaticity brought about by removal of a π -electron. This increased twist also appears to affect electronic delocalization (Figure 40). In **36**, electron density can be seen to be distributed across the entire aromatic system. However, on oxidation a region of lower electron density (darker blue) can be seen where ring D joins ring A (Figure 2) along with a region of higher electron density (green area) in rings B and C. Significant bond lengthening is also found in four of the six C-C bonds in ring D (see Supplementary information). This is consistent with the increased twist in ring D decreasing π -bonding and electronic delocalization in and around this ring.

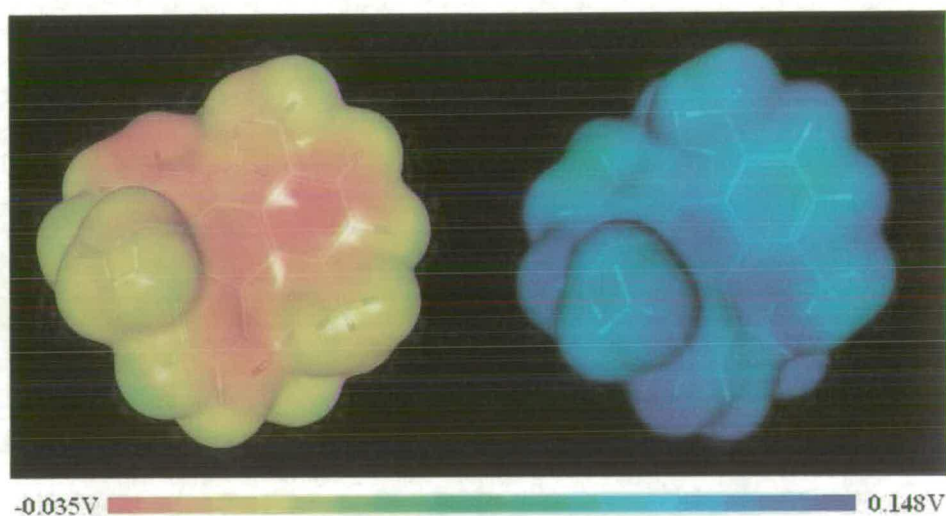


Figure 40: Electrostatic potential maps for the optimized geometries of **36** and **36**⁺. Red is electron rich, blue is electron poor. As well as the overall decrease in electron density on oxidation (an overall shift in color from red to blue), the potential map for **36**⁺ also reveals the decrease in π -bonding and delocalization after oxidation – a blue electron poor region is clearly seen where ring D is joined to ring C.

4.9) Conclusions

In summary, the model compound 1,4,5,8,9,12-hexamethyltriphenylene **36** has been prepared for the first time. X-ray studies have revealed a highly distorted C_2 structure with 53° end-to-end twist. We have shown through experiment and computation that **36** displays dynamic conformational interchange in solution, and have provided computational evidence that this phenomenon is active in all hindered triphenylene systems. We have also shown it to be fluorescent in the blue and electroactive, as well as possessing good solvent solubility and electroactivity. Fluorescence, electrochemical measurements and calculations have shown that both the excited state and oxidized forms of **36** show significant differences in geometry, consistent with the decrease in π -bonding brought about by excitation and by oxidation, which leads to an increase to 60° end-to-end twist.

5) Future Work

5.1) New liquid crystalline complexes

Supramolecular liquid crystals of the core + corona type described in this work are yet to reach the levels of order associated with conventional covalent systems. Interestingly, attention in this area has moved from concentrating upon symmetric molecules to those with dipoles.¹⁰³ This might be a route to gaining greater alignment control.

5.2) Alignment of liquid crystal complexes

In order to overcome the difficulties in aligning liquid crystals on surfaces, a new technique has recently been developed.⁴⁶ An elastomeric stamp can be moulded and smoothed to nanometre precision. When placed on top of a film in the isotropic state, the elastomer is wetted uniformly by the liquid crystal. This removes the surface tension effects at the air interface and causes the liquid crystal phase to align as for the pressed film (Figure 29, p64).

5.3) Polymerisation of aligned films

Initially an attempt must be made to characterise the films of complex 1.47 using the above alignment technique. If the films are proved not to align on gold, a new complex will be required with lower melting point. Kato and co-workers successfully formed aligned films incorporating initiator, the key point was the lower isotropisation temperature of their material.¹⁰⁴

5.4) Formation of Nanoporous Arrays

The realisation of the etching step may help to confirm the structure of the aligned film. Further etching experiments should be conducted using a variety of solvent mixtures to remove the benzotri(imidazole) from the polymer matrix. Electrochemistry could be used to detect whether the pores reach the substrate, XPS to determine that the nitrogen-rich core has been removed and AFM to visualise the pores.

5.5) Further Extensions

Chapter 4 presents a mutually exclusive line of research, nevertheless, the silyl triflate intermediate developed for the synthesis of 1,4,5,8,9,12-hexamethyltriphenylene could be very useful for the synthesis of other distorted aromatics. Studies have begun in this area with some promising results; not presented here as inconsistent with the project title. Orthogonal benzyne precursors could be applied in a combination of benzyne Diels-Alder reactions⁴² and palladium cyclisations.¹⁰⁵ This would allow an efficient modular approach to large “twistacenes” previously synthesised by low-yielding linear syntheses.

Acknowledgements

I am grateful to the following:

- Dr. Trent Galow giving me the opportunity to research such an interesting area of science.
- For the liquid crystal project: Jürgen Huck, Chris Wong and Rob Horner for some related syntheses, Dr. Olivier Gaudin and Prof. Ifor Samuel for our collaboration and particularly for the ellipsometry, Alistair Kilgour for DSC training, Dr. John Craven for help with the microscopy, Dr. Steve Francis for help with IR spectroscopy, Dr. Nic Mellor for training on X-ray scattering, Dr. Ron Brown for XPS work, Prof. Mark Bradley for use of a UV lamp and custom built hotstage, and Toby Cull for useful discussions.
- For the Molecule with a Twist: Yi Wang for initial synthetic and ^1H NMR work. Mark McConnel for molecular modelling, John Henry and Dr. Andrew Mount for our collaboration, manuscript preparation, electrochemistry, fluorescence and related modelling of the oxidised systems, Peter A. Wood and Dr. Simon Parsons for single crystal X-Ray diffraction, Dr. Andrew Turner, Dr. Herbert Fruchtl, Prof. David Leigh, Dr. Ian Sadler, Dr. Anita Jones, John Miller, and Jaclyn Henderson for useful discussions.
- This work has made use of the resources provided by the EaSTCHEM Research Computing Facility (<http://www.eastchem.ac.uk/rcf>). This facility is partially supported by the eDIKT initiative (<http://www.edikt.org>).
- The University of Edinburgh and The Royal Society for funding.

- Elise, whose steadfast tolerance and understanding has lifted me whenever all seemed lost.

Experimental section:

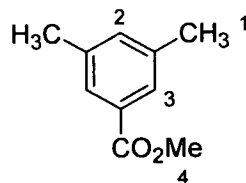
<i>Experimental section:</i>	92
Materials and methods	94
Preparation of methyl (3,5-dimethyl)benzoate (14).....	95
Synthesis of methyl (3-(bromomethyl)-5-methyl)benzoate.....	95
Formation of methyl (3,5-di(bromomethyl)benzoate ¹⁰⁷ (11).....	96
Generation of 1,3-bis(triisopropylsilyloxy)propan-2-ol (38).....	97
Preparation of 3,5-bis(1,3-di(triisopropylsilyloxy)propyl-2-oxymethyl)benzoic acid (39)	98
Synthesis of 1-bromo-9-methacroyloxynonane (13) by Mitsunobu esterification	99
Generation of pivaldehyde dimethyl acetal (43).....	100
Synthesis of 2- <i>tert</i> -butyl-1,3-dioxycyclohept-5-ene ⁶⁸ (21).....	100
Preparation of 1,3-dioxy-2- <i>tert</i> -butyl-5- <i>p</i> -styrylcyclohept-4-ene (19)	101
Attempted synthesis of 2,4,6-tris(1 -benzylimidazol-2-yl)-1,3,5-triazine (24) via nucleophilic substitution	102
Formation of 1-benzyl-2-cyanoimidazole ⁷¹ (26)	103
Attempted synthesis of 2,4,6-tris(1-benzylimidazol-2-yl)-1,3,5-triazine (24) via cyclotrimerisation of 1-benzyl-2-cyanoimidazole (26)	104
Preparation of <i>N</i> -(2-amino-2-oxoethyl)benzamide (44)	105
Synthesis of <i>N</i> -(aminomethyl)benzamide hydrochloride (45).....	106
Preparation of <i>N</i> -(aminomethyl)benzamide (31)	106
Synthesis of 3,5-dichloro-2,4,6-trinitroanisole (50).....	107
Synthesis of 1,3,5-trichloro-2,4,6-trinitrobenzene (51)	107
Synthesis of 1,3,5-triamino-2,4,6-trinitrobenzene (52).....	108
Synthesis of 2,2',2''-Tributylbenzotris(imidazole) (47).....	109
Preparation of 3,4,5-tris(11'-hydroxyundecyloxy)benzoic acid (55)	110
Synthesis of 3,4,5-Tris(11'-acryloyloxyundecyloxy)benzoic acid ⁷⁶ (1)	111
3,4,5-Tris(11'-methacryloyloxyundecyloxy)benzoic acid (48)	112

Liquid crystal analysis details	113
Procedure for formation of supramolecular complexes 48.47 and 1.47	114
Bulk measurements:	115
<i>Differential Scanning Calorimetry</i>	115
Polarised optical microscopy on bulk material	121
<i>Calibration of the stage</i>	121
X-ray scattering to observe liquid crystal phase of complex 1.47	124
Bulk polymerisation	125
Thin film measurements.....	129
<i>Representative procedure for spin-casting</i>	129
<i>Polarised optical microscopy</i>	129
<i>Acrylate complex, thinner films (~120 nm)</i>	131
<i>Etching, XPS – preliminary measurements</i>	133
2-Bromo-3,6-dimethylphenol (46).....	134
(2-Bromo-3,6-dimethylphenoxy)trimethylsilane (62)	134
3,6-Dimethyl-2-(trimethylsilyl)phenyltrifluoromethanesulfonate (63)	135
1,4,5,8,9,12-Hexamethyltriphenylene (36)	136
Crystal data and structure refinement for 1,4,5,8,9,12-Hexamethyltriphenylene 36 (C ₂₄ H ₂₄)	137
Comparison of RMS Deviation.....	138
Comparison of angles between planes	139
FT-IR Spectrum of 1,4,5,8,9,12-Hexamethyltriphenylene 36.	139
Variable-Temperature ¹³ C NMR Study of 1,4,5,8,9,12-Hexamethyltriphenylene 36.....	140
Fluorescence of 1,4,5,8,9,12-Hexamethyltriphenylene 36.	141
Cyclic Voltammogram of 1,4,5,8,9,12-Hexamethyltriphenylene showing the irreversibility of 36.....	142
Computational studies of 36.	143

Materials and methods

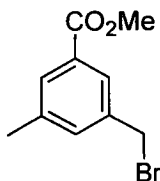
^1H NMR and ^{13}C NMR spectra were recorded on a Bruker ARX 250 spectrometer using the carbon signal of the deuterated solvent as internal standard. Mass spectra were recorded on KRATDS MS50Tc Spectrometers (both EI and FAB, nominal and accurate). Electrospray mass spectrometry was carried out on a Micromass Platform II mass spectrometer with an applied voltage of $-35 - +45$ V, the sign of the charge is stated. UV/Vis spectra were recorded on a Lambda 900 spectrometer. Melting points were determined using an Electrothermal 9100 melting point apparatus and were uncorrected. Single crystal X-ray diffractions were determined by a Bruker Smart Apex CCD diffractometer. IR spectra were recorded on a JASCO FTIR 430Plus spectrometer. All reactions were carried out under nitrogen unless otherwise stated. Analytical TLC was carried out on Merck aluminium backed plates coated with silica gel 60F254. Column chromatography was performed over Fisher silica gel 60Å, particle size 35-70 μm . Components were visualised using UV light (254 nm), H_2SO_4 / EtOH dip or KMnO_4 / OH $^-$ dip, I_2 . Solvents described as dry were purchased as anhydrous grade in the cases of DCM, THF and methanol and dried over molecular sieves (3 or 4 Å) in the cases of DMF and toluene. All starting materials were obtained from commercial suppliers and were used without further purification unless otherwise stated.

Preparation of methyl (3,5-dimethyl)benzoate¹⁰⁶ (**14**)



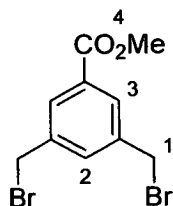
To a 250 mL round-bottomed flask was added 3,5-dimethylbenzoic acid (15.0 g, 0.100 mol), methanol (85 mL) and concentrated H₂SO₄ (few drops). The reaction mixture was stirred at reflux for 16 h whereupon TLC [Hexane: EtOAc, 4:1] indicated that the reaction was complete. The solvent was removed by rotary evaporation and the residue treated with EtOAc (50 mL) and NaOH (30 mL, 1 M (aq)). The organic layer was separated and washed with water (25 mL), dried over MgSO₄, filtered and concentrated *in vacuo* to yield **14** (15.4 g, 93.9 mmol, 94%). ¹H NMR (250 MHz, CDCl₃, 293 K): δ (ppm) = 2.28 (s, 6H, CH₃-1), 3.81 (s, 3H, CO₂CH₃), 7.12 (d, 1H, ArH-2), 7.58 (d, 2H, ArH-3).

Synthesis of methyl (3-(bromomethyl)-5-methyl)benzoate



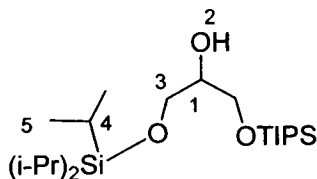
NBS (5.631 g, 31.9 mmol, 1.05 eq) and methyl benzoate **14** (5 g, 30.5 mmol, 1 eq) were dissolved in a 1 L quartz vessel in 400 mL acetonitrile. The solution was degassed with nitrogen before (20 min) and during irradiation (90 min) in a UV reactor at 254 nm. The solvent was evaporated and the residue subjected to chromatography [SiO₂/ Hexane: EtOAc, 17:3]. The majority of fractions containing dibrominated ester **11** were retained for latter purification. The remaining starting material was mostly discarded and the remaining mid fractions (6.08 g, 68% mono-bromo ester, 13% starting material **14**, 13% dibrominated ester **11**) were used without further purification for the next stage of the reaction sequence.

Formation of methyl (3,5-di(bromomethyl)benzoate)¹⁰⁶ (11)



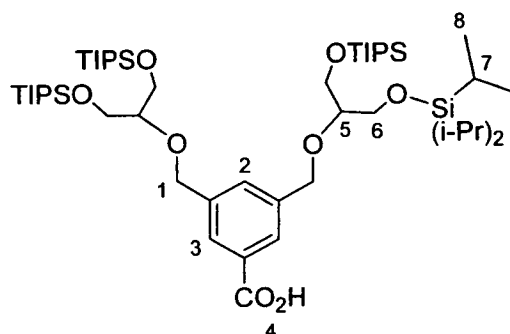
Previous reaction product (6.08 g) and NBS (2.015g, 11.3 mmol, 50% of remaining bromine equivalents required for dibromination of **14** and remaining monobrominated ester) were dissolved in a quartz vessel in 400 mL acetonitrile. The solution was degassed with nitrogen before (20 min) and during irradiation (120 min) in a UV reactor at 254 nm whereupon TLC [Hexane: EtOAc, 3:2] indicated that no further reaction was occurring. Following removal of the solvent *in vacuo* the residue was combined with the previous product fraction and subjected to column chromatography [SiO₂/ Hexane: EtOAc, 17:3] to yield **11**, (3.03 g 30 % based upon methyl benzoate **14**). ¹H NMR (250 MHz, CDCl₃, 293 K): δ (ppm) = 3.98 (s, 3H, CH₃-4), 4.55 (s, 4H, CH₂-1), 7.66 (m, 1H, ArH-2), 8.05 (m, 2 H, ArH-3).

Generation of 1,3-bis(triisopropylsilyloxy)propan-2-ol¹⁰⁷ (38)



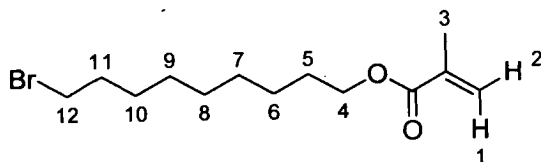
Glycerol (0.561 g, 6.09 mmol, 1 eq) was weighed into a dried 250 mL round-bottomed flask, imidazole (1.70 g, 24.9 mmol, 4.1 eq) and dry DMF (40 mL) were added. The solution was stirred and triisopropylsilyl chloride (2.35 g, 2.60 mL, 12.2 mmol, 2 eq) was added over 20 min and the reaction mixture stirred for 16 h. TLC [Hexane: EtOAc, 5:1 and 20:1] indicated good conversion to the product. The solvent was removed by rotary evaporation and the residue subjected to column chromatography [SiO₂/ Hexane: EtOAc/ 15:1] to yield **38** (2.91 g, 88%). ¹H NMR (250 MHz, CDCl₃, 293 K): δ (ppm) = 1.11 (septet J = 4 Hz, 6H, CH-4), 1.11 (d J = 4.2 Hz, 36H, CH₃-5), 2.62 (s, br, 1H, OH-2), 3.81 (m, 5H, CH₂-3 & CH-1).

Preparation of 3,5-bis(1,3-di(triisopropylsilyloxy)propyl-2-oxymethyl)benzoic acid (39)



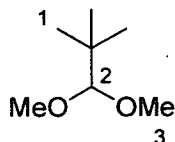
To a dry 50 mL round-bottomed flask were added NaH (70.4 mg - 60% weight suspension in mineral oil, 1.75 mmol, 5 eq) and dry THF (10mL) which was brought to reflux. A solution of propanol derivative **38** (0.284 g, 0.704 mmol, 2 eq) and dibrominated ester **11** (0.113 g, 0.352 mmol, 1 eq) in 10 mL dry THF was added over 5 hours. The solution was stirred at for 16 h then NaH (70.4 mg, 1.74 mmol, 5 eq) was added and the reaction stirred for a further 24 h whereupon no change was observed by TLC [Hexane: EtOAc, 10:1]. The reaction was quenched with water (10 mL) then neutralised with 1M HCl. The organic phase was extracted by the addition of diethyl ether (20 mL). The aqueous phase was then extracted with two more aliquots of diethyl ether (2×20 mL). The combined organic phases were washed with saturated brine (5 mL) then dried over MgSO₄ and filtered. The solvent was removed by rotary evaporation and the residue subjected to column chromatography [SiO₂/ Hexane: EtOAc/ Gradient, Hexane → 10: 1] to yield **39** (51.6 mg, 17%) as a thick oil. ¹H NMR (250 MHz, CDCl₃, 293 K): δ (ppm) = 1.10 (s, br, 84H, CH-7 & CH₃-8), 3.54 (m, 2H, CH-5), 3.75 (m, 4H, CH₂-6), 4.73 (s, 4H, CH₂-1), 7.51 (m, 1H, ArH-2), 7.95 (m, 2H, ArH-3). IR (NaCl disc) wavenumber (cm⁻¹) = 2200-3500 (br, O-H stretch), 1695 (sharp, C=O stretch). MS (ESI -ve) *m/z* = 954.9 (Predicted *m/z* [M]⁻ (954.6) or [M-H]⁺ (953.6)).

Synthesis of 1-bromo-9-methacroyloxynonane (**13**) by Mitsunobu esterification



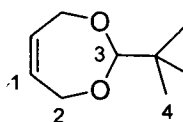
9-Bromononanol **41** (0.2 g, 0.896 mmol, 1 eq) was dissolved in dry THF (5 mL) in a dry 25mL round-bottomed flask. Triphenylphosphine (0.353 g, 1.34 mmol, 1.5 eq) and methacrylic acid (0.115 g, 0.115 mL, 1.34 mmol, 1.5 eq) were added and the reaction mixture cooled to 0 °C. Diisopropylazodicarboxylate (0.271 g, 0.265 mL, 1.34 mmol, 1.5 eq) was then added. The mixture was stirred for 2 h whereupon TLC [Hexane: EtOAc/ 10:1] showed good conversion to the product. The reaction was quenched by the slow addition of 20 mL MeOH/H₂O. The organic phase was separated following the addition of a further 120 mL H₂O and 15 mL EtOAc, washed with water (2 × 20 mL) then dried over MgSO₄. Following filtration and concentration by rotary evaporation the mixture was separated by column chromatography [SiO₂/ Hexane: EtOAc/ 20:1] to yield **13** (0.194 g, 75%). ¹H NMR (250 MHz, CDCl₃, 293 K): δ (ppm) = 1.7 (m, 10H, CH₂-6, 7, 8, 9, & 10), 1.94 (m, 2H, CH₂-11), 2.09 (m, 2H, CH₂-5), 2.29 (s, 3H, CH₃-3), 3.65 (t, 2H, CH₂-12), 4.37 (t, 2H, CH₂-4), 5.79, 6.34 (s, 1H + 1H, CH-1 & 2). ¹³C NMR (63 MHz, CDCl₃, 293 K): δ (ppm) = 18.70, 26.31, 28.50, 28.977, 29.04, 29.50, 29.67, 33.18, 34.31, 65.14, 125.49, 139.94, 167.9. 13 of 13 expected signals. Elemental analysis: Found 53.69% C, 8.39% H; Expected C₁₃H₂₃BrO₂ 53.61% C, 7.96% H.

Generation of pivaldehyde dimethyl acetal¹⁰⁸ (43)



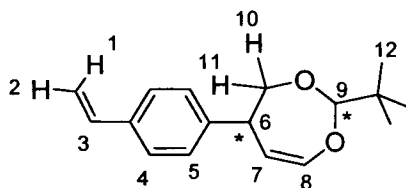
Pivaldehyde **42** (4.35 g, 50.5 mmol, 1.25 eq), trimethyl orthoformate (4.29 g, 4.42 mL, 40.4 mmol, 1 eq) and dry methanol (2 mL) were added to a dry 50 mL round-bottomed flask followed by 3 drops of conc. H₂SO₄. The mixture was stirred overnight and monitored by NMR showing 65% conversion to **43**. The reaction was completed by the addition of a further 0.5 eq trimethyl orthoformate. The moisture sensitive product **43** (5.37 g, 81%) was purified by careful fractional vacuum distillation directly from the reaction mixture (85 °C, 400 mBar). ¹H NMR (250 MHz, CDCl₃, 293 K): δ (ppm) = 1.03 (s, 3H, CH₃-1), 3.61 (s, 6H, CH₃-3), 3.61 (m, 1H, CH-2).

Synthesis of 2-*tert*-butyl-1,3-dioxycyclohept-5-ene⁶⁷ (21)



Cis-2-butene-1,4-diol (3.25 g, 36.9 mmol) and *p*-toluene sulphonic acid dihydrate (30 mg), were added to dimethyl acetal **42** (5.37 g, 0.406 mol) in a 50 mL round-bottomed flask and the mixture subjected to rotary evaporation (200 mBar, 25 °C) for 2 hours. The reaction was then driven towards completion and the product **21** (4.00 g, 62%) purified by careful fractional vacuum distillation (19 mBar, 75 °C) using a dry ice condenser. ¹H NMR (250 MHz, CDCl₃, 293 K): δ (ppm) = 0.990 (s, 12H, CH₃-4), 4.17 (s, 1H, CH-3), 4.23, 4.52 (2 × d – J = 15 Hz, 2H + 2H, CH₂-2), 5.74 (m, 2H, CH-1).

Preparation of 1,3-dioxy-2-*tert*-butyl-5-*p*-styrylcyclohept-4-ene (19)

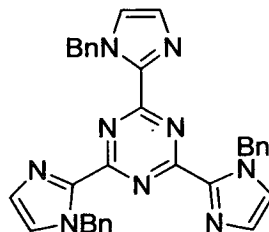


A microwave reaction vessel was charged with 4-bromostyrene **22** (0.28 g, 0.2 mL, 1.53 mmol, 4 eq), cyclic acetal **21** (59.7 mg, 3.82 mmol, 1 eq), triethylamine (0.193 g, 0.268 mL, 1.91 mmol, 5 eq), Pd(OAc)₂ (2.5 mg, 1.14×10^{-5} mol, 3 mol %), (\pm)-2,2'-bis(diphenylphosphino)-1,1'-binaphthalene (22.7 mg, 3.42×10^{-5} mol, 9 mol %) and toluene (0.5 mL). The vessel was sealed (in aerobic conditions) and irradiated in a microwave reactor at 135 °C with cooling for 45 min; this equated to a power of ~120 W. The reaction mixture was then filtered through a celite plug, washed with toluene. The solvent was removed by rotary evaporation and the residue purified by column chromatography [SiO₂/ Hexane: Toluene/ 9: 1] yielding a white solid (20 mg, 21%). The analytical data obtained were consistent with a mixture of two diastereomers as indicated by the chiral centres marked by asterisks.^{xvii} ¹H NMR (250 MHz, CDCl₃, 293 K): Diastereomer a) δ (ppm) = 0.97 (s, 9H), 3.07 (t - J = 11 Hz, 1H), 3.77 (m, 1H), 4.01 (dd - J = 11, 5 & 1.1 Hz, 1H), 4.13 (s, 1H), 4.71 (m, 1H), 5.15 (d - J = 11 Hz, 1H), 5.65 (d - J = 17 Hz, 1H), 6.35 (dd - J = 7 & 3 Hz, 1H), 6.62 (dd - J = 18 & 11 Hz, 1H), 7.15 (m, 4H). MS (ESI +ve) - m/z = 256.92 (~258) \rightarrow [M]⁺.

Diastereomer b) δ (ppm) = 0.97 (s, 9H), 3.58 (m, 1H), 3.76 (dd - J = 12 & 3 Hz, 1H), 4.10 (d J = 10 Hz, 1H), 4.31 (s, 1H), 4.90 (t - J = 7 Hz, 1H), 5.25 (d - J = 11 Hz, 1H), 5.72 (d - J = 17 Hz, 1H), 6.35 (d - J = 7 Hz, 1H), 6.72 (dd - J = 18 & 11 Hz, 1H), 7.31 (m, 4H). MS (ESI +ve) m/z = 258.09 \rightarrow [M]⁺.

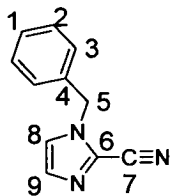
^{xvii} ¹H NMR appeared consistent with compound **19** but before substantial (> 2 mg), analytically pure samples of each diastereomer were isolated, it became clear that the next step was not efficient and that the synthetic route had an unreasonable number of steps given the simpler alternatives available. Therefore further synthetic attempts for compound **19** were abandoned.

Attempted synthesis of 2,4,6-tris(1-benzylimidazol-2-yl)-1,3,5-triazine (24) via nucleophilic substitution



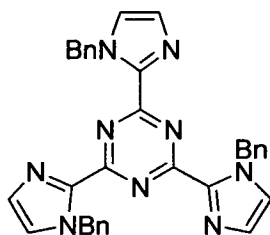
1-Benzylimidazole **27** (1.00 g, 6.22 mmol, 2 eq) was added to a dry 100 mL round-bottomed flask with 15 mL dry THF, the solution was degassed for 20 min then cooled to -78 °C. *n*-Butyllithium (3.16 mL, 2 M solution in pentanes, 2 eq) was added over 1 h. The mixture was stirred for a further hour at -78 °C, cyanuric chloride **25** (0.583 g, 3.16 mmol, 2 eq, in 10 mL dry THF) was then added and the reaction stirred at -78 °C → RT for 18 h. The reaction mixture was quenched by the addition of methanol (5 mL) and an NMR spectrum taken of the crude residue following removal of the solvent *in vacuo*. The broad signals in the NMR were characteristic of polymerisation of the imidazole.

Formation of 1-benzyl-2-cyanoimidazole⁷⁰ (**26**)



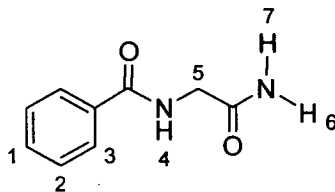
A solution of DMAP (2.45 g, 20.0 mmol, 2.5 eq) in 40 mL dry DMF at 10 °C in a 100 mL round-bottomed flask. Cyanogen bromide (2.12 g, 20.0 mmol, 2.5 eq) was added and the solution allowed to warm to RT whereupon a yellow precipitate formed. The suspension was cooled to 10 °C and *N*-benzylimidazole **27** (1.27 g, 8.00 mmol, 1 eq) was added and the reaction mixture stirred for 16 h whereupon no further reaction was observed by TLC [Hexane: EtOAc/ 7: 3]. Saturated NaHCO₃ solution (250 mL) was added carefully followed by EtOAc (100 mL). The mixture was stirred for 1 h then the organic layer separated. The aqueous phase was extracted twice more with 2 × 100 mL EtOAc and the combined organic extracts were washed with 2 × 50 mL water, dried over MgSO₄, filtered and the solvent removed by rotary evaporation. The residue was subjected to column chromatography [SiO₂/ hexane: EtOAc/ 7: 3] to yield **26** (0.493 g, 33%). ¹H NMR (250 MHz, CDCl₃, 293 K): δ (ppm) = 5.34 (s, 2H, CH₂-5), 7.12 (d J = 1.0 Hz, 1H, CH - 8/9), 7.36 (m, 6H, Ar-H 1 & 2 & 3 & CH - 8/9). ¹³C NMR (63 MHz, CDCl₃, 293 K): δ (ppm) = 51.29 (C-5), 122 (C- 4/ 6/ 7) 123.1, 127.6, 128.8, 129.2, 131.9 (C - 1/ 2/ 3/ 8/ 9), 134.1 (C- 4/ 6/ 7).

Attempted synthesis of 2,4,6-tris(1-benzylimidazol-2-yl)-1,3,5-triazine (24) via cyclotrimerisation of 1-benzyl-2-cyanoimidazole (26)



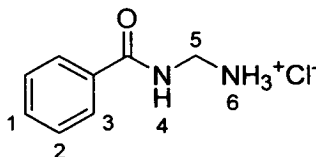
1-Benzyl-2-cyanoimidazole **26** (0.183 g, 1.00 mmol), yttrium trifluoromethanesulphonate (1.10 mg, 10 mol %) and piperidine (0.100 ml, 1.00 mmol) were sealed into a microwave reaction vessel (aerobic conditions). The reaction mixture was stirred at 130 °C for 45 minutes. The residue was washed out of the flask with acetonitrile and was subjected to column chromatography following evaporation of the solvent. This yielded a mixture containing 1-benzylimidazole-2-carboxylic acid and other intermediates according to mass spectrometry and NMR. The reaction was also tested in the presence of solvent (xylene) and with ytterbium trifluoromethanesulphonate with the same results.

Preparation of *N*-(2-amino-2-oxoethyl)benzamide (44)



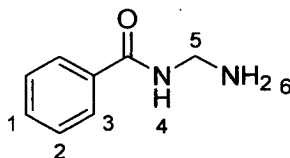
Glycinamide hydrochloride **33** (0.200 g, 1.81 mmol, 1 eq), chloroform (10 mL) and triethylamine (0.403 g, 0.559 mL, 3.97 mmol, 2.2 eq) were added to a 50 mL round-bottomed flask and the reaction mixture stirred for 15 min. Benzoyl chloride (0.254 g, 0.210 mL, 1.81 mmol, 1 eq) was added over 30 min and the mixture stirred for 2 h. Saturated sodium hydrogen carbonate solution (3 cm³) was added and the organic layer containing by-products of the reaction was separated. The aqueous phase was extracted with two further aliquots of chloroform (2 × 5 mL). The combined chloroform phases were back extracted with 0.1 M HCl (20 mL) then with water (20 mL). The benzamide **44** was then extracted with EtOAc (5 × 20 mL) from the combined aqueous phases arising from the initial work-up and back-extraction. The EtOAc extracts were dried over MgSO₄, filtered and concentrated *in vacuo* to yield **44** (0.263 g, 81%). ¹H NMR (250 MHz, DMSO-d₆, 293 K): δ (ppm) = 3.82 (d – J = 5 Hz, 2H, CH₂-5), 7.07, 7.41 (both s, br, 1H + 1H, NH – 6 & 7), 7.51, 7.90 (m, 3H + 2H, Ar – H 1, 2 & 3), 8.69 (t, br, 1H, NH – 4).

Synthesis of *N*-(aminomethyl)benzamide hydrochloride (45)



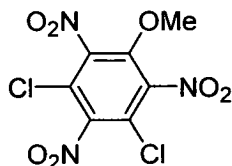
I,I-Bis(trifluoroacetoxy)iodobenzene (1.29 g, 3.00 mmol, 1.5 eq) was dissolved in 6 mL acetonitrile / distilled water. Diamide 44 (0.356 g, 2.00 mmol, 1 eq) was added and the solution stirred for 18 h. The reaction mixture was then diluted with 30 mL distilled water and acidified with 4 mL conc. HCl. The organic impurities were then removed by extraction with ether (3 × 5 mL); the combined ether extracts were then back extracted with 10 mL 10% HCl solution. The combined aqueous phases were concentrated and the residue recrystallised from ethanol/ ether to yield 45 (0.307 g, 82%). ¹H NMR (250 MHz, DMSO-*d*₆, 293 K): δ (ppm) = 4.26 (d – J = 6 Hz, 2H, CH₂ – 5), 7.44, 7.80 (m, 3H + 2H, Ar – H - 1, 2 & 3), 8.25 (s, br, 3H, NH₃ – 6), 9.51 (s, br, 1H, NH – 4).

Preparation of *N*-(aminomethyl)benzamide (31)



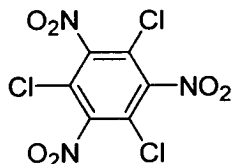
Hydrochloride salt 45 (0.305 g, 1.63 mmol, 1 eq) was dissolved in 8 mL methanol. Triethylamine (0.157 g, 0.218 mL, 1.55 mmol, 0.95 eq) was added and the mixture stirred for 5 min. DCM (92 mL) was added and the resulting suspension of triethylamine hydrochloride filtered through a basic alumina plug which was then washed with a further (400 mL DCM: MeOH, 92:8). The solution was concentrated *in vacuo* at room temperature to yield 31 (0.164 g, 1.09 mmol, 67%). ¹H NMR (250 MHz, DMSO-*d*₆, 293 K): δ (ppm) = 1.94 (s, br, 2H, NH₂ – 6), 3.97 (d – J = 6 Hz, 2H, CH₂ – 5), 7.44, 7.75 (m, 3H + 2H, Ar – H - 1, 2 & 3), 8.75 (s, br, 1H, NH – 4). Product was unstable and used immediately.

Synthesis of 3,5-dichloro-2,4,6-trinitroanisole¹⁰⁹ (50)



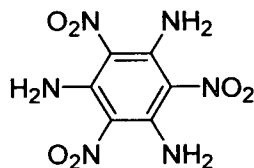
To an ice-cooled, stirred solution of conc. HNO₃ (21 mL) and conc. H₂SO₄ (50 mL) in a 100 mL flask fitted with a condenser, 3,5-dichloroanisole **49** (10.0 g, 56.0 mmol) was added slowly. The cooling bath was removed after 5 min and the suspension was heated to 105 °C over 20 min and refluxed for 1.5 h. The mixture was then cooled to room temperature and poured onto ice. The product was filtered, washed with water, and recrystallised from hexane: toluene 2:1 (13.9 g, 79% yield). m.p. = 93-95 °C (lit = 94-95)

Synthesis of 1,3,5-trichloro-2,4,6-trinitrobenzene¹⁰⁹ (51)



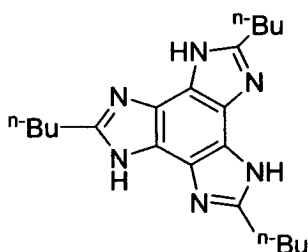
Thionyl chloride (0.94 mL, 13.0 mmol) and dimethylformamide (0.82 mL, 10.6 mmol) was added to a solution of **50** (3 g, 9.6 mmol) in toluene (10 mL) at 50 °C. The mixture was stirred and heated to 95 °C over a period of 20 min and refluxed at that temperature for 1h. Water (20 mL), was added and the organic phase separated. The aqueous phase was extracted with toluene (2 × 20 mL). The combined organic phases were dried over magnesium sulfate, heated with activated carbon for 30 min and filtered through celite. The solvent was removed *in vacuo* to give a cream-colored solid which was recrystallised from acetic acid (2.72 g, 79% yield). m.p. = 194-196 °C (lit. 195-196 °C)

Synthesis of 1,3,5-triamino-2,4,6-trinitrobenzene (52)



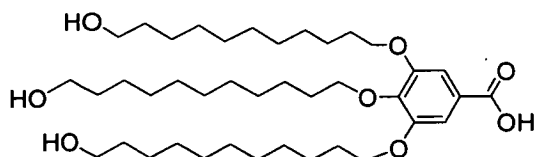
Ammonia was introduced via a balloon to a stirred solution of **51** (5.81 g, 18.3 mmol) in toluene (150 mL) contained in a 1 L 3-necked flask. The mixture was sonicated for 2 minutes every 2 hours over a 12 hour period. After a further 12 h stirring the supernatant solution over the bright yellow precipitate became colourless. The mixture was filtered, washed sequentially with toluene, hot water, and acetone, and dried yielding a bright yellow solid (4.19 g, 87% crude yield). The product was used for the next stage without further purification.

Synthesis of 2,2',2''-Tributylbenzotris(imidazole) (47)



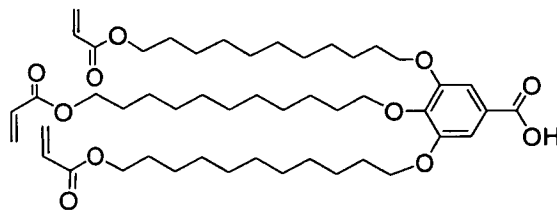
Compound **52** (1 g, 3.87 mmol) was suspended in EtOAc (80 mL) in a 250 mL 3-necked flask fitted with a condenser and the mixture degassed with argon. 10% Pd/C (260 mg) was added and the suspension heated to 60°C. The vigorously stirred suspension was degassed with hydrogen and hydrogenated at normal pressure for 5 h after which the suspension became colourless. The solvent was removed *in situ* and freshly distilled valeric anhydride (7 mL, Ar degassed) was added to the residue. Heating to 60 – 70 °C under argon resulted in a gel-like suspension of acetylated hexaaminobenzene to which HCl (28 mL of a 37% solution + 52 mL of water) was added. The mixture was heated at reflux overnight under argon. It was then transferred to 2 × sealed pressure tubes (equipped with a high-vacuum quality stopcock) and heated under argon to 180 °C for 6 h, and then cooled. The catalyst was removed by filtration through celite and washed with hot water. The filtrate was made basic using 35% NH₃ in water solution and checked by pH paper. The mixture was refluxed at 110 °C in a 500 mL flask for 7 min and allowed to cool overnight. The aqueous mixture was extracted with Et₂O (3 × 100 mL) and DCM (3 × 100 mL). The combined organic phases were evaporated to dryness without the use of drying agent and subjected to column chromatography [SiO₂/ CHCl₃ : MeOH/ 100:3, saturated with NH₃ gas] to yield (180 mg, 13%) of crude material. To reach the high purity required for LC studies the material was recrystallised three times from wet ethyl acetate. ¹H NMR (250 MHz, CDCl₃ 293 K): Elemental analysis – found: C 65.49 % H 8.36 % N 21.14% expected C₂₁H₃₀N₆.1H₂O C, 65.59%; H, 8.39%; N, 21.86%. ESI MS m/z = 367.2 [M + H⁺]

Preparation of 3,4,5-tris(11'-hydroxyundecyloxy)benzoic acid⁷⁵ (55)



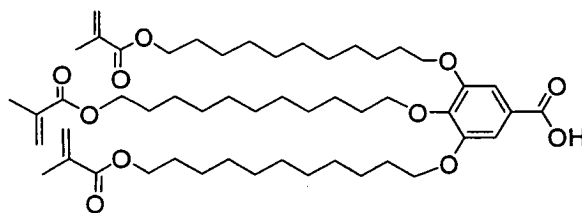
Methyl gallate **53** (2.48 g, 13.5 mmol) was dissolved in dry DMF (80 mL) in a 250 mL round-bottomed flask. K_2CO_3 (18.6 g) was added and the mixture stirred at 75 °C for 30 min. 11-bromoundecanol **54** (11.17 g, 44.4 mmol) was added over 10 minutes and the reaction stirred for a further 11 h at 75 °C. Upon cooling the precipitate was removed by filtration, the solvent was removed *in vacuo* and the residue dissolved in 100 mL water and 100 mL EtOAc. The aqueous phase was separated and extracted with EtOAc (2 × 100 mL). The combined organic layers were evaporated into a 250 mL R.B. flask and dissolved in 60 mL MeOH and 20 mL Water. NaOH (3 g) was added and the mixture stirred at reflux overnight. Upon cooling the mixture was made acidic with 1 M aqueous HCl and extracted with EtOAc (3 × 100 mL). The combined organic layers were washed with water (100 mL) and dried over $MgSO_4$. The resulting white solid was recrystallised from tepid EtOAc to yield (7.76 g, 84 %). 1H NMR (250 MHz, d_6 -DMSO 293 K): δ (ppm) = 1.45 (s, br, 48H), 1.59 (m, 6H), 1.95 (m, 6H), 4.17 (m, 6H), 4.48 (s, 3H), 7.37 (s, 2H).

Synthesis of 3,4,5-Tris(11'-acryloyloxyundecyloxy)benzoic acid **75** (**1**)



55, (6 g, 8.8 mmol), N,N-dimethylaniline, (5.58 mL, 44.1 mmol) and THF (50 mL) were loaded into a 250 mL 3-necked RB flask protected from light. Acryloyl chloride (3.50 mL, 44 mmol) was added slowly. After 5 hours the reaction was complete (T.L.C.) solvent was removed at R.T. by rotary evaporation. The residue was subjected to column chromatography [SiO₂/ Hexane: EtOAc/ 3:1] and evaporated into a 250 mL RB flask protected from light. To the mixed ester-anhydride species **57**, 15 mL pyridine and 5 mL water were added and the mixture heated to reflux under nitrogen for 10 minutes. The mixture was cooled to 0 °C and acidified with HCl (10% aq.) the acid products were extracted with Et₂O (3 × 20 mL). EtOAc (20 mL) was added and the methacrylic acid removed by washing with Na₂CO₃ (sat. aq). The low density solvents were removed and the organic extracts redissolved in CHCl₃ and the mixture washed with HCl (30 mL, 10% aq.) and distilled water (3 × 20 mL). The organic layer was dried over MgSO₄, filtered through celite and evaporated to yield **1** (1.62 g, 22% after recrystallisation from EtOAc). ¹H NMR (250 MHz, CDCl₃, 293 K): δ (ppm) = ¹H NMR (250 MHz, CDCl₃, 293 K): δ (ppm) = 1.25 – 1.56 (m, 42H), 1.55 - 1.96 (m, 12H), 4.06 (q, 6H), 4.18 (t, 6H), 5.84 (complex d, 3H, J = 10.3 Hz), 6.12 (dd, 3H, J = 17 Hz & 10 Hz), 6.41 (d, 3H, J = 17 Hz), 7.34 (s, 2H).

3,4,5-Tris(11'-methacryloyloxyundecyloxy)benzoic acid (**48**)



Compound **55**, (2.11 g, 3.1 mmol), pyridine, (5.00 mL, 61.8 mmol) and dioxane (20 mL) were loaded into a 100 mL 3-necked RB flask protected from light. The dissolution was completed by stirring at 60 °C for 5 min. Following cooling to R.T. methacryloyl chloride (1.81 mL, 18.5 mmol) was added slowly. After 5 hours the reaction was complete (T.L.C.) solvent and pyridine was removed at R.T. by rotary evaporation. The residue was subjected to column chromatography [SiO_2 / Hexane: EtOAc/ 7:1] and evaporated into a 250 mL RB flask protected from light. To the mixed ester-anhydride species **56**, 15 mL pyridine and 5 mL water were added and the mixture heated to reflux under nitrogen for 10 minutes. The mixture was cooled to 0 °C and acidified with HCl (10% aq.) the acid products were extracted with Et_2O (3 × 20 mL). EtOAc (20 mL) was added and the methacrylic acid removed by washing with Na_2CO_3 (sat. aq.). The low density solvents were removed and the organic extracts redissolved in CHCl_3 and the mixture washed with HCl (30 mL, 10% aq.) and distilled water (3 × 20 mL). The organic layer was dried over MgSO_4 , filtered through celite and evaporated to yield **48** (1.62 g, 60%). ^1H NMR (250 MHz, CDCl_3 , 293 K): δ (ppm) = 1.52 (s, 30H), 1.68 (m, 6H), 1.88 (m, 6H), 2.02 (m, 6H), 4.23 (m, 6H), 4.34 (t, 6H), 5.75 (s, 3H), 6.30 (s, 3H), 7.51 (s, 2H). ^{13}C NMR (63 MHz, CDCl_3 , 293 K): δ (ppm) = (172.0, 167.9, 153.2, 143.3, 136.9, 124.0, - 6 of 7 expected quaternary C) (125.5 - CH_2 methacrylate) (108.9 - CH aromatic) (73.8, 69.5, 65.2, 30.7, 29.9, 29.8, 29.7, 29.6, 29.0, 26.4, - 10 of 11 expected CH_2 aliphatic signals) (18.7 - CH_3).

Elemental analysis predicted 70.55% C, 9.56% H, found 70.81% C, 10.1% H. MS (ESI -ve) $m/z = 884 \rightarrow [\text{M}-(\text{H}^+)]^-$.

Liquid crystal analysis details

Spectrophotometric grade or fresh distilled chloroform was used. It was ensured that neither the pipettes used nor the vials contained contaminants such as soluble plasticers or adhesives. Glass coverslips used were supplied by Fisher (16 mm, round 0.13-0.17 mm thick). They were cleaned by sonication for 1 minute in acetone and 1 minute in isopropyl alcohol and blown dry with air. Gold coated silicon wafers were supplied by Georg Albert (100 nm Au adhered by 5 nm Ti on 111 Si, cut into ~ 10 mm squares). These were cleaned by holding in piranha solution for 30 seconds then rinsed with copious distilled water and washed and dried as for the glass slides.

Thicknesses of films were measured by the group of Prof. Ifor Samuel, Organic Semiconductor Centre, St. Andrews, using a Woolam M2000 ellipsometer. The films were annealed either with a Linkam THMS600 Heating and Freezing Stage, or a custom built hotstage. This allowed the heating and slow cooling of the samples as described. Phase behaviour was investigated with a Perkin Elmer Pyris 6 DSC. Best results were obtained using crimped pans as opposed to sealed ones. Bulk samples were polymerised at 365 nm in a UV photoreactor. Film samples were irradiated in a glass chamber purged with nitrogen using a 365 nm 100W UVP spotlight. X-ray scattering data was collected on a Bruker AXS D8 diffractometer using a scintillation counter detector such that small angles could be accessed.

Procedure for formation of supramolecular complexes **48.47** and **1.47**

In a round bottomed flask one equivalent of benzotri(imidazole) **47** and three equivalents of methacrylate derivative **48** or acrylate derivative **1** were combined. CHCl_3 : MeOH 10:1 was added with sonication until complete dissolution was achieved. The solvent was removed by rotary evaporation and the complex redissolved in CHCl_3 . The solution was once again evaporated to dryness and the chloroform addition and removal was repeated two further times to yield a translucent waxy solid. **48.47** - ^1H NMR (250 MHz, CDCl_3 , 293 K): δ (ppm) = 1.18 (t, 9H, $J = 7.4$ Hz), 1.50 - 2.05 (m, 174H), 2.10 (s, 27H), 2.19 (quintet, 6H, $J = 7.2$ Hz), 3.34 (t, 6H, $J = 7.8$ Hz), 4.22 (m, 36H). ^{13}C NMR (63 MHz, CDCl_3 , 293 K): δ (ppm) = (172.3, 167.8, 153.1, 152.6, 142.3, 136.9, 128.3, 121.2 - 8 of 9 expected quaternary C) (125.5 - CH_2 methacrylate) (108.9 - CH aromatic) (73.8, 69.5, 65.2, 30.7, 30.1, 30.1, 30.0, 29.9, 29.8, 29.6, 29.0, 28.3, 26.5, 26.4, 22.7 - 16 of 16 expected CH_2 aliphatic signals) (18.7, 14.2 - 2 of 2 expected CH_3 signals). **1.47** - ^1H NMR (250 MHz, CDCl_3 , 293 K): δ (ppm) = 1.09 (t, 9H, $J = 7.4$ Hz), 1.30 - 2.00 (m, 174H), 2.09 (quintet, 6H, $J = 7.2$ Hz), 3.27 (t, 6H, $J = 7.8$ Hz), 4.12 (m, 36H), 5.84 (complex d, 3H, $J = 10.3$ Hz), 6.12 (dd, 3H, $J = 17$ Hz & 10 Hz), 6.41 (d, 3H, $J = 17$ Hz), 7.47 (s, 2H).

Bulk measurements:

Differential Scanning Calorimetry

The material (6-9 mg) was added to the DSC pan as a highly concentrated solution in DCM. Solvent was removed at reduced pressure overnight before crimping. The heating rate was 10 °C/min and the samples were heated over a range of – 50 °C to 90 °C. A number of experiments were carried out on complex **48.47** to determine the phase behaviour of the materials and the effect of initiator and/or inhibitor.

- (a) First sample of complex **48.47**

- (b) Second sample of complex **48.47**

- (c) Complex **48.47** (b) doped with 0.8% w/w TMBPO

- (d) Complex **48.47** (b) doped with 0.8% w/w TMBPO and 0.02% w/w MEHQ

- (e) Complex **48.47** (b) doped with 0.1% w/w MEHQ

The behaviour of complex **1.47** was also investigated

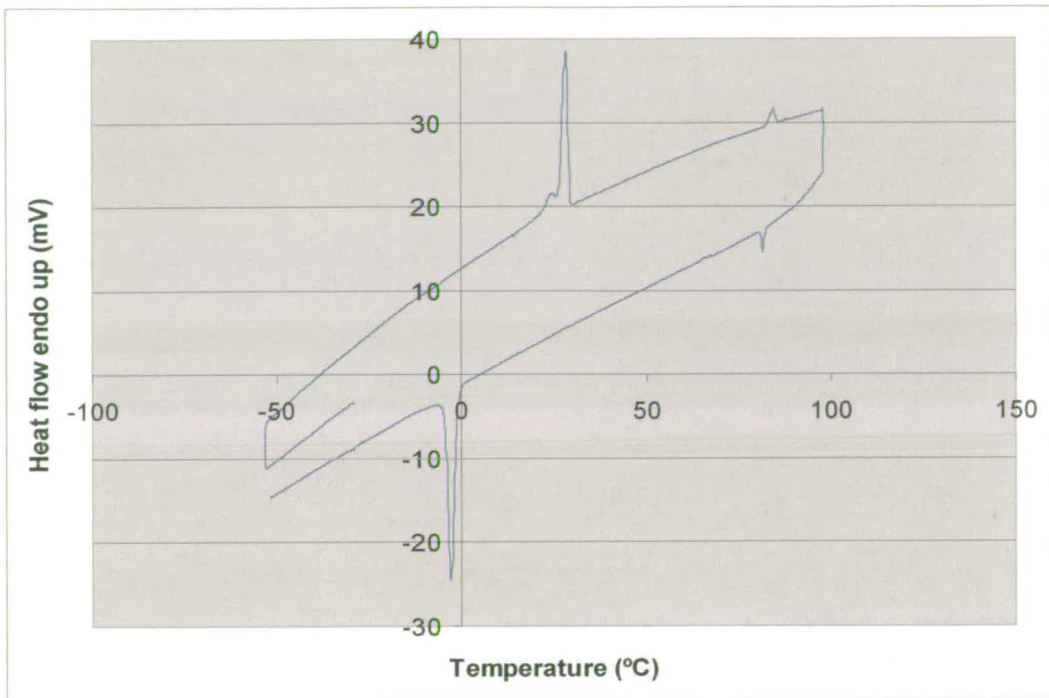


Figure 41: DSC trace of sample (a) Complex 48.47a scan 1

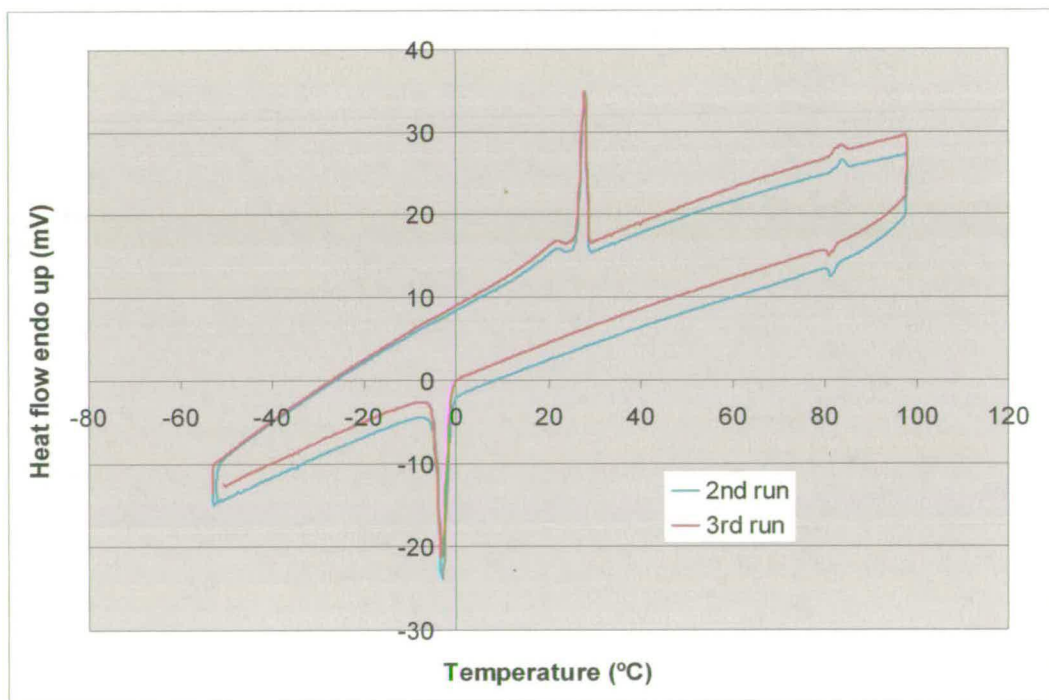


Figure 42: DSC trace of sample (a), Complex 48.47a, scans 2 and 3

Experiment			(a)	(b)	(c)	(d)	(e)
Scan 1 Heat	K → Col	Onset (°C)	18.9	14.0		15.0	15.7
		Peak(s) (°C)	(21.4) ^c 27.6	(23.1) ^c 26.5		(24.5) ^c 27.2	27.5
		ΔH (J/g)	30.0	35.6		39.5	30.7
	Col → I	Onset (°C)	81.5	73.5		-	65.0
		Peak(s) (°C)	84.5	76.0		-	65.7
		ΔH (J/g)	2.1	1.7		-	-0.5
Scan 1 Cool	I → Col	Onset (°C)	83.1	73.0	-	-	
		Peak(s) (°C)	81.4	71.0	-	-	
		ΔH (J/g)	-1.4	-0.8	-	-	
	Col → K	Onset (°C)	0.8	3.8	-3.0	2.5	1.5
		Peak(s) (°C)	-2.9	0.0	-8.5	-1.2	-2.9
		ΔH (J/g)	-32.7	-40.0	-42.0 ^a	-40.3	-36.8
Scan 2 Heat	K → Col	Onset (°C)	18.9	14.0	13.8	15.0	15.7
		Peak(s) (°C)	(21.4) ^c 27.6	26.8	21.9	(24.5) ^c 27.2	27.5
		ΔH (J/g)	29.6	33.7	38.8	38.3	27.6
	Col → I	Onset (°C)	81.2	72.2	-	-	63.2 ^b
		Peak(s) (°C)	83.9	74.3	-	-	63.9 ^b
		ΔH (J/g)	1.7	1.0	-	-	-0.3 ^b
Scan 2 Cool	I → Col	Onset (°C)	83.1	73.0	-	-	-
		Peak(s) (°C)	81.4	72.5	-	-	-
		ΔH (J/g)	-1.5	-0.8	-	-	-
	Col → K	Onset (°C)	0.8	3.6	-5.0	2.4	1.5
		Peak(s) (°C)	-2.9	-0.3	-8.2	-1.2	-2.9
		ΔH (J/g)	-32.4	-38.9	-2.1 ^a	-40.1	-36.0
Scan 3 Heat	K → Col	Onset (°C)	24.6	15.5			
		Peak(s) (°C)	27.6	27.7			
		ΔH (J/g)	25.9	34.8			
	Col → I	Onset (°C)	81.1	71.1			
		Peak(s) (°C)	83.9	71.4			
		ΔH (J/g)	1.7	0.8			
Scan 3 Cool	I → Col	Onset (°C)	83.4				
		Peak(s) (°C)	81.0				
		ΔH (J/g)	-1.3				
	Col → K	Onset (°C)	0.8				
		Peak(s) (°C)	-2.9				
		ΔH (J/g)	-31.5				

Table 4: Peak onsets, maxima and enthalpy changes for phase transitions of complex 48.47. ^a The enthalpy change for the Col → K transition decreases markedly. ^bThis is not the expected type of Col → I phase change, note the negative enthalpy on heating and the lower than expected transition temperature. The DSC experiments would have been repeated much more thoroughly were it not for a lack of training provision and poor computer equipment. ^c The numbers in parantheses indicate that an unresolvable transition occurred before the melting point.

The general behaviour of samples (a) and (b) is similar, the disparities (Table 4) likely stem partly from the two-component nature of the complex (weighing error) and additionally from the fact that the small, broad peaks are close to the detection limits of the machine. Formulation (c) appears to polymerise thermally – as displayed by the large reduction in freezing enthalpy, the sample was also hardened following the DSC experiment. Apart from a strange negative enthalpy change for sample (e), none of the liquid crystalline phase changes observed for samples (a) and (b) were observed for samples (c), (d) and (e). The behaviour of impure or wet samples of complex 48.47 was essentially the same as that of sample (d). Fine structure was present in the K → Col transition which disappeared for samples (c) and (e).

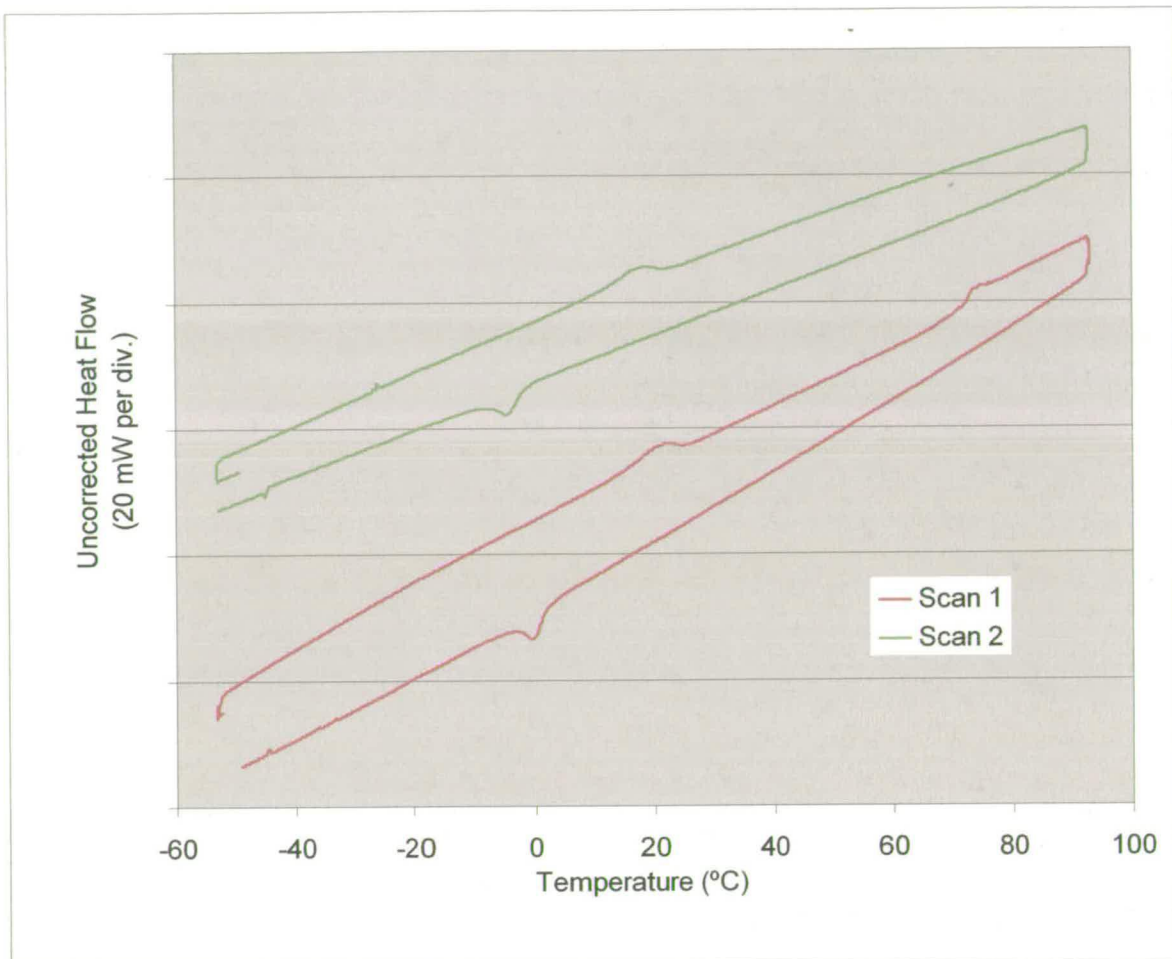


Figure 43: DSC trace of Complex 1.47, scans 1 and 2

Experiment	Observed Transition	Data type	Data
Scan 1 Heat	K → Col	Onset (°C)	14.5
		Peak(s) (°C)	21.9
		ΔH (J/g)	15.4
	Col → I	Onset (°C)	71.8
		Peak(s) (°C)	74.9
		ΔH (J/g)	4.29
Scan 1 Cool	I → Col	Onset (°C)	-
		Peak(s) (°C)	-
		ΔH (J/g)	-
	Col → K	Onset (°C)	2.29
		Peak(s) (°C)	-0.73
		ΔH (J/g)	-16.6
Scan 2 Heat	K → Col	Onset (°C)	12.7
		Peak(s) (°C)	19.5
		ΔH (J/g)	14.5
	Col → I	Onset (°C)	-
		Peak(s) (°C)	-
		ΔH (J/g)	-
Scan 2 Cool	I → Col	Onset (°C)	-
		Peak(s) (°C)	-
		ΔH (J/g)	-
	Col → K	Onset (°C)	0.64
		Peak(s) (°C)	-4.65
		ΔH (J/g)	-14.5

Table 5: DSC data for acrylate liquid crystalline complex 1.47

The isotropisation enthalpy of complex 1.47 is relatively high at 4.29 J/g. It exhibits less reversible behaviour than complex 48.47, no peaks corresponding to liquid crystalline phases are detected following the initial isotropisation.

Polarised optical microscopy on bulk material

Calibration of the stage

The temperature reading on the linkam hotstage was calibrated by placing crystals of melting point standards on a glass coverslip and comparing observed melting point to standard melting point.

	Expected Melting Range	Median Melting Point	Experiment A: Melting Range	Experiment A: Median Melting points	Experiment B: Melting Range	Experiment B : Median Melting points	Average Measured Temperature
Standard 1	51.1	51.55	60.3	61.15	61.1	61.9	61.525
	52		62		62.7		
Standard 2	68	69	79.4	80.9	78.6	79.65	80.275
	70		82.4		80.7		
Standard 3	107	107	116	117.45	117.2	118.85	117.325
	107		118.9		120.5		

Table 6: Linkam Hotstage calibration results

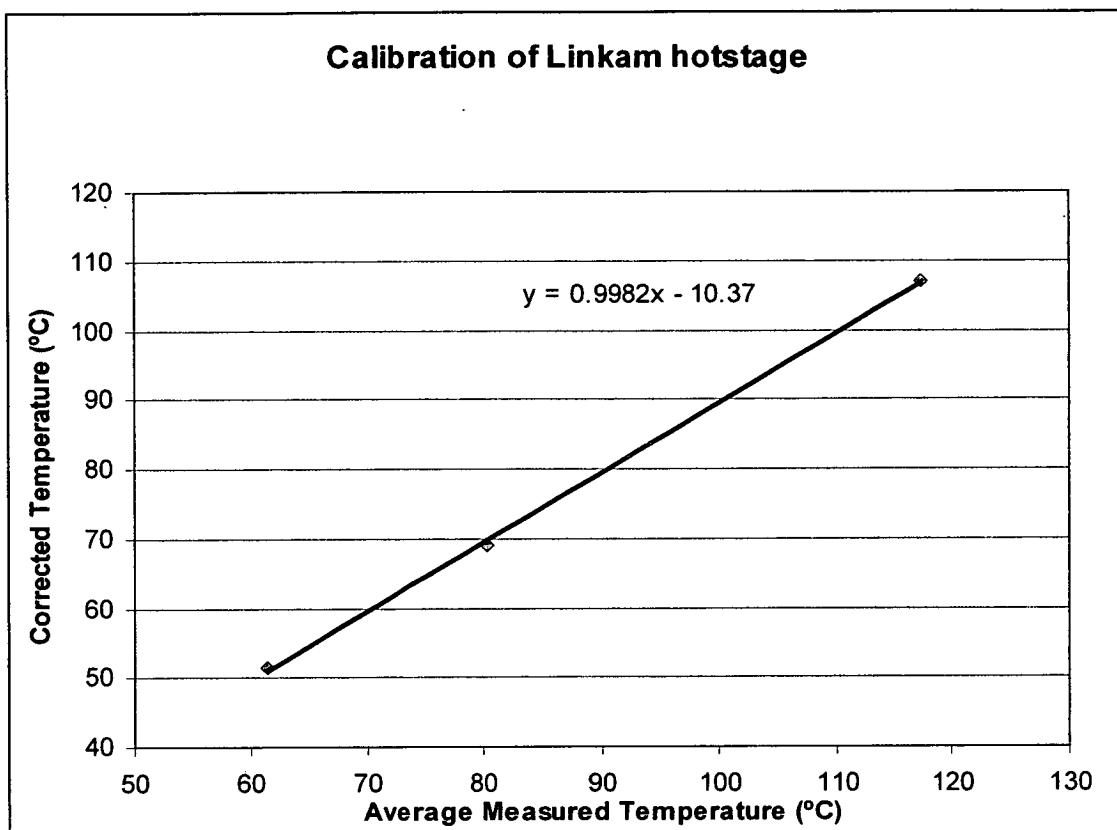


Figure 44: Calibration graph for Linkam hotstage

A relationship was thus found to allow all temperatures recorded on the hot-stage to be corrected. A thick film was made by drop coating and dried under vacuum. The crude films had the texture shown (Figure 45a) this most likely represents the plastic or crystalline phase. Melting into the columnar phase occurred slowly and the birefringent colours observed changed slightly upon heating. Isotropisation occurred at 97 °C (Figure 45e and f), the sample could now be intimately sandwiched with a second clean coverslip (Figure 45g). The texture observed upon slow cooling is shown in (Figure 45i).

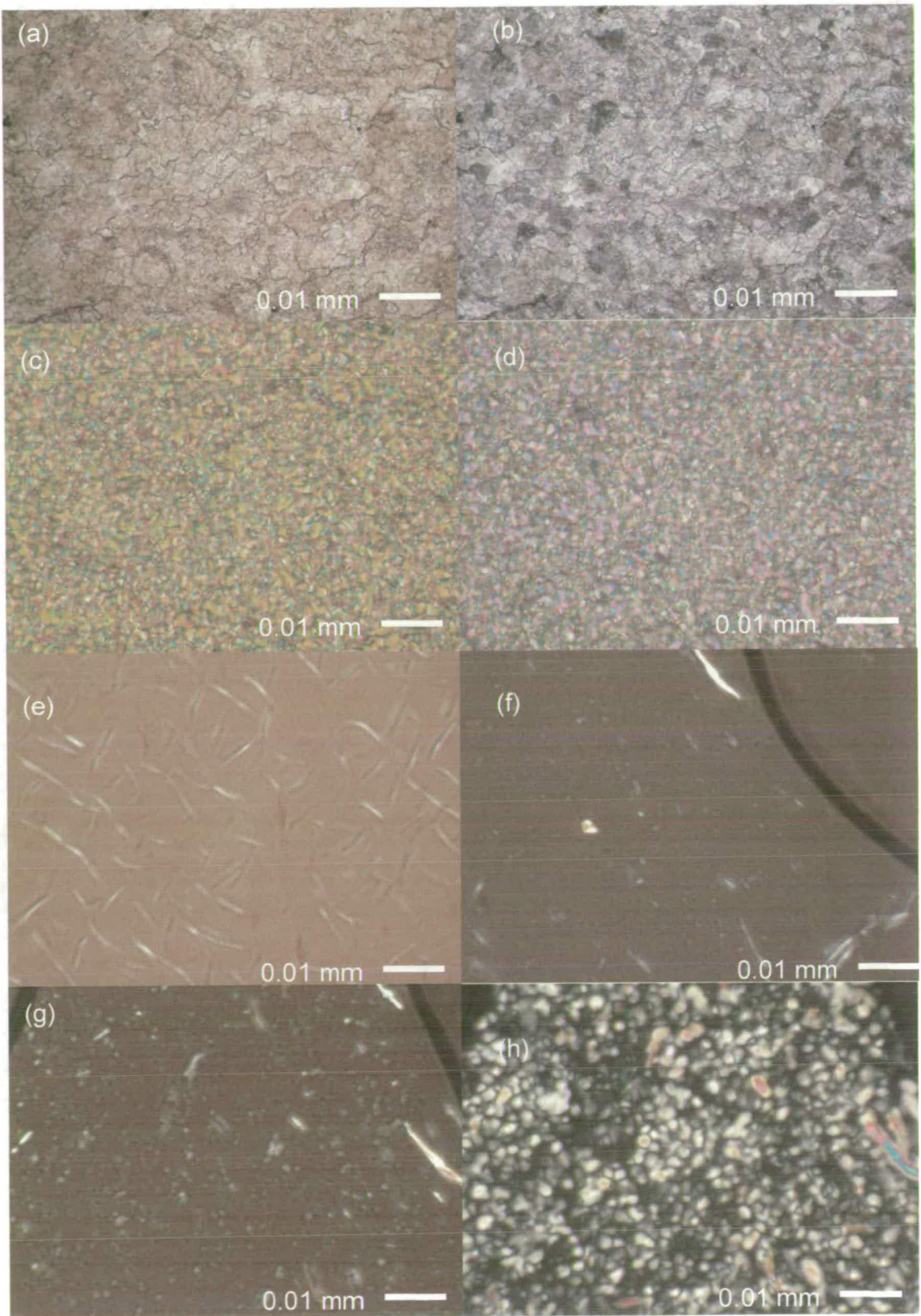


Figure 45: a) Texture of uncovered thick film at 25 °C under parallel polarisers; b) 25 °C, crossed polarisers; c) 50 °C under parallel polarisers; d) 50 °C, crossed polarisers; e) 97 °C, crossed polarisers; f) Sandwiched with second glass slide and reheated to 97 °C under crossed polarisers; g) Cooled slowly (0.5 °C / min) to 50 °C, crossed polarisers, h) Cooled to 25 °C, crossed polarisers.

The temperature of isotropisation was 97 °C when measured by microscopy. A texture characteristic of columnar phases grew when the sample was cooled slowly from the isotropic (Figure 45 f-h)

X-ray scattering to observe liquid crystal phase of complex 1.47

As the heating stage was not available at the required time, complex 1.47 was annealed on a glass slide as for the microscopy samples and trapped in the liquid crystal phase by polymerisation prior to X-ray analysis. Following polymerisation (1 h) the polymer was analysed on a rotating stage.

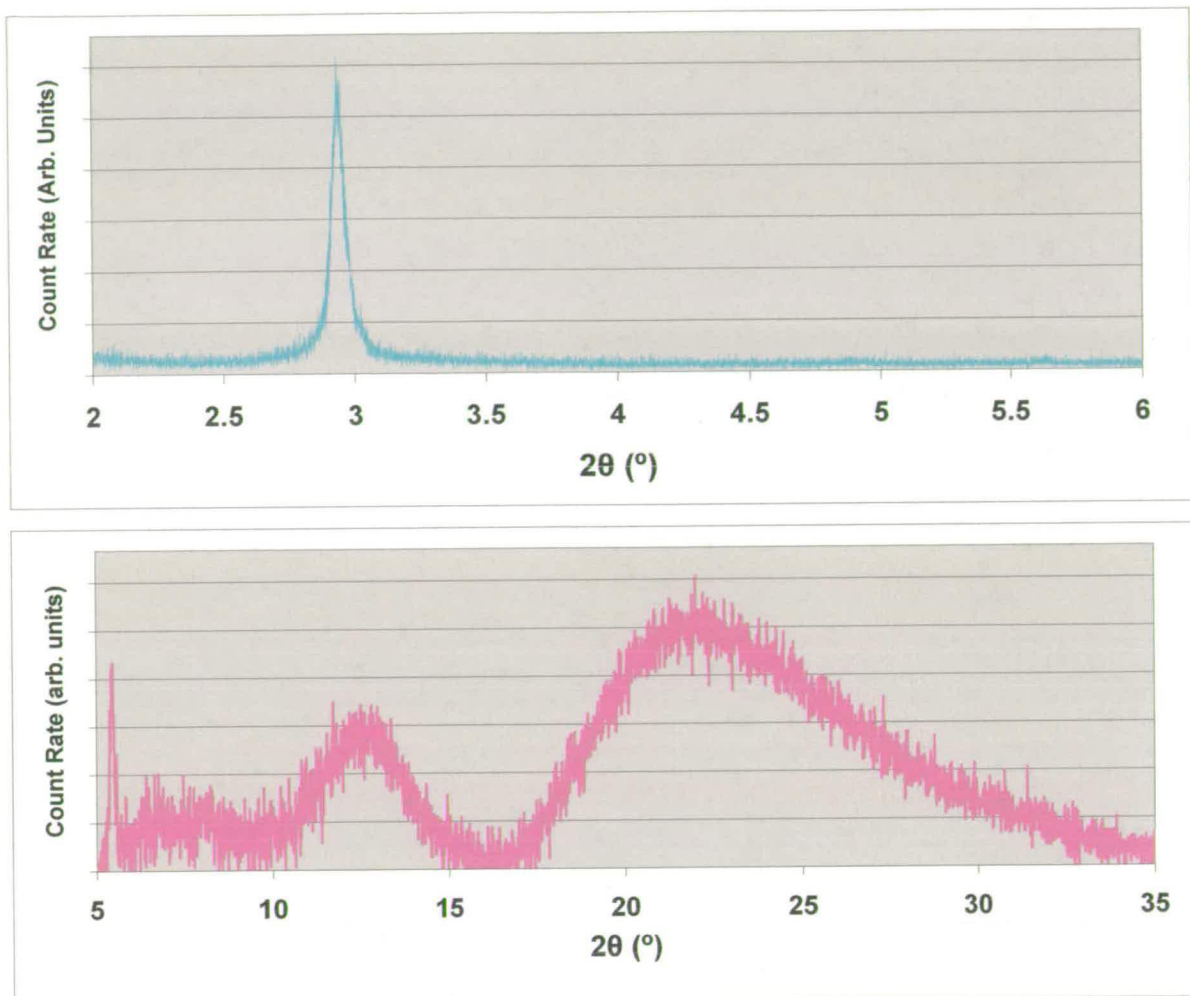


Figure 46: X-ray scattering was performed in two separate experiments using the scintillation counter detector for low angles (above) and the PSD detector for wide angles (below).

Bulk polymerisation

Methacrylate complex **48.47** (289.4 mg, 0.287 mmol) was dissolved in chloroform (2 mL) with the initiator 2,2-dimethoxy-2-phenylacetophenone (7.2 mg, 2.5 % w/w). The formulation was coated on the inside of a quartz tube (12 mm diam.). The mixture was irradiated under nitrogen for 1 h (365 nm, UV photoreactor). The polymer produced was relatively hard and insoluble in DCM-methanol mixtures. The MAS ^1H NMR spectrum was unfortunately very broad and no ^{13}C spectrum was possible due to the low sensitivity of the probe.

In order to reduce the weight fraction of initiator required, the more efficient initiator, 2,4,6-trimethylbenzoylphosphine oxide in combination with the inhibitor MEHQ (methyl hydroquinone) was used. FTIR spectroscopy was used to determine the extent of polymerisation. Samples were prepared by drop casting a solution of the required formulation on to a KBr disc. The samples were analysed before and after polymerisation by normal transmission FTIR spectroscopy. Peak heights were calculated as demonstrated in Figure 47.

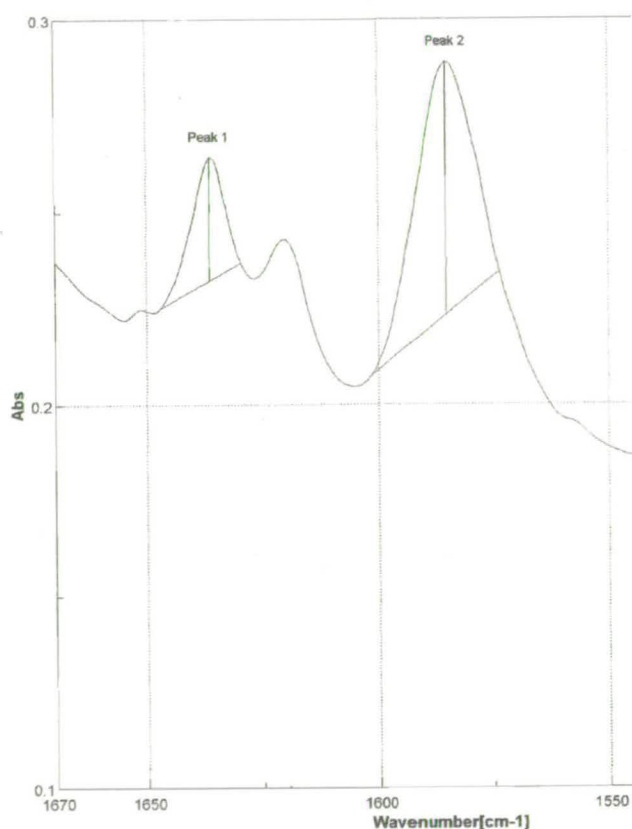


Figure 47: Portion of FTIR spectrum of complex 1.47 in absorbance units. Peak heights were calculated as an average height for two peak base points. Points were the same for each spectrum and were chosen to minimise the inclusion of shoulders in the calculation.

The degree of methacrylate conversion was determined as follows:

$$\text{Conversion (Ratio)} = \frac{((\text{absorbance ratio before poly}) - (\text{absorbance ratio after poly}))}{(\text{height ratio before poly})}$$

Conversion (direct) =

$\frac{\text{Height difference}}{\text{Original height}}$

Experiment	Methacrylate LC 0.8% TMBPO 0.1% MEHQ				Methacrylate LC 0.4% TMBPO 0.1% MEHQ		Methacrylate LC 0.5% DMPA 0.1% MEHQ	
	0 (not annealed)	0 (annealed)	10	60	0	60	0	60
methacrylate C=C str height Absorbance units Peak = 1638 cm ⁻¹ B1 = 1647 cm ⁻¹ B2 = 1633 cm ⁻¹	3.49E-02	3.32E-02	1.12E-02	3.11 E-03	1.36 E-02	4.21 E-03	3.18 E-02	1.86 E-02
Aromatic C=C str height Absorbance units Peak = 1586 cm ⁻¹ B1 = 1573 cm ⁻¹ B2 = 1602 cm ⁻¹	6.67E-02	5.97E-01	6.68E-02	5.06 E-02	2.01 E-02	1.55 E-02	7.03 E-02	6.43 E-02
Ratio	0.52	0.60	0.17	0.06	0.67	0.27	0.45	0.29
Difference of Ratios			0.43	0.54		0.40		0.16
% methacrylate conversion by ratio method	Ratio the same within experimental error – No evidence of methacrylate decomposition		72	90		60		36
% methacrylate conversion by direct method			68	91		69		42

Table 7: Showing calculation of conversion of methacrylate groups in complex 48.47 during polymerisation.

Experiment	Acrylate LC	
	0	60
Acrylate C=C str height Absorbance units Peak = 1636 cm^{-1} B1 = 1647 cm^{-1} B2 = 1630 cm^{-1}	3.21E-02	1.28E-02
Aromatic C=C str height Absorbance units Peak = 1585 cm^{-1} B1 = 1573 cm^{-1} B2 = 1602 cm^{-1}	6.57E-02	5.12E-02
Ratio	0.49	0.25
Difference of Ratios		0.24
% Acrylate conversion (ratio)		49
% Acrylate conversion (direct)		60

Table 8: Showing calculation of conversion of acrylate groups during polymerisation.

Thin film measurements

Representative procedure for spin-casting

For a 2.25% w/v solution, 7.4 mg of the liquid crystalline complex was dissolved in 0.5 mL chloroform. The coverslip or wafer, once in place on the spin caster, was covered with 3-4 drops of the desired solution and spinning was commenced immediately. Films were stored in a dessicator. Varying the concentration of the casting solution and the speed of spinning led to differing film thicknesses. As shown below, faster spinning or a less concentrated solution led to thinner films.

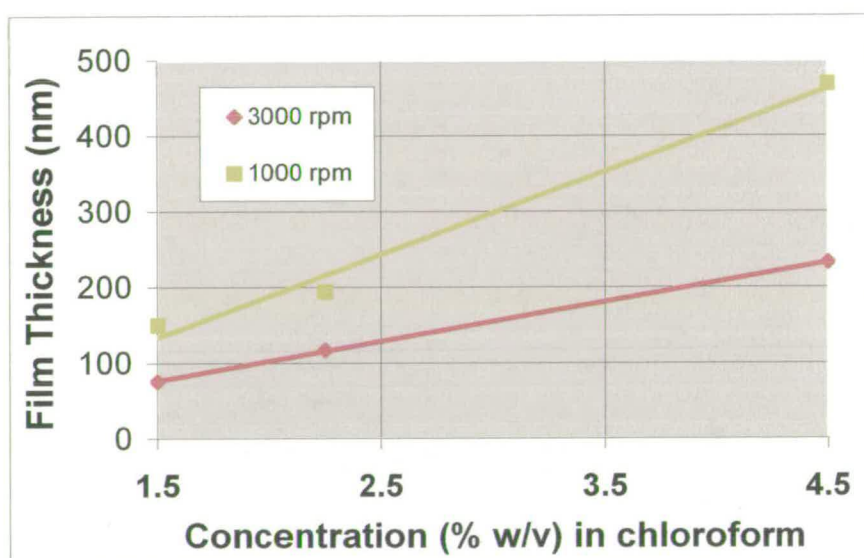


Figure 48: Graph showing the relationship between film thickness and concentration at two different spin speeds.

Polarised optical microscopy

A spin cast film of methacrylate complex **48.47** exhibited the textures shown (Figure 49) upon heating and cooling. In this case isotropisation occurred at a lower temperature setting due to the thinner film. The films were held at the isotropisation temperature for 1 hour prior to slow cooling (0.5 °C/min).

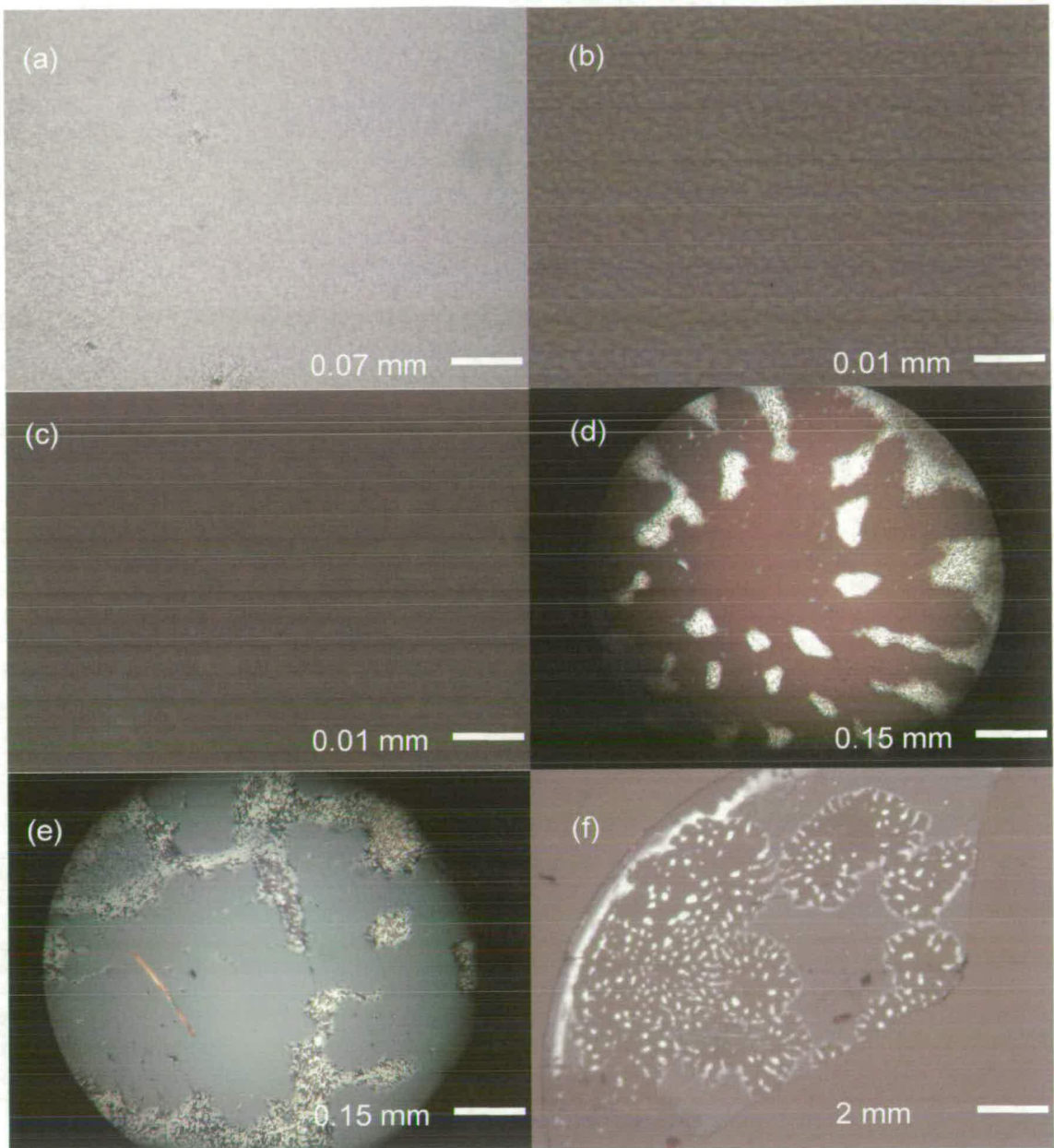


Figure 49: a) Texture of thin film before annealing, 25 °C, crossed polarisers; b) 50 °C under crossed polarisers; c) 90 °C, crossed polarisers; d) After holding at 90 °C for 1 hour and slow cooling to 25 °C under crossed polarisers; e) similar to (d), polarisers not quite crossed; f) View of part of coverslip showing extent of aligned domains.

Incorporation of initiators caused difficulties with alignment of thin films as demonstrated by the examples below:

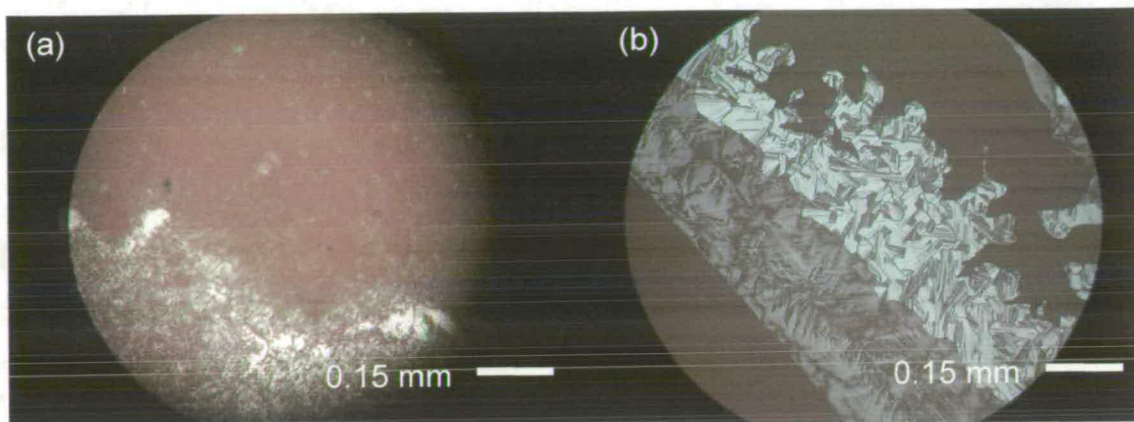


Figure 50: a) Methacrylate complex containing 2.5% w/w 2,2-dimethoxy-2-phenylacetophenone at 130 °C under crossed polarisers after slow heating; b) Methacrylate complex containing 0.8% w/w 2,4,6-trimethylbenzoylphosphine oxide at 45 °C under crossed polarisers.

Some alignment of the acrylate complex 1.47 appeared to occur upon long-term annealing of thin films at 40 °C. This procedure was similar to that used by Kim and co-workers.⁵⁶ Dendritic domains grew as shown in (Figure 51).

Acrylate complex, thinner films (~120 nm)

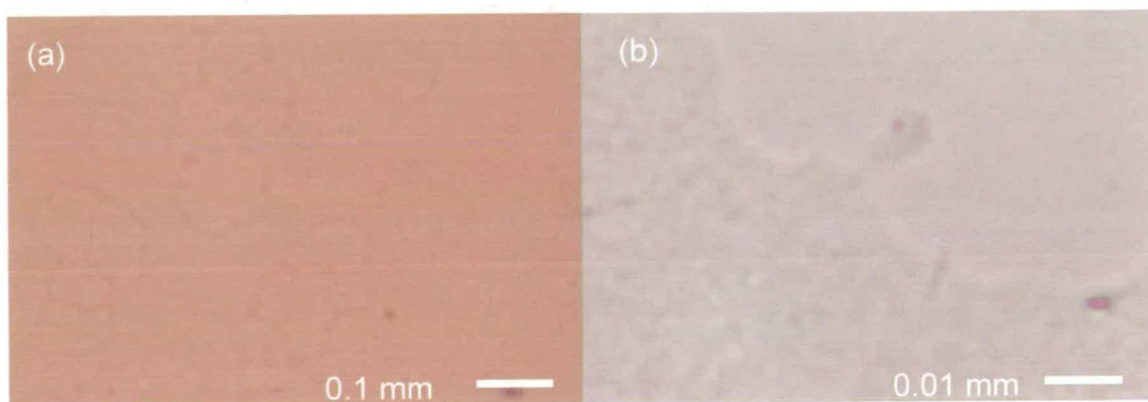


Figure 51: a) Texture under crossed polarisers after heating for 12 h at 40 °C. Aligned area at high magnification. Note that the contrast is low due to the thinness of the film and the field is light due to compensation by the camera.

Acrylate complex, thicker films (>300 nm)

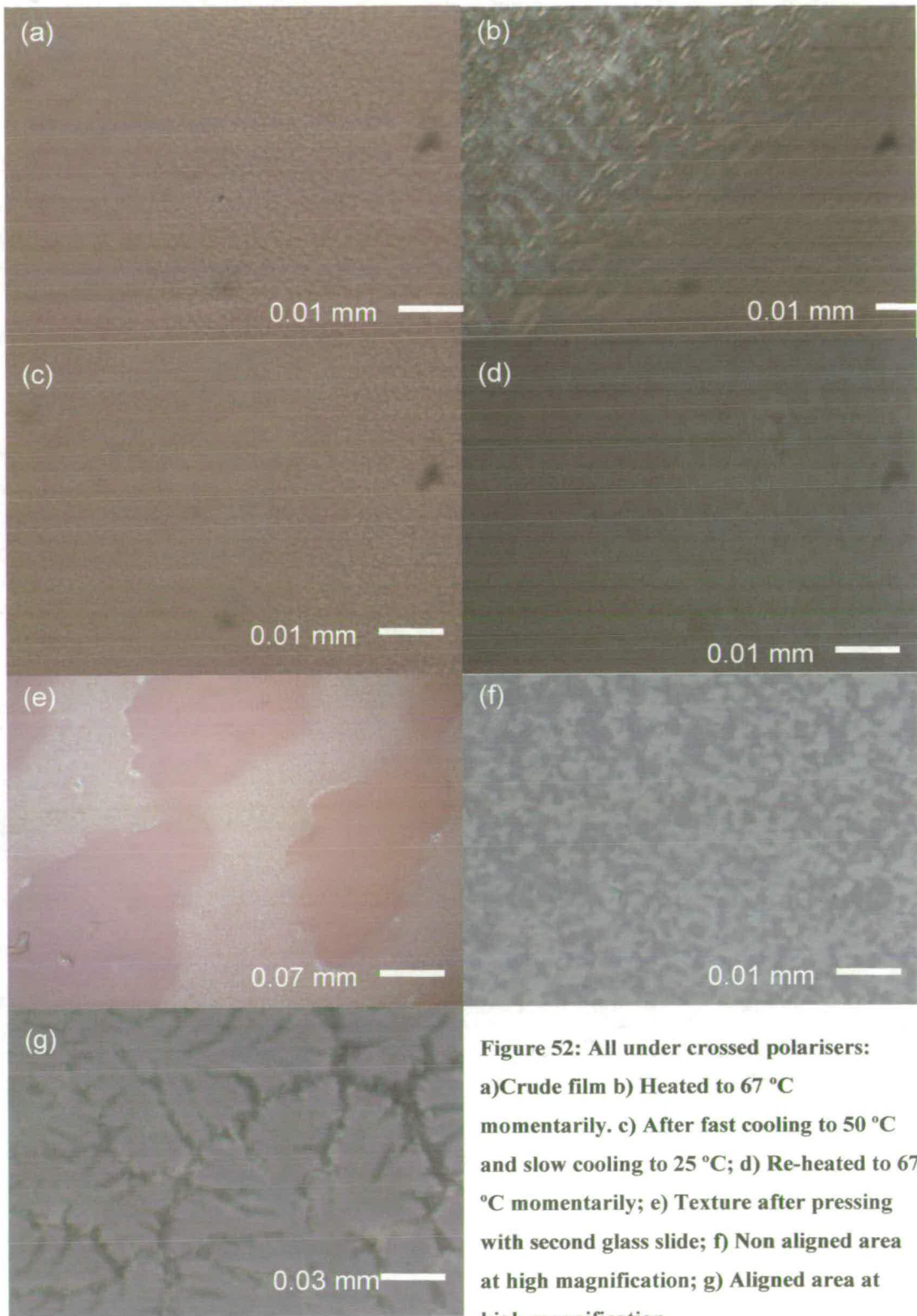


Figure 52: All under crossed polarisers:
a) Crude film b) Heated to 67 °C momentarily. c) After fast cooling to 50 °C and slow cooling to 25 °C; d) Re-heated to 67 °C momentarily; e) Texture after pressing with second glass slide; f) Non aligned area at high magnification; g) Aligned area at high magnification.

Small areas of alignment were also achieved for thick films of the acrylate complex **1.47**. After momentary heating to 67 °C the sample was pressed and cooled slowly from 50 °C to room temperature.

Etching, XPS – preliminary measurements

The samples of blank gold substrates, core **47** and corona **1** have been characterised initially. The samples of core **47** and corona **1** were spotted on to gold coated silicon wafers as solutions in methanol and DCM respectively. The samples were purged for 24 h before analysis.

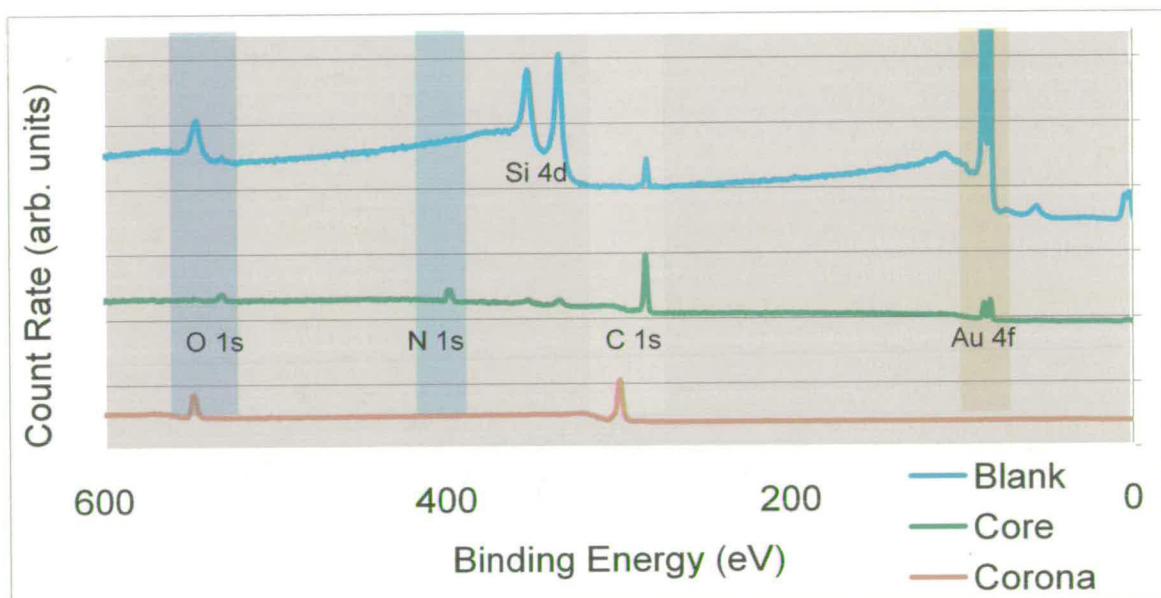
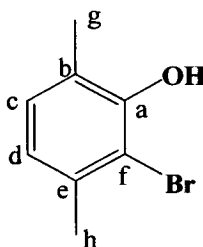


Figure 53: Initial XPS characterisation of components. No impurities appear to be present, however silicon is observed on the gold surface

Thin films (100-500 nm) were formed on gold on silicon substrates. Following 12 h annealing at 40 °C, the films were polymerised and sonicated in 1:1 MeOH : 3N HCl. The films did not deteriorate, XPS characterisation will be attempted in future.

2-Bromo-3,6-dimethylphenol (46)



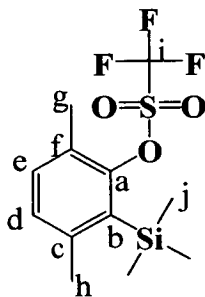
In a 1 L three-necked RB flask fitted with a dry tube, 2,5-dimethylphenol **61** (20.1 g, 16.5 mmol) was dissolved in CS₂ (600 mL) and the mixture degassed with N₂ and protected from light, then cooled to 15 °C. NBS (32.9 g, 18.5 mmol, 1.12 eq) was added slowly. The mixture was stirred and warmed to R.T. over 3 h, the solvent was removed *in vacuo* and the residue filtered through a short silica plug and eluted with hexanes. Kügelrohr distillation (80 °C, 0.5 mbar) gave the desired bromophenol as a colorless oil. Yield: 25.8 g (78%); ¹H NMR (250 MHz, CDCl₃): δ = 7.17 (d, 1H, *J*=7.5 Hz), 6.94 (d, 1H, *J*=7.5 Hz), 5.89 (s, 1H), 2.58 (s, 3H), 2.50 (s, 3H). ¹³C NMR (150 MHz, CDCl₃): δ = 150.7 (C, C-a), 136.0 (C, C-e), 129.7 (CH, C-c), 123.1 (C, C-b), 122.2 (CH, C-d), 113.5 (C, C-f), 23.3 (CH₃, C-h), 16.8 (CH₃, C-g).

N.B. It was discovered that the bromophenol is unstable, so has to be stored under N₂ atmosphere and in the dark. Reaction repeated twice.

(2-Bromo-3,6-dimethylphenoxy)trimethylsilane (62)

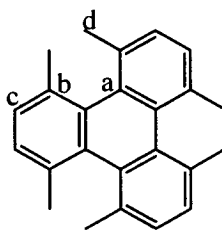
A mixture of 2-bromo-3,6-dimethylphenol (31.2 g, 155 mmol) and HMDS (325 mL, 10 eq) was stirred at 80 °C in a dry three-neck flask under N₂ atmosphere for 48 h. Excess NH₃ and unreacted HMDS were flushed carefully through a diaphragm pump with a flow of nitrogen. After ¹H NMR confirmation of near quantitative formation of the corresponding silane **62**, the crude product was employed in the next step without further purification. Yield: 41.4 g (98%); ¹H NMR: δ = 6.87 (d, 1H, *J*=7.5 Hz), 6.70 (d, 1H, *J*=7.5 Hz), 2.29 (s, 3H), 2.12 (s, 3H), 0.23 (s, 9H).

3,6-Dimethyl-2-(trimethylsilyl)phenyltrifluoromethanesulfonate (**63**)



The crude product **62** (19.9 g, 72.7 mmol) was dissolved in dry THF (350 mL) in a 1 L RB flask. The solution was cooled to $-100\text{ }^{\circ}\text{C}$ (liquid $\text{N}_2/\text{Et}_2\text{O}$ bath) and BuLi (49.9 mL, 1.6 M solution in hexanes, 1.1 eq) was added over 5 min. The mixture was stirred for 30 minutes and the temperature reached $-80\text{ }^{\circ}\text{C}$. The mixture was cooled again to $-100\text{ }^{\circ}\text{C}$, Tf_2O (14.7 mL, 1.2 eq) was added over 5 minutes, and stirring was continued for 30 minutes while the temperature reached $-80\text{ }^{\circ}\text{C}$. Cold satd. aq. NaHCO_3 (200 mL) was added, and the aqueous layer extracted with Et_2O (3 x 200 mL). The combined organic layers were dried over Na_2SO_4 , filtered and concentrated under reduced pressure. The residue was purified by flash column chromatography on silica gel with hexanes to afford the silyl triflate **63**. Yield: 15.74 g (66%); ^1H NMR(250 MHz, CDCl_3): δ =7.03 (d, 1H, J =7.5 Hz), 6.91 (d, 1H, J =7.5 Hz), 2.33 (s, 3H), 1.97 (s, 3H), 0.24 (s, 9H). ^{13}C NMR (150 MHz, CDCl_3): δ =148.6 (C, C-a), 142.6 (C, C-c), 131.5 (CH, C-e), 131.2 (C, C-b), 128.7 (C, C-f), 126.9 (CH,C-d), 116.9 (CF_3 , C-i, q $J_{\text{C-F}}$ = 5.1 Hz), 21.6 (CH_3 , C-h), 15.1 (CH_3 , C-g), 0.0 (CH_3 , C-j).

1,4,5,8,9,12-Hexamethyltriphenylene (36)



To a 1 L three necked RB flask, a solution was prepared by dissolving **63** (15.1 g, 46.4 mmol) in dry MeCN (450 mL) then deoxygenated. Pd(dba)₂ (2.10 g, 2.30 mmol) and anhydrous CsF (13.9 g, 92 mmol) were added and stirred under N₂ at room temperature overnight. Then, the reaction mixture was concentrated by rotary evaporation (~50 mL) and transferred to a separating funnel. CH₂Cl₂ (150 mL) and H₂O (100 mL) were added and the organic layer collected. The aqueous layer was washed with CH₂Cl₂ (2 × 100 mL). The organic layers were combined, dried over Na₂SO₄, filtered and concentrated under reduced pressure. The residue was purified by flash column chromatography on silica gel with hexanes to provide white crystals of **36**. The crude product was recrystallized slowly from EtOH to give pure material suitable for X-ray. Yield: 9.42 g (65%); mp: 160-162 °C; ¹H NMR (250 MHz, CDCl₃): δ = 7.31 (s, 6H), 2.54 (s, 18H). ¹³C NMR (150 MHz, CDCl₃): δ = 133.5 (C, C-a), 131.4 (C, C-b), 129.3 (CH, C-c), 22.9 (CH₃, C-d). MS: *m/z* = 312 (M⁺, 100), 154 (M - C₁₂H₁₂, 73), 77 (M - C₁₈H₁₉, 51). UV/Vis (CH₂Cl₂): λ_{max} (ε_{max}) = 235 (12500), 281 (23200) nm (Lmol⁻¹cm⁻¹). FT-IR (cm⁻¹): 3044, 2986, 2949, 2866, 1456, 1378. Elemental analysis: calculated C 92.24%, H 7.74%; actual C 92.26%, H 7.67%.

Crystal data and structure refinement for 1,4,5,8,9,12-Hexamethyltriphenylene 36 (C₂₄H₂₄)

X-ray diffraction data were collected at 150 K using Mo-K alpha radiation on a Bruker Smart Apex CCD diffractometer. The sample was a colourless plate of dimensions 0.42 x 0.34 x 0.11 mm. The structure was solved by direct methods (SIR92) and refined as a twin formed by a two-fold rotation about [100] using CRYSTALS. The twin scale factor was 0.1582(19) and final conventional R-factor was 0.0652; other crystal and refinement statistics are available in the cif which forms part of the supplementary material available with this paper. Analysis of the geometry of the crystal structure was accomplished using PLATON.

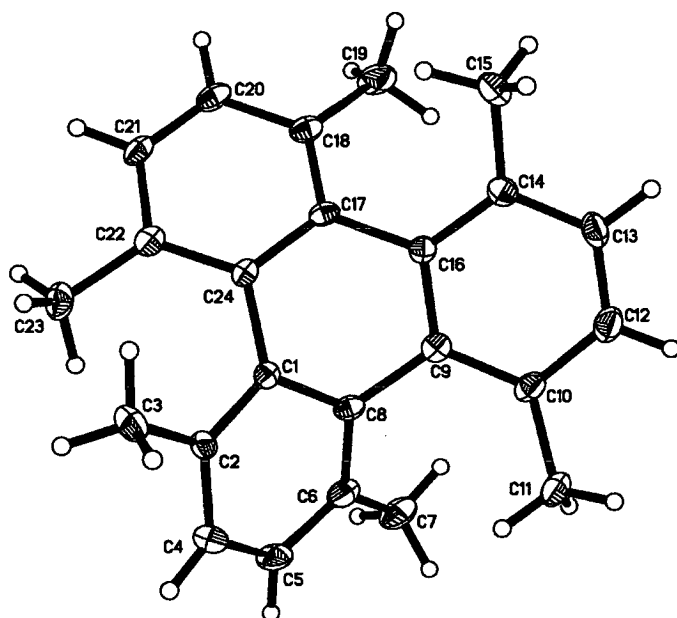


Figure 54 Molecular Structure of 1,4,5,8,9,12-hexamethyltriphenylene 36. Thermal ellipsoids drawn at 50% probability. Hydrogen atoms represented by white circles.

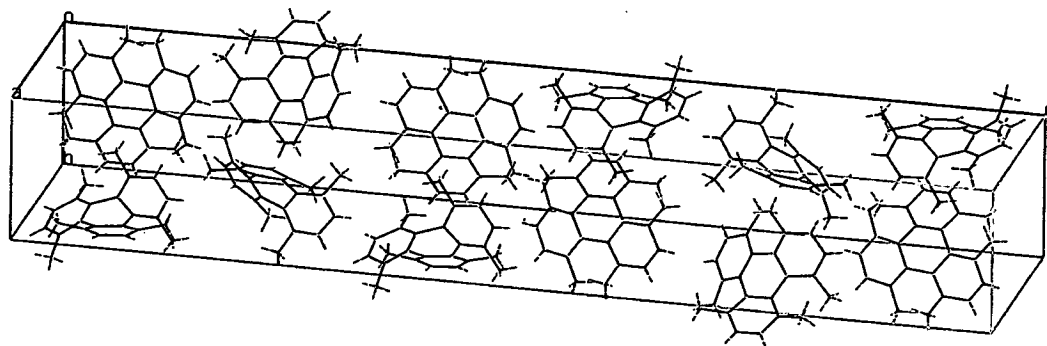


Figure 55: Unit cell of 1,4,5,8,9,12-hexamethyltriphenylene 36. Hydrogen atoms represented by white sticks.

Comparison of RMS Deviation

A measure of distortion from planarity of **36** can be achieved by comparing least squares planes (rms deviation). The central ring A, which is most distorted (non-benzenoid) has the highest rms deviation. The rings with lowest deviation (rings B and D) are consistent with the most in tact 'planar' benzenoid rings.

Plane 1 (ring C) : $0.9914(2)x - 0.1186(17)y + 0.0547(18)z = 0.134$
(C1-2-4-5-6-8)

Plane 2 (ring A): $0.8082(9)x - 0.5398(13)y - 0.2355(16)z = 0.257$
(C1-8-9-16-17-24)

Plane 3 (ring B) : $0.6532(13)x - 0.4723(15)y - 0.5918(14)z = 0.053$
(C9-10-12-13-14-16)

Plane 4 (ring D) : $-0.5543(13)x + 0.8272(9)y + 0.00920(16)z = 0.055$
(C17-18-20-21-22-24)

Comparison of angles between planes

Another measure of distortion of **36** can be achieved by comparing the plane angles:

$$\text{Plane 1 (ring C) } \angle \text{ Plane 2 (ring A) } = 31.52^\circ$$

$$\text{Plane 3 (ring C) } \angle \text{ Plane 2 (ring A) } = 22.75^\circ$$

$$\text{Plane 4 (ring C) } \angle \text{ Plane 2 (ring A) } = 23.63^\circ$$

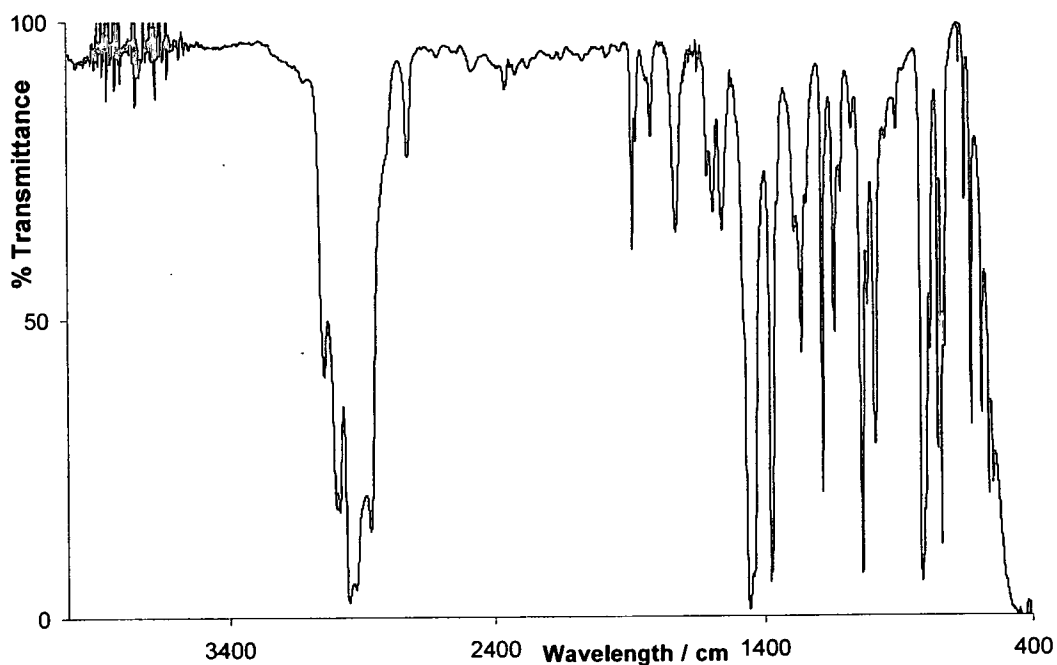
Non-bonded contacts:

$$\text{C3} - \text{C23} = 2.941 \text{ \AA.}$$

$$\text{C15} - \text{C19} = 3.005 \text{ \AA.}$$

$$\text{C11} - \text{C7} = 2.985 \text{ \AA.}$$

FT-IR Spectrum of 1,4,5,8,9,12-Hexamethyltriphenylene **36**.



Variable-Temperature ^{13}C NMR Study of 1,4,5,8,9,12-Hexamethyltriphenylene 36.

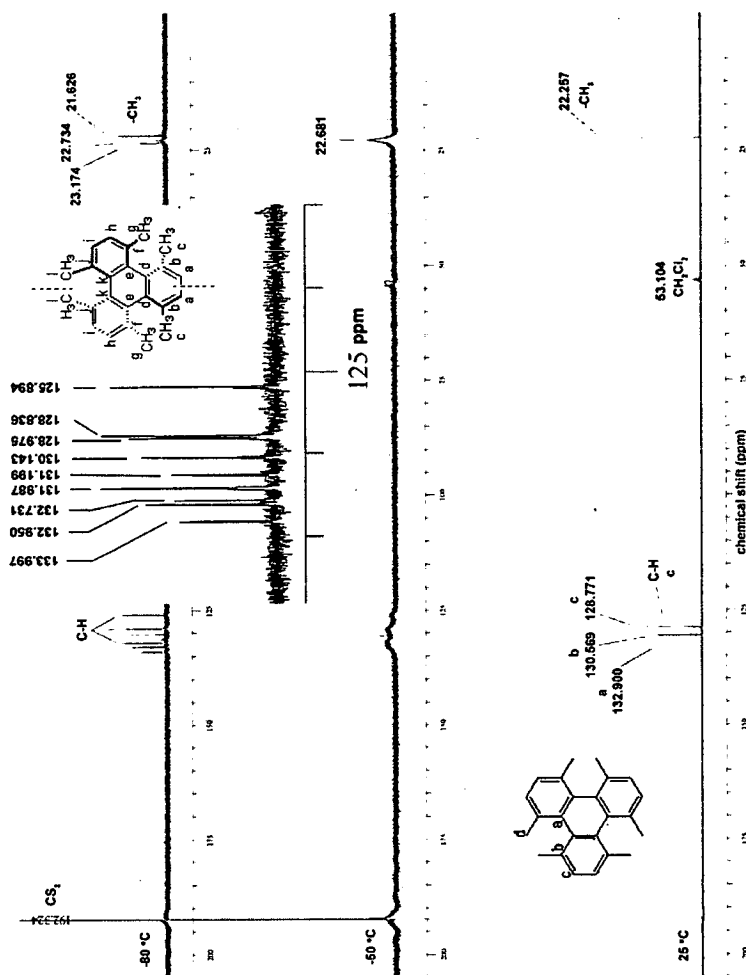


Figure 56: ^{13}C VT-NMR study of 36. At $25\text{ }^\circ\text{C}$, only four peaks are seen which is consistent with rapid conformational interconversions. At $-50\text{ }^\circ\text{C}$, broadening of these signals is observed as the rate of interconversion decreases. At $-80\text{ }^\circ\text{C}$, the nine aromatic peaks and three methyl peaks are revealed. These twelve peaks are indicative of a C_2 symmetric structure. The peaks at 125.894, 128.836, and 131.987 ppm correspond to C-H carbons in different environments. The three methyl peaks (21.626, 22.734, and 23.174 ppm) also relate to different environments.

Fluorescence of 1,4,5,8,9,12-Hexamethyltriphenylene 36.

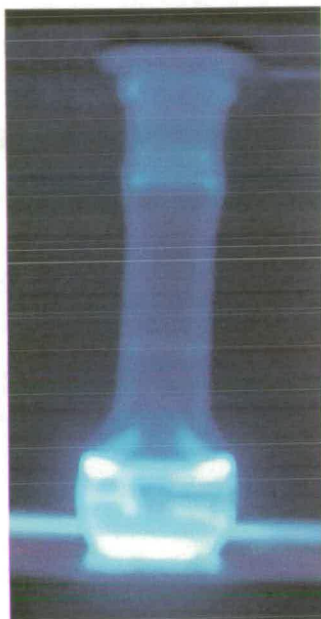


Figure 57: Blue fluorescence of 36. [36] = 20 mg/mL in CH₂Cl₂.

Cyclic Voltammogram of 1,4,5,8,9,12-Hexamethyltriphenylene showing the irreversibility of 36.

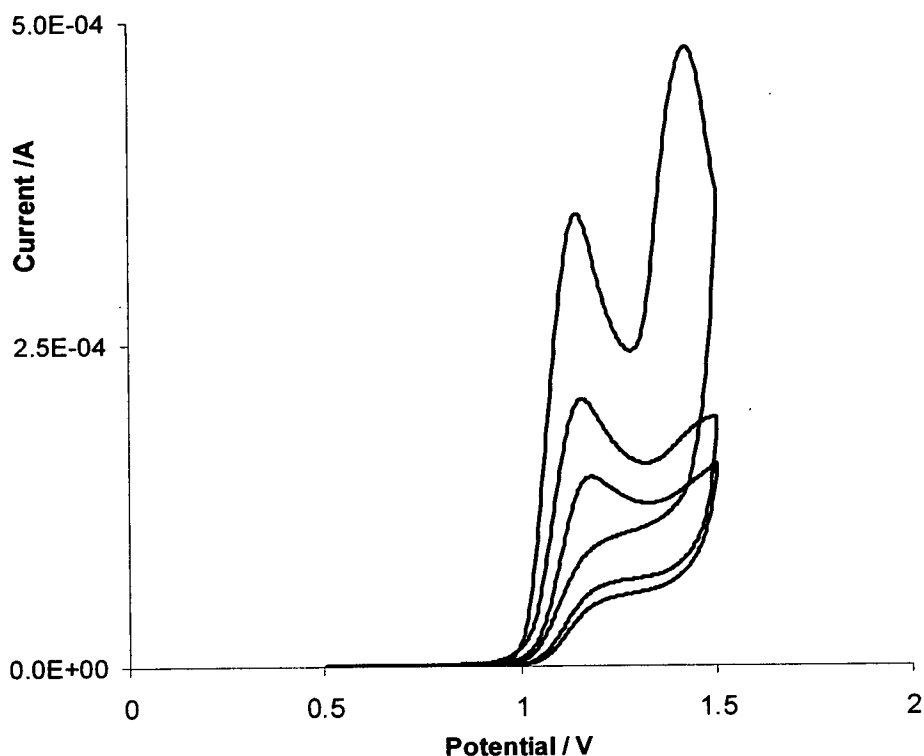
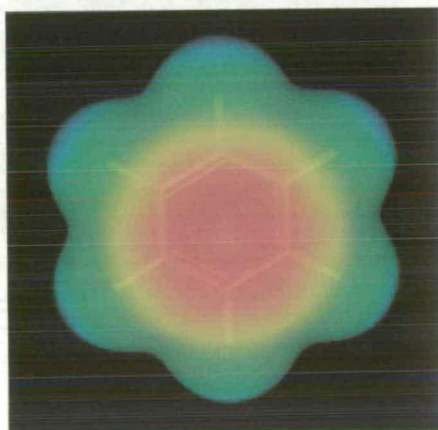
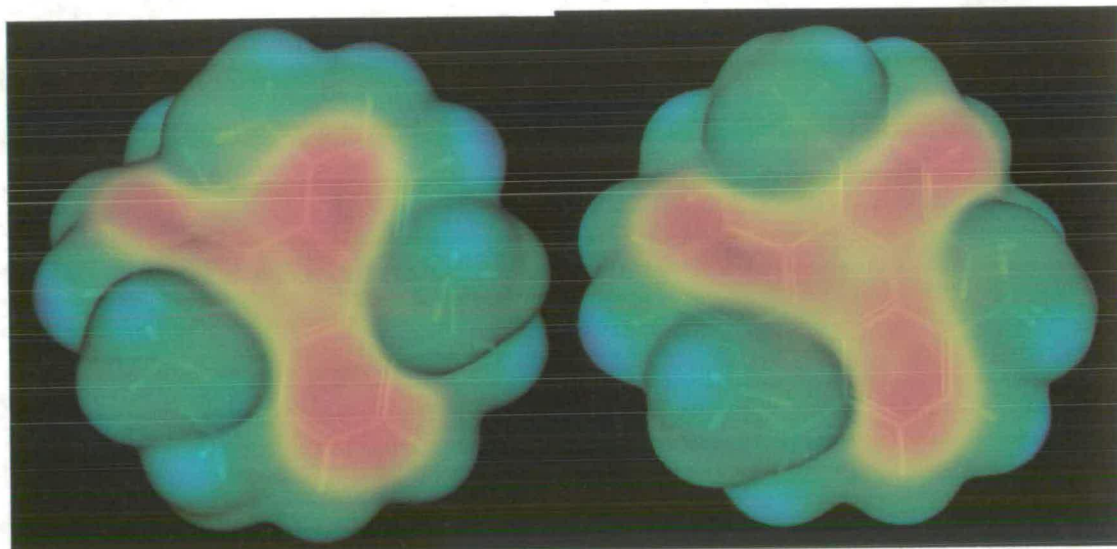


Figure 58: Cyclic voltammogram of 36 (three scans) with sweep rate of 20 mV/s. [36] = 1 mM in acetonitrile. Reference electrode was made in-house and consists of a Ag wire dipped into a solution of AgClO_4 (0.01 M) in background electrolyte solution, with a potential of +0.437 V vs SCE. Background electrolyte solution consists of 0.1 M anhydrous LiClO_4 in acetonitrile (dried; distilled). Counter electrode is a 2 cm^2 Pt gauze, working electrode was a 0.387 cm^2 Pt rotating-disc electrode. Electrodes were connected to a three-electrode potentiostat AUTOLAB PGSTAT30 (Eco Chemie B.V) equipped with GPES 4.9 software.

Computational studies of 36.

Figure 59: Electrostatic Potential Maps of 1,4,5,8,9,12-Hexamethyltriphenylene 5. C_2 Conformer is top left and the D_3 conformer top right (both are optimized geometries). Red electron rich, blue electron poor.

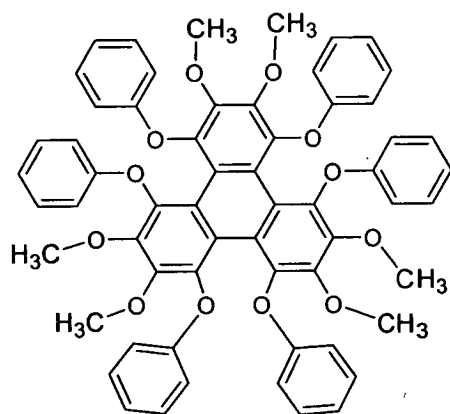


LEFT: Electrostatic Potential Map of Benzene (for comparison).

Note the redder electron-rich areas 'localized' over the outer benzene rings of the C_2 conformer, and the lesser amount of negative charge situated over the central ring. Contrary to this, in the D_3 system there is less redder negative charge on the outer

rings (delocalized) and slightly more located over the central ring. This supports the theory that hindered triphenylene systems can be seen as three separate aromatic joined by low order bonds.

The full structure of the *mimic* employed for calculation of the C_2-C_2 transition state of the peraryloxytriphenylenes 58a-c.



Mimic used
for
aryloxy-
systems in
calculations

Figure 60: Table 5. Table of RMS values determined for comparison of X-ray and Molecular Modelling.

		RMS deviation
AM1	X-ray 1	0.0406
AM1	X-ray 2	0.0454
AM1	X-ray 3	0.0491
HF 6-31Gdp	X-ray 1	0.0303
HF 6-31Gdp	X-ray 2	0.0512
HF 6-31Gdp	X-ray 3	0.0548
RHF 6-311Gdp	X-ray 1	0.0321
RHF 6-311Gdp	X-ray 2	0.0525
RHF 6-311Gdp	X-ray 3	0.0564
B3LYP 6-31Gdp	X-ray 1	0.0280
B3LYP 6-31Gdp	X-ray 2	0.0435
B3LYP 6-31Gdp	X-ray 3	0.0475
B3LYP 6-311Gdp	X-ray 1	0.0282
B3LYP 6-311Gdp	X-ray 2	0.0466
B3LYP 6-311Gdp	X-ray 3	0.0509

The X-ray structures correspond to 3 different molecules within a unit cell. Note, due to weak diffraction of H's in X-ray structures, the RMS deviations for the carbon skeletons were compared, to give meaningful numbers.

Visual Molecular Dynamics (VMD 1.8.5) software was used to calculate RMS deviations. This program is available free from the internet.

RMSD for carbon skeletons of X-ray structures = 0.0388

Mean RMSD

AM1 and all X-rays = 0.0450

HF 6-31Gdp and all X-rays = 0.0454

RHF 6-311Gdp and all X-rays = 0.0470

B3LYP 6-31Gdp and all X-rays = 0.0396

B3LYP 6-31Gdp and all X-rays = 0.0419

Table 9: Calculated bond lengths (Å) for 36 (neutral) and 36^{•+} (radical cation)

	36	36^{•+}	36^{•+} - 36
C(1) – C(2)	1.411413	1.425211	0.013798
C(1) – C(8)	1.434101	1.457091	0.02579
C(1) – C(24)	1.481616	1.452136	-0.02948
C(2) – C(4)	1.398635	1.384559	-0.01408
C(4) – C(5)	1.388897	1.414965	0.026068
C(5) – C(6)	1.398635	1.384557	-0.01408
C(6) – C(8)	1.411413	1.425215	0.013802
C(8) – C(9)	1.481619	1.452132	-0.02949
C(9) – C(10)	1.420612	1.434667	0.014055
C(9) – C(16)	1.431033	1.437711	0.006678
C(10) – C(12)	1.397935	1.399232	0.001297
C(12) – C(13)	1.381661	1.378618	-0.00304
C(13) – C(14)	1.394897	1.411073	0.016176
C(14) – C(16)	1.410279	1.398352	-0.01193
C(16) – C(17)	1.474818	1.47658	0.001762
C(17) – C(18)	1.410279	1.398353	-0.01193
C(17) – C(24)	1.431032	1.437707	0.006675

C(18) – C(20)	1.394898	1.411074	0.016176
C(20) – C(21)	1.381662	1.378615	-0.00305
C(21) – C(22)	1.397936	1.399233	0.001297
C(22) – C(24)	1.420609	1.434666	0.014057

Bibliography

- 1 Stryer, L. "Biochemistry", 4th edn.; W. H. Freeman and company, New York, 1999.
- 2 a) Greig, L. M.; Philp, D. *Chem. Soc. Rev.* **2001**, *30*, 287–302. b) Lawrence, D. S.; Jiang, T.; Levett, M. *Chem. Rev.* **1995**, *95*, 2229-2260.
- 3 Whitesides, G. M.; Mathias, J. P.; Seto, C. T. *Science*, **1991**, *254*, 1312-1318.
- 4 Bong, D. T.; Clark, T. D.; Granja, J. R.; Ghadiri, M. R. *Angew. Chem.* **2001**, *113*, 1016 – 1041; *Angew. Chem. Int. Ed.* **2001**, *40*, 988 – 1011.
- 5 Kato, T.; Mizoshita, N. *Current opinion in solid state and materials science*, **2002**, *6*, 579-587.
- 6 Keizer, H. M.; Sijbesma, R. P. *Chem. Soc. Rev.* **2004**, 226-234.
- 7 Butler, P. J. G.; Klug, A. *Nature New Biol.* **1971**, *229*, 47 - 50.
- 8 Butler, P. J. G. *J. Gen. Virol.* **1984**, *65*, 253 - 279. Produced a diagram and mechanism subsequently reproduced by the following website amongst others: www.vu-wien.ac.at/i123/ALLVIR/SELFASSEMB1.HTML and http://mrsec.wisc.edu/Edetc/technologist/thumbnails/Matt/Virus_diagram.jpg
- 9 a) A. Klug, *Angew. Chem., Int. Ed. Engl.*, **1983**, *22*, 565. b) A. Klug, *Phil. Trans. R. Soc. Lond., Ser. B*, **1999**, *354*, 531.
- 10 Laitinen, O. H.; Marttila, A. T.; Airene, K. J.; Kulik, T.; Livnah, O.; Bayer, E. A.; Wilchek, M.; Kulomaa, P. *J. Biol. Chem.*, **2001**, *276*, 8219-8224.
- 11 Pris, L. J.; Reinhoudt, D. N.; Timmerman, P. *Angew. Chem. Int. Ed.* **2001**, *40*, 2382-2426.
- 12 Jorgensen, J. L.; Pranata, J. *J. Am. Chem. Soc.* **1990**, *112*, 2008-2010.
- 13 Zimmerman, S. C.; Murray, T. J. *Tet. Let.*; **1994**, 4077-4080.
- 14 Sijbesma, R. P.; Beijer, F. H.; Brunsveld, L.; Folmer, B. J. B.; Hirschberg, J. H. K. K.; Lange, R. F. M.; Lowe, J. K. L.; Meijer, E. W. *Science*, **1997**, *278*, 1601 - 1604.
- 15 Berl, V.; Schmutz, M.; Krische, M. J.; Khoury, R. G.; Lehn, J.-M. *Chem. Eur. J.* **2002**, *4*, 1227-1243.
- 16 El-ghayoury, A.; Schenning, P. H. J.; van Hal, P.A.; van Duren, J. K. J.; Janssen, R. A. J.; and E. W. Meijer. *Angew. Chem. Int. Ed.* **2001**, *40*, 3660-3663.
- 17 Hartgerink, J. D.; Clark, T. D.; Ghadiri, M. R. *Chem. Eur. J.* **1998**, *4*, 1367-1372.
- 18 Smith, D. K.; *J. Chem. Ed.* **2005**, *82*, 393-400.
- 19 Fernandez-Lopez, S.; Kim, H. S.; Choi, E. C.; Delgado, M.; Granja, J. R.; Khasanov, A.; Kraehenbuehl, K.; Long, G.; Weinberger, D. A.; Wilcoxon, K. M.; Ghadiri, M. R. *Nature* **2001**, *412*, 452–455.
- 20 Couet, J. D.; Jeyaprakash, S.; Kopyshv, A.; Santer, S.; Biesalski, M. *Angew. Chem. Int. Ed.* **2005**, *44*, 3297 –3301.

-
- 21 Song, J.; Cisar, J. S.; Betoizzi, C. R. *J. Am. Chem. Soc.* **2004**, *126*, 8459-8465.
- 22 Mouffouk, F.; Higgins, S.J.; Brown, S.J.; Sedghi, N.; Eccleston, B.; and Reeman, S. *Chem. Comm.*, **2004**, *20*, 2314 – 2315.
- 23 a) Zeng, F.; Zimmerman, S. C.; Kolotuchin, S. V.; Reichert, D. E. C.; Ma, Y. *Tetrahedron*, **2002**, *58*, 825-843. b) Zeng, F.; Zimmerman, S. C.; Ma, Y. *J. Am. Chem. Soc.* **2002**, *124*, 13757-13769.
- 24 Chandrasekhar, S.; Sadashiva, B. K.; Suresh, K. A. *Pramana*, **1977**, *9*, 471.
- 25 Kato, T.; Mizoshita, N.; Kishimoto, K. *Angew. Chem.* **2006**, *118*, 44 – 74; *Angew. Chem. Int. Ed.* **2006**, *45*, 38 – 68.
- 26 D. M. Walba, E. Korblova, R. Shao, J. E. MacLennan, D. R. Link, M. A. Glaser, N. A. Clark, *Science* **2000**, *288*, 2181 – 2184.
- 27 Percec, V.; Johansson, G.; Ungar, G.; Zhou, J. *J. Am. Chem. Soc.* **1996**, *118*, 9855-9866
- 28 Collins, P.J.; Hird, M. "Introduction to liquid crystals" Taylor & Francis, **1997**.
- 29 Höger, S.; *Chem. Eur. J.* **2004**, *10*, 1320 – 1329.
- 30 Barbera, J.; Rakitin, O. A.; Ros, M. B.; Torroba, T. *Angew. Chem. Int. Ed.* **1998**, *37*, 296-299.
- 31 Chandkhar, S.; Ranganath, G. S. *Rep. Prog. Phys.* **1990**, *53*, 57-84.
- 32 Kouwer, P. H. J.; Jager, W. F.; Mijs, W. J.; Picken, S. J. *J. Mat. Chem.*, **2003**, *13*, 458-469.
- 33 Crawford, Gregory P.; Hurt, Robert H. *Encyclopedia of Nanoscience and Nanotechnology.* **2004**, *6*, 879-905.
- 34 Hamelinck, P. J.; Huck, W. T. S. *J. Mater. Chem.*, **2004**, *11*, 381-385.
- 35 Fechtenkötter, A.; Tchegotareva, N.; Watson, M.; Müllen, K. *Tetrahedron*, **2001**, 3769-3783.
- 36 Simpson, C. D.; Wu, J.; Watson, M. D.; Muellen, K. *J. Mat. Chem.* **2004**, *14*, 494-504.
- 37 Bouligand, Y. *J. Physique*, **1980**, *41*, 1297-1307.
- 38 Hatsusaka, K.; Ohta, K.; Yamamoto I.; Shirai, H. *J. Mater. Chem.*, **2001**, *11*, 423-430
- 39 Yip, W. C.; Bhat, A. Gururaj; Kwok, H. S. "Room temperature laser deposited indium tin oxide films for display applications." Materials Research Society Symposium Proceedings. **1994**, *345*, 261-265.
- 40 Vij, J. K.; Kocot, A.; Perova, T. S. *Mol. Cryst. & Liq. Cryst.* **2003**, *397*, 531-544.
- 41 Yoshio, M.; Mukai, T.; Ohno, H.; Kato, T. *J. Am. Chem. Soc.* **2004**, *126*, 994-995.
- 42 Yoshio, M.; Mukai, T.; Ohno, H.; Kato, T. *J. Am. Chem. Soc.* **2006**, *128*, 5570-5577.
- 43 Jung, H. T.; Kim, S. O.; Ko, Y. K.; Yoon, D. K.; Hudson, S. D.; Percec, V.; Holerca, M. N.; Cho, W. D.; Mosier, P. E.; *Macromolecules*, **2002**, *35*, 3717-3731.
- 44 Grelet, E.; Bock, H., *Europhys. Lett.* **2006**, *73*, 712-718.
- 45 Boden, N.; Bushby, R. J.; Clements, J.; Movaghar, B. *J. Mater. Chem.*, **1999**, *9*, 2081-2086.
- 46 Schmidtke, J. P.; Friend, R. H.; Kastler, M.; Müllen, K.; *J. Chem. Phys.* **2006**, *124*, 174704
- 47 Liu, C. Y.; Fechenkötter, A.; Watson, M. D.; Müllen, K.; Bard, A. J. *Chem. Mater.* **2003**, *15*, 124.
- 48 C. M. Paleos, D. Tsiourvas, *Liq. Cryst.* **2001**, *28*, 1127 – 1161.

- 49 Kanie K.; Yasuda T.; Ujiie S.; Kato T. *Chem. Commun.* **2000**, 1899-1900.
- 50 Kraft, A.; Reichert, A.; Kleppinger, R.; *Chem. Commun.* **2000**, 1015-1016.
- 51 Lee, J. H.; Han, M.-J.; Hwang, S. H.; Jang, I.; Lee, S. J.; Yoo, S. H.; Jho, J. Y.; Park, S.-Y., *Tetrahedron Letters* **2005**, *46*, 7143-7146.
- 52 Piermattei, A.; Giesbers, M.; Marcelis, A. T. M.; Mendes, E.; Picken, S. J.; Crego-Calama, M.; Reinhoudt, D. N. *Angew. Chem. Int. Ed.* **2006**, *45*, 7543-7546.
- 53 Stepien, M.; Donnio, B.; Sessler, J. L.; *Angew. Chem. Int. Ed.* **2007**, *46*, 1431-1435.
- 54 Tomalia, D. A.; *Nature Mat.* **2003**, *2*, 711-712.
- 55 Xu, J.; Liu, X.; Kok-Peng Ng, J.; Lin, T.; He, C. *J. Mater. Chem.*, **2006**, *16*, 3540-3545.
- 56 Lee, H. K.; Lee, H.; Ko, H. K.; Chang, Y. J.; Oh, N. K.; Zin, W. C.; Kim, K. *Angew. Chem. Int. Ed.* **2001**, *40*, 2669-2670.
- 57 Xu, Y.; Gu, W.; Gin, D. L.; *J. Am. Chem. Soc.* **2004**, *126*, 1616.
- 58 Sidorenko, A.; Tokarev, I.; Minko, S.; and Stamm, M.; *J. Am. Chem. Soc.*, **2003**, *125*, 12211-12216.
- 59 Tuominen, M. T.; Russell, T. P. *Science*, **2000**, *290*, 2126-2129.
- 60 Liang, C.; Hong, K.; Guiochon, G. A.; Mays, J. W.; Dai, S. *Angew. Chem. Int. Ed.* **2004**, *43*, 5785-5789.
- 61 Lee, M.; Park, M.H.; Oh, N.K.; Zin, W.C.; Jung, H.T.; Yoon, D.K. *Angew. Chem. Int. Ed.* **2004**, *43*, 6466-6468.
- 62 Hawker, C. J.; Wooley, K. L. *Science* **2005**, *309*, 1200.
- 63 Chand, P.; Babu, Y. S.; Bantia, S.; Chu, N.; Cole, L. B.; Kotia, P. L.; Layer, W. G.; Montgomery, J. A.; Pathak, V. P.; Petty, S. L.; ShROUT, D. P.; Walsh, D. A.; Walsh, G. M. *J. Med. Chem.* **1997**, *40*, 4030-4052.
- 64 Choi, J. Y.; Kim, J.; Furukawa, H.; Chae, H. K. *Chem. Lett.*, **2006**, *35*, 1054-1055.
- 65 Wang, Yi.; MSc by research thesis, University of Edinburgh, **2006**.
- 66 Greene, T. W.; Wuts, G. M. "Protective Groups in Organic Synthesis." Wiley, **1999**.
- 67 a) Gianni, M. H.; Adams, M. *J. Org. Chem.* **1975**, *40*, 450-453. b) Frauenrath, H.; Runsink, J. *J. Org. Chem.* **1987**, *52*, 2707-2712.
- 68 Koga, Y.; Sodoka, M.; Shibasaki, M. *Tet. Let.* **1994**, 2227-2230.
- 69 a) Forsberg, J. H.; Spaziano, V. T.; Klump, S. P.; Sanders, K. M. *J. Heterocyclic Chem.* **1988**, *25*, 767-770. b) Milata, V.; Claramunt, R. M.; Cabildo, P.; Santa Maria, M. D.; Cornago, P.; Infantes, L.; Cano, F. H.; Elguero, J. *Heterocycles*, **2001**, *55*, 905-924. c) de la Hoz, A.; Diaz-Ortiz, A.; Elguero, J.; Martinez, L. J.; Moreno, A.; Sanchez-Migallon, A. *Tetrahedron*, **2001**, *57*, 4397-4403.
- 70 Whitten, J. P.; McCarthy, J. R.; Matthews, D. P. *Synthesis*, **1988**, 470-473.
- 71 Khalaj, A.; Ghafari M. *Tet. Let.* **1986**, *27*, 5019-5020.
- 72 Radhakrishna, A. S.; Parham, M. E.; Riggs, R. M.; Loudon, G. M. *J. Org. Chem.* **1979**, *44*, 1746-7.

- 73 a) Ioannis, K.; Campas, H. M.; Rovirá I Virgili University, European patent **2003**, W003062456. b) Jobst, G. Moser, I. Varahram, M.; Svasek, P.; Aschauer, E.; Trajanoski, Z.; Wach, P.; Kotanko, P.; Skrabal, F.; Urban, G. *Anal. Chem.* **1996**, *68*, 3173-3179.
- 74 Nguyen, P.; Douce, L.; Ziessel, R.. *Tet. Lett.* **2002**, *43*, 5441-5444.
- 75 Smith, R. C.; Fischer, W. M.; Gin, D. L., *J. Am. Chem. Soc.* **1997**, *119*, 4092-4093.
- 76 Kumar, S.; Naidu, J. J.; Shankar Rao, D. S.; *J. Mat. Chem.*, **2002**, *12*, 1335-1341.
- 77 Torikai, A.; Ohno, M.; Fueki, K. *J. App. Polymer Sci.*, **2003**, *41*, 1023-1032.
- 78 Sahlen, F.; Trollsas, M.; Hult, A.; Gedde, U. W., *Chem. Mater.* **1996**, *8*, 382-388.
- 79 Bleyl, I.; Erdelen, C.; Etzbach, K. -H.; Paulus, W.; Schmidt, H. -W.; Siemensmeyer, K.; Haarer, D. *Mol. Cryst. & Liq Cryst.* **1997**, *299*, 149-155.
- 80 Tani, K.; Stoltz, B. M. *Nature* **2006**, *441*, 731-734.
- 81 Hiyama, Y.; Brown, T. L. *J. Phys. Chem.* **1981**, *85*, 1698-1700.
- 82 Hursthouse, M. B.; Smith, V. B.; Massey, A. G. *J. Fluor. Chem.* **1977**, *10*, 145-156.
- 83 Shibata, K.; Kulkarni, A. A.; Ho, D. M.; Pascal, R. A., Jr. *J. Org. Chem.* **1995**, *60*, 428-434.
- 84 (a) Pascal, R. A., Jr. *Chem. Rev.* **2006**, *106*, 4809-4819. (b) Shibata, K.; Kulkarni, A. A.; Ho, D. M.; Pascal, R. A., Jr. *J. Am. Chem. Soc.* **1994**, *116*, 5983-5984.
- 85 Smith, V. B.; Massey, A. G. *Tetrahedron* **1969**, *25*, 5495-5501.
- 86 (a) Lu, J.; Ho, D. M.; Vogelaar, N. J.; Kraml, C. M.; Pascal, R. A., Jr. *J. Am. Chem. Soc.* **2004**, *126*, 11168-11169. (b) Niemz, A.; Rotello, V. M. *Chem. Rev.* **1999**, *32*, 44-52. (c) Kroto, H. W. *Recent Research Developments in Applied Physics* **2002**, *5*, 409-436. (d) Watson, M. D.; Fechtenkötter, A.; Müllen, K. *Chem. Rev.* **2001**, *101*, 1267-1300. (e) Wu, Y-T.; Siegel, J. S.; *Chem. Rev.* **2006**, *106*, 4843-4867. (f) Tsefrikas, V. M.; Scott, L. T.; *Chem. Rev.* **2006**, *106*, 4868-4884.
- 87 Barnett, L.; Ho, D. M.; Baldrige, K. K.; Pascal, R. A., Jr. *J. Am. Chem. Soc.* **1999**, *121*, 727-733.
- 88 Frampton, C. S.; MacNicol, D. D.; Rowan, S. J. *J. Mol. Struct.* **1997**, *405*, 169-178.
- 89 Nishinaga, T.; Inoue, R.; Matsuura, A.; Komatsu, K. *Org. Lett.* **2002**, *4*, 1435-1438.
- 90 (a) Factual end-to-end twists: **58b** 45.2°, **59** 40.2° **60** 56.6°. Predicted (computed) twist: **61** 61°. Unsubstituted triphenylene 2°. (b) A 1:1 cocrystal of perfluoro **59** and triphenylene gives corresponding twists of 33° and 16°. Weck, M.; Dunn, A. R.; Matsumoto, K.; Coates, G. W.; Lobkovsky, E. B.; Grubbs, R. H. *Angew. Chem. Int. Ed.* **1999**, *38*, 2741-2745.
- 91 Peña, D.; Pérez, D.; Guitián, E.; Castedo, L. *Eur. J. Org. Chem.* **2003**, *7*, 1238-1243.
- 92 Peña, D.; Pérez, D.; Guitián, E.; Castedo, L. *Org. Lett.* **1999**, *1*, 1555-1557.
- 93 Peña, D.; Cobas, A.; Pérez, D.; Guitián, E. *Synthesis* **2002**, 1454-1458.
- 94 Peña, D.; Escudero, S.; Guitián, D. P. E.; Castedo, L. *Angew. Chem. Int. Ed.* **1998**, *37*, 2659-2661.
- 95 Peña, D.; Pérez, D.; Guitián, E.; Castedo, L. *J. Am. Chem. Soc.* **1999**, *121*, 5827-5828.

- 96 Peña, D.; Pérez, D.; Guitián, E. *Angew. Chem. Int. Ed.* **2006**, *45*, 3579-3581.
- 97 (a) Peña, D.; Cobas, A.; Pérez, D.; Guitián, E.; Castedo, L. *Org. Lett.* **2000**, *2*, 1629-1632. (b) Bennett, M. A.; Kopp, M. R.; Wenger, E.; Willis, A.C. *J. Organomet. Chem.* **2003**, *667*, 8-15.
- 98 (a) Altomare, A.; Cascarano, G.; Giacovazzo, G.; Guagliardi, A.; Burla, M.C.; Polidori, G.; Camalli, M. *J. Appl. Cryst.* **1994**, *27*, 435. (b) Betteridge, P.W.; Carruthers, J.R.; Cooper, R.I.; Prout, K.; Watkin, D.J.; *J. Appl. Cryst.* **2003**, *36*, 1487. (c) Spek, A.J. PLATON. University of Utrecht, The Netherlands, **2006**.
- 99 Gaussian 03, Revision C.02, Frisch, M. J.; Trucks, G. W.; Schlegel, H. B.; Scuseria, G. E.; Robb, M. A.; Cheeseman, J. R.; Montgomery, Jr., J. A.; Vreven, T.; Kudin, K. N.; Burant, J. C.; Millam, J. M.; Iyengar, S. S.; Tomasi, J.; Barone, V.; Mennucci, B.; Cossi, M.; Scalmani, G.; Rega, N.; Petersson, G. A.; Nakatsuji, H.; Hada, M.; Ehara, M.; Toyota, K.; Fukuda, R.; Hasegawa, J.; Ishida, M.; Nakajima, T.; Honda, Y.; Kitao, O.; Nakai, H.; Klene, M.; Li, X.; Knox, J. E.; Hratchian, H. P.; Cross, J. B.; Bakken, V.; Adamo, C.; Jaramillo, J.; Gomperts, R.; Stratmann, R. E.; Yazyev, O.; Austin, A. J.; Cammi, R.; Pomelli, C.; Ochterski, J. W.; Ayala, P. Y.; Morokuma, K.; Voth, G. A.; Salvador, P.; Dannenberg, J. J.; Zakrzewski, V. G.; Dapprich, S.; Daniels, A. D.; Strain, M. C.; Farkas, O.; Malick, D. K.; Rabuck, A. D.; Raghavachari, K.; Foresman, J. B.; Ortiz, J. V.; Cui, Q.; Baboul, A. G.; Clifford, S.; Cioslowski, J.; Stefanov, B. B.; Liu, G.; Liashenko, A.; Piskorz, P.; Komaromi, I.; Martin, R. L.; Fox, D. J.; Keith, T.; Al-Laham, M. A.; Peng, C. Y.; Nanayakkara, A.; Challacombe, M.; Gill, P. M. W.; Johnson, B.; Chen, W.; Wong, M. W.; Gonzalez, C.; and Pople, J. A.; Gaussian, Inc., Wallingford CT, 2004.
- 100 Kirby, E.P.; Steiner, R.F. *J. Phys. Chem.* **1970**, *74*, 4480.
- 101 Xu, Q.; Duong, H.M.; Wudl, F.; Yang, Y.; *App. Phys. Lett.* **2004**, *85*, 3357-3359.
- 102 Morrison, D.J.; Trefz, T.K.; Piers, W.E.; McDonald, R.; Parvez, M. *J. Org. Chem.* **2005**, *70*, 5309-5312.
- 103 Foster, E. J.; Jones, R. B.; Lavigueur, C.; Williams, V. E., *J. Am. Chem. Soc.* **2006**, *128*, 8569-8574.
- 104 Yoshio, M.; Kagata, T.; Hoshino, K.; Mukai, T.; Ohno, H.; Kato, T., *J. Am. Chem. Soc.* **2006**, *128*, 5570-5577.
- 105 Jayanth, T. T.; Jeganmohan, M.; Cheng, C. H. *J. Org. Chem.* **2004**, *69*, 8445-8450.
- 106 Ryu, E. H.; Yan, J.; Zhong, Z.; Zhao, Y., *J. Org. Chem.* **2006**, *71*, 7205-7213.
- 107 Han, L.; Razdan, R. K., *Tetrahedron Letters* **1999**, *40*, 1631-1634.
- 108 Seebach, D.; Aebi, J. D.; Gander-Coquoz, M.; Naef, R., *Helvetica Chimica Acta* **1987**, *70*, 1194-1216.
- 109 Ott, Donald G.; Benziger, Theodore M., **1990**, 8 pp, US 4952733
- 110 Shibata, K.; Kulkarni, A. A.; Ho, D. M.; Pascal, R. A., Jr., *J. Am. Chem. Soc.* **1994**, *116*, 5983-4.
- 111 Smith, V. B.; Massey, A. G., *Tetrahedron* **1969**, *25*, 5495-501.

-
- 112 Lu, J.; Ho, D. M.; Vogelaar, N. J.; Kraml, C. M.; Pascal, R. A., Jr., *J. Am. Chem. Soc.* **2004**, *126*, 11168-11169.
- 113 Barnett, L.; Ho, D. M.; Baldrige, K. K.; Pascal, R. A., Jr., *J. Am. Chem. Soc.* **1999**, *121*, 727-733.
- 114 Hart, H.; Lai, C.-y.; Chukuemeka Nwokogu, G.; Shamouilian, S., *Tetrahedron* **1987**, *43*, 5203-5224.